Spring 1-1-2012

The Effect of Wind Turbine Wakes on Summertime Midwest Atmospheric Wind Profiles as Observed with Ground Based Doppler LIDAR

Michael Edward Rhodes
University of Colorado at Boulder, michael.e.rhodes@gmail.com

The Effect of Wind Turbine Wakes on Summertime Midwest Atmospheric Wind Profiles as Observed with Ground Based Doppler LIDAR

by

Michael Edward Rhodes

B.S., North Carolina State University, 2008

A thesis submitted to the

Faculty of the Graduate School of the

University of Colorado in partial fulfillment

of the required for the degree of

Master of Science

Department of Aerospace Engineering Sciences

2012

This thesis entitled:

The Effect of Wind Turbine Wakes on Summertime Midwest Atmospheric Wind Profiles as Observed with Ground Based Doppler LIDAR

written by Michael Edward Rhodes

has been approved for the Department of Aerospace Engineering Sciences

_____

(Prof. Julie K. Lundquist, Committee Chair)

_____

(Prof. Jeff Thayer)

Date_____

The final copy of this thesis has been examined by the signatories, and we find that both the content and the form meet acceptable presentation standards of scholarly work in the above mentioned discipline.

Rhodes, Michael Edward (M.S., Aerospace Engineering Sciences)

The Effect of Wind Turbine Wakes on Summertime Midwest Atmospheric Wind Profiles as Observed with Ground Based Doppler LIDAR

Thesis directed by Assistant Professor Julie K. Lundquist

This study examines the influences of modern multi-megawatt wind turbine generator wakes on wind profiles. Principles of wind LIDAR technology and operation are discussed in preparation for analysis of the LIDAR dataset. Surface and wind LIDAR observations were collected from June 30, 2011 to August 16, 2011 in central Iowa. Two identical Windcube LIDAR systems were compared for two days at the beginning of the observation period and found to agree with good correlation in both wind speed and wind direction measurements at 20m vertical intervals from 40m to 220m above the surface. For the remainder of the field campaign, one LIDAR was located 2 rotor diameters (D) directly south of a wind turbine; the other LIDAR was moved 3 D North of the same wind turbine. Data from the two LIDAR dataset was filtered for the prevailing southerly flow in order to simultaneously capture inflow and waked conditions with the respective LIDAR. Data were compared between the upwind and downwind LIDARs for horizontal and vertical wind speed, wind shear, wind direction, wind directional shear, horizontal and vertical turbulence intensity, turbulent kinetic energy, and the power law coefficient (alpha). Results indicate measurable reductions in waked wind speeds at heights spanning the wind turbine rotor (40m to 120m). Turbulent and wind shear quantities increase in the wake of the turbine rotor. Results also indicate that the power law coefficient below turbine hub height may be a parameter that quickly identifies whether the downwind LIDAR was sampling turbine wake or free flow conditions. Changes in quantities downwind of the wind turbine are also shown to vary with inflow wind speed and time of day. Results are consistent with the few observations available from other studies; this dataset contributes higher temporal and spatial resolution data to provide a dataset which will be useful for turbine wake model validation.

Table of Contents

List of Tables and Figures

Tables

Figures

1 Introduction

A global transition to renewable energy sources is possible due to abundant renewable resources and technology (Jacobson and Delucchi 2011). Tremendous wind energy potential exists in the United States Midwest (Figure 1) which makes wind energy a leading renewable energy source for the United States (Milligan et al. 2009). Additionally, wind energy is the least expensive (9-12 ¢/kWh) utility-scale renewable energy technology, while the wind industry still expects many years of growth (Komor, 2009).

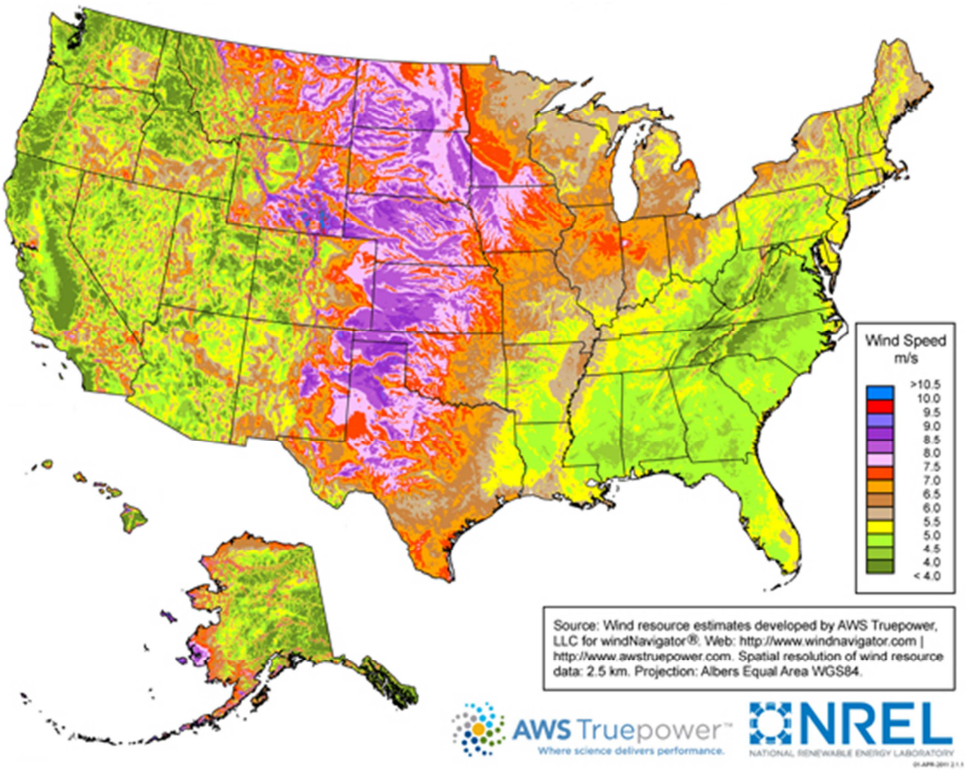

Figure 1: 80 m wind resource map of the United States. The purple colors indicate higher annual 80 m wind speeds and the greens show low wind speeds. (http://www.windpoweringamerica.gov)

The Midwest provides plentiful wind energy, and the region also serves as the hub of US agriculture (Figure 2). Corn and other crops are an important part of the local economy, and possible impacts of energy production on these crops are real concerns. Consequently, the unknown impact of turbine wakes on local agriculture could alter the future of wind energy development in the Midwest.

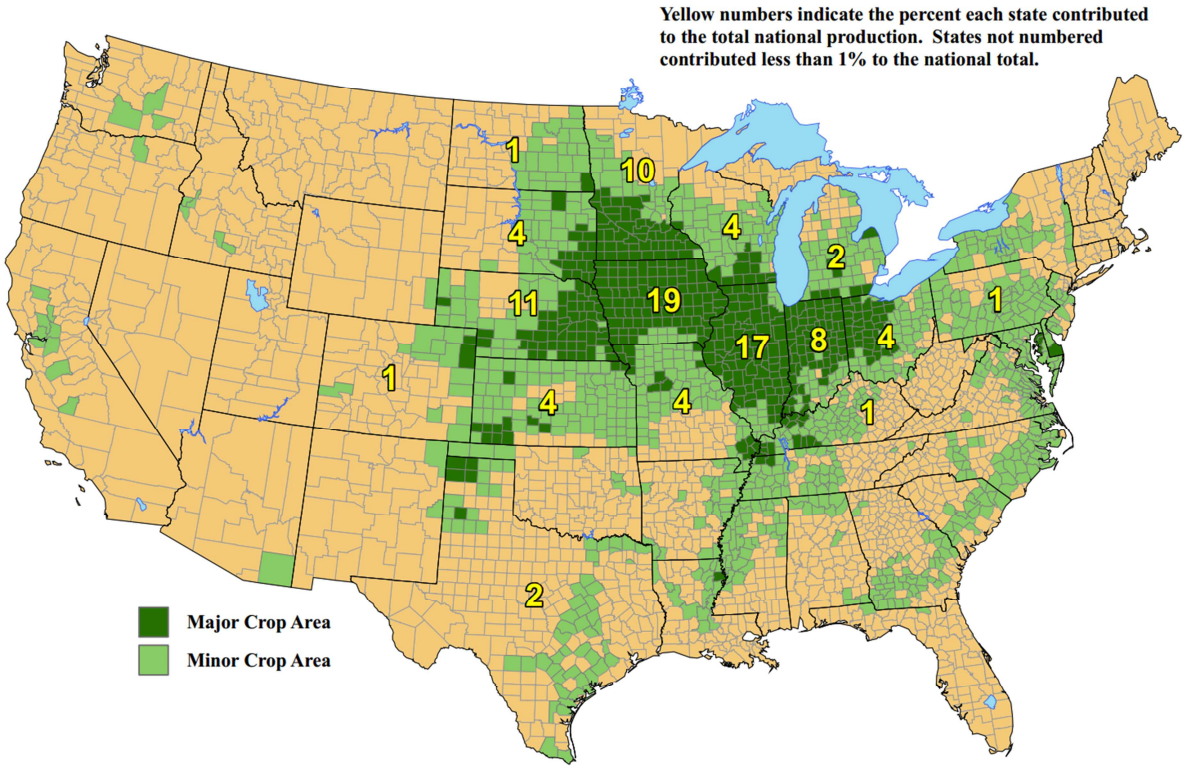

Figure 2: United States corn production by county.
(http://www.usda.gov/oce/weather/pubs/Other/MWCACP/Graphs/USA/corn.pdf)

In particular, concern exists that increased turbulence in turbine wakes may alter the exchange of heat and moisture with the soil and vegetative canopies (Baidya Roy 2011). Altered surface fluxes may lead to changes in the growing behavior of agricultural crops, but wind turbine wakes have not yet been determined to have a beneficial or detrimental impact on crop growth (Rajewski et al. 2012). Detailed observations of the atmosphere and surface exchanges upwind and downwind of operational turbines are essential to determine wake impact on the atmosphere and then on local crops.

Agriculture is directly influenced by the atmospheric boundary layer (ABL). The Midwest tend to follow a distinct daily cycle of ABL behavior due to flat terrain (Figure 3) (Stull 1988). Shortly after local sunrise, the surface begins to warm from direct solar radiation. A warmer surface creates convective overturning and turbulent mixing in the ABL. Before sunset the surface begins to cool slowly creating a stably stratified layer that persists until sunrise the following morning. Day time conditions are characterized

by more turbulence and generally slower wind speeds than at night. Night time flow can be described with reduced turbulence, higher wind speeds, and wind direction shear.

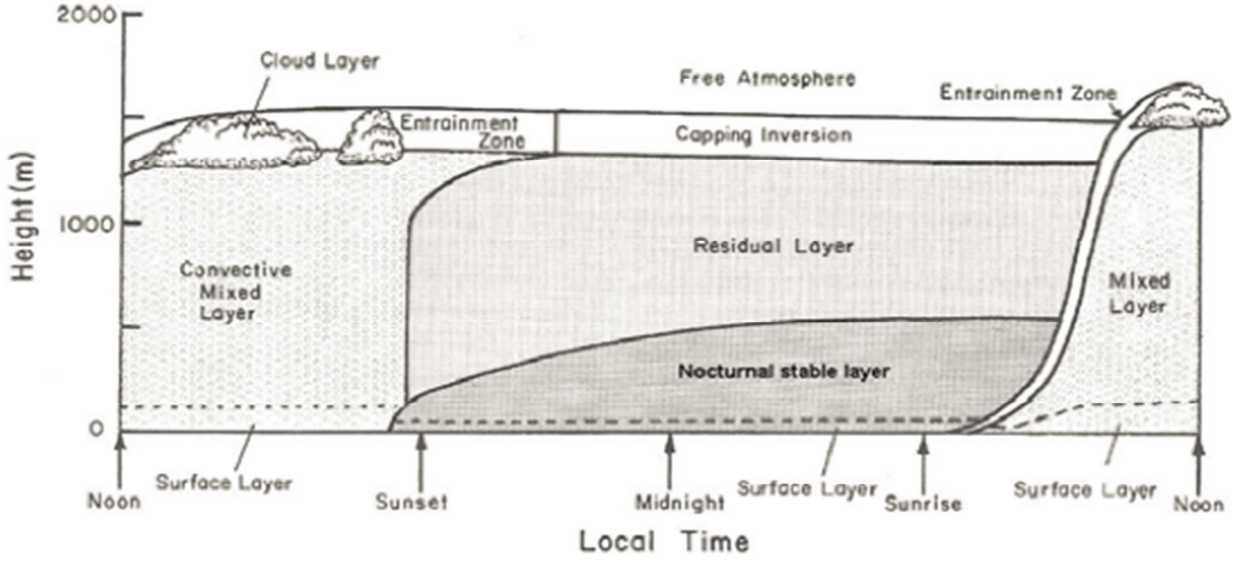

Figure 3: The atmospheric boundary layer typical of summer-time Midwest. (Stull 1988)

A wind farm, most commonly used for utility-scale applications, is a group of hundreds of individual horizontal-axis wind turbines (typically of capacity 1.5 MW or greater) installed over an area on the order of 100 km^2. Each turbine in the wind farm has blades that produce electricity by converting horizontal momentum in the wind into rotation of a generator. The area swept by the turbine blades is known as the rotor disk. A region of reduced wind speeds and increased turbulence, called the wake, exists downwind of each turbine as a result of the interaction between the wind and rotor. Wakes from upwind turbines are responsible for decreased power output at downwind turbines in the wind farm (Barthelmie et al. 2010). Because turbine wakes have removed momentum from the wind, less momentum is available for the downwind turbines to extract.

Wind turbines cause atmospheric changes over a range of scales. Laboratory, computer simulation, and observational studies all guide our understanding of the impacts of wind turbines on both the atmosphere and the surface. Chamorro and Porté-Agel (2010) used a wind tunnel to measure the effects of a model wind turbine on fluid flow. They measured mean and turbulence values of the flow under neutral and stable conditions and found signatures of turbine wakes up to 20 rotor diameters downwind. Furthermore,

they found the wake momentum deficit to be axially-symmetric while the turbulence characteristics of the turbine wake were concentrated above hub height. Chamorro and Porté-Agel did not take measurements of unstable flow conditions, which are often present during daytime, or of stable conditions, which dominate nighttime flow regimes.

A Large Eddy Simulation (LES) model and wind tunnel comparison by Wu and Porté-Agel (2010) found that the wind tunnel is not a robust representation of the full atmospheric boundary layer environment. A LES model run by Lu and Porté-Agel (2011) compared atmospheric flow with and without the presence of a "very large wind farm." The model did not perform well in unstable conditions. Results in stable conditions indicate a significant impact of the wind farm on boundary layer height, wind speed, turbulent kinetic energy, turbulent fluxes, and the kinetic energy power spectrum at least 8D downstream. While both LES and wind tunnel studies provide insights into what might be expected from field campaigns, only field campaigns are able to show real wind farm-atmosphere dynamics. Of course, test conditions may not be controlled during a field campaign as they can be in a wind tunnel or in simulations.

Field campaigns typically involve both *in situ* and remote sensing instrumentation. Standard atmospheric wind measurements are made with *in situ* measurements with cup or sonic anemometers, which must be mounted on towers that can interfere with measurement of the wind field. Additionally, towers pose logistical problems due to the large size. Tethered kites and remotely piloted vehicles outfitted with onboard hotwire anemometers (Högström et al. 1988; Baker and Walker 1984; Frehlich et al. 2003; Kocer et al. 2011) can observe details of turbulent environments at multiple locations on the scale of seconds to minutes without the flow disruption towers cause. Remote sensing technology, including acoustic, microwave, and laser systems have the ability to measure the atmosphere at multiple locations. Light Detection and Ranging (LIDAR) systems offer the ability to measure high above the ground and over long distances without having to erect a large meteorological tower at each desired measurement location. One such LIDAR system is the Leosphere Windcube (Courtney, Wagner, and Lindelöw 2008), which will be discussed in detail in the following chapter.

Previous observational campaigns on turbines show that downwind of a turbine there is a readily measurable wake region characterized by decreases in horizontal wind speed and increased turbulence (Baker and Walker 1984; Högström et al. 1988; Käsler et al. 2010). One other study suggests slightly increased temperatures downwind of large wind farms (Baidya Roy 2011). Trujillo et al. (2011) mounted a scanning LIDAR system on the back of a modern multi-megawatt wind turbine to more closely examine the wind turbine wake dynamics. They conclude that wake shape is largely determined by otherwise undisturbed atmospheric flow interaction with small eddies. However, Kelley et al. (2006) demonstrate that different geographic locations experience dissimilar atmospheric flow based on geographic characteristics upwind of the wind farm. Kelley's findings imply that Trujillo's LIDAR measurements taken on the west coast of Denmark may not apply in other locations. Other studies support Kelley's findings that individual turbine wakes show differences due to local effects such as topography, siting, and atmospheric conditions (Baker and Walker 1984; Käsler et al. 2010) and are not generally symmetric downwind of a single turbine (Högström et al. 1988). In our study, we are interested in learning more about turbine wake characteristics located in the Midwest. In particular, nocturnal flow in the Midwest often experiences a jet-type structure in the wind profile, known as a nocturnal low-level jet (Blackadar, 1957; Whiteman et al., 1997, Banta et al., 2002). We use LIDAR to evaluate the effect of wind turbine wakes on Midwest atmospheric profiles of mean and turbulent quantities.

Chapter 2 of this thesis provides information on the Windcube LIDAR used to collect data for analysis. In Chapter 0, specifics of the field deployment are discussed in addition to the behavior of wind turbine wakes based on inflow wind speed and height. Chapter 4 discusses an averaged, or canonical, day approach to quantifying wake properties. To demonstrate that the canonical method is representative of individual wakes, two cases studies reveal wake dynamics. Finally, the conclusion summarizes the findings of this dataset and outlines future work.

2 Windcube LIDAR System

The Windcube operates by transmitting a laser pulse of infrared light (1.54 μm) sequentially in four cardinal compass directions each directed approximately 30° down from vertical. The offset from vertical in conjunction with the four directions allows the Windcube to calculate the three wind velocity components (Figure 4). For each direction, the Windcube sends out a 10μJ, 200ns pulse at a repetition rate of 10kHz for approximately one second (Table 1). As the LASER light travels through the atmospheric boundary layer, some of the light is backscattered off aerosols, which are assumed to be traveling with the wind. If the scattering object has a component of velocity along the line of sight (LOS), the backscattered frequency will experience a Doppler shift in frequency. Information from each one second pulse window is ranged based on time of flight. Each range gate is then averaged with other pulses from the same range gate in order to determine the most accurate LOS velocity for each user-specified height. The four LOS velocities from one rotation of the LASER then produce a profile of the three wind velocity components. Data from each height is really the combination of data averaged over a vertical extent of approximately 20 m.

Components of wind data from the Windcube are reported in an coordinate system that does not conform with the standard meteorological component system (Stull 1988; Pauliac 2009). The Windcube system reports +u as North to South, +v as East to West, and +z towards the ground. For this report all wind components are rotated to the standard meteorological system with +u pointing to the East, +v pointing North, and +w pointing upward from the surface.

As described above, the Windcube laser light is backscattered off of aerosols. The backscattered light returns to the detector window where it then passes through an Acousto-Optic Modulator (AOM). The AOM allows the Windcube to accurately distinguish the wind direction of the return signal through polarity comparison (Courtney, Wagner, and Lindelöw 2008). Unfortunately, the exact algorithm for the retrieval is not publicly available due to proprietary reasons.

Performances	
Range	40 to 200m
Accumulation Time	0.5 s
Data output frequency	1 Hz
Probed length	20m
Scanning cone angle	~30°
Speed Accuracy	0.2m/s
Speed range	Up to 45m/s
Direction Accuracy	1.5°
Data Availability	> 95% up to 150 m*
Laser	
Wavelength	1,54 µm
Pulse energy	10 µJ
Eye safety	IEC 60825-1
Environmental	
Temperature Range	-15 to +40°C with Temperature Control Unit*
Operating humidity	IP65
Rain protection	Wiper (with water pump)
Compacity	Portable (2persons)
Dimensions	
Weight	60 Kg
Dimensions	900X550X550mm
Power Supply Specifications	
Electric Power Supply	27 DC
Power consumption	111W (without wiper, window heating ruban and temperature control)/ 375W Total with Temperature Control/ 400W Peak

Table 1: Basic operating specifications for the Windcube (Pauliac 2009).

2.1 Errors and Uncertainties

The most significant source of error in the Windcube measurements involves an assumption of homogenous flow. Radial velocities from four different directions (Figure 4) are averaged together to define three components of wind during one rotation of the prism, which requires approximately 4 seconds. Each height reported by the Windcube represents a volume measurement. Table 2 compares the representative volume, diameter of the measurement volume, line of sight depth, and vertical depth of each wind cube measurement for heights of 40m to 220m in 20m increments for α=27.85° cone angle (Figure 4), which is a common cone angle for a Windcube.

Measurement Height (m)	Vertical Depth (m)	LOS Depth (m)	Diameter of Measurement Area (m)	Representative Volume (m^3)
40	26.5	30.0	42.3	1120

60	26.5	30.0	63.4	1680
80	26.5	30.0	84.5	2240
100	26.5	30.0	105.7	2800
120	26.5	30.0	126.8	3360
140	26.5	30.0	147.9	3920
160	26.5	30.0	169.1	4480
180	26.5	30.0	190.2	5040
200	26.5	30.0	211.3	5600
220	26.5	30.0	232.5	6160

Table 2: Lengths and volumes of windcube measurement compared with the measurement height for a cone angle of 27.85°.

The atmospheric boundary layer is inherently turbulent (Stull 1988), thus the winds are changing velocity at time scales ranging from minutes to fractions of a second. Turbulent time scales are similar to the measurement time scales of Windcube measurement, so there is uncertainty at the smallest time scales (Mikkelsen 2009). Results shows ten-minute averages of LIDAR-retrieved velocities agree well with those measured by cup and sonic anemometers (Courtney, Wagner, and Lindelöw 2008). However, turbulence estimates provided by the Windcube show some disagreement with turbulence measurements from sonic anemometers (Sathe et al. 2011). The disagreement in sonic and LIDAR measurements may be due to the difference in measuring volume (Sathe et al. 2011) and time scales. The Windcube uses a vertical depth averaging of 26m and a time scale on the order of one second to calculate its data while sonic anemometers measure volumes of 10cm or less at a rate of 20Hz.

Complex terrain upwind of the Windcube exacerbates the error in calculated wind. Complex terrain reduces the validity of the homogenous flow assumption (Peña et al. 2010). For the field study described herein, the gently sloping terrain of central Iowa in conjunction with agricultural crops dominates the landscape with wind turbines located throughout the region.

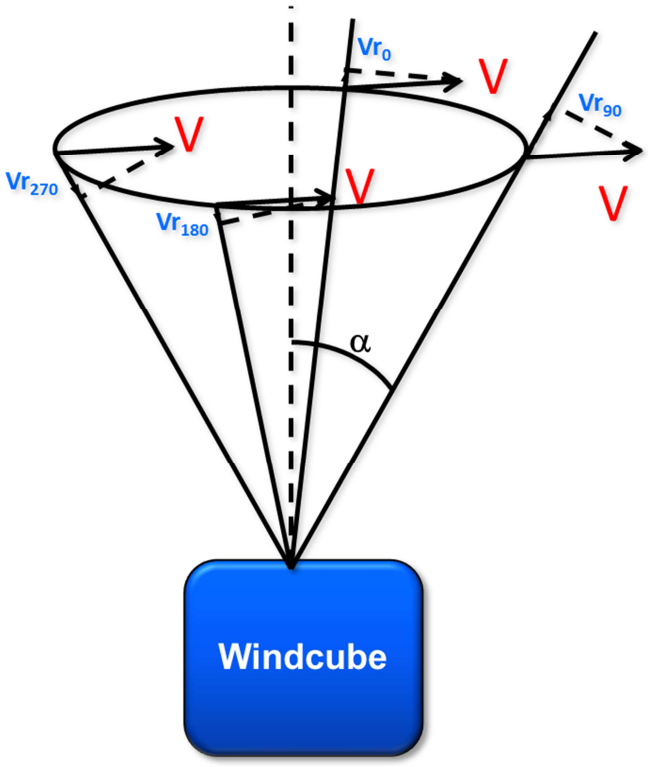

Figure 4: Schematic of Windcube operating principle (adapted from NRG Systems).

2.2 Prior Validation

The Windcube system has been the focus of multiple validation studies. One of the first validation papers to compare the Windcube with the industry standard cup anemometer was produced by Deutsche WindGuard (Albers, Janssen, and Mander 2008). They compare 10 minute averaged values of wind speed, direction, turbulence, and statistics of these values between a cup anemometer and the Windcube prototype at 99m and 135m above the surface. The 2008 WindGuard study found the Windcube and cup anemometer highly correlated with R^2 values in the mid to upper 90%. However, the turbulence intensity calculation is not as highly correlated between the cup anemometer and Windcube with R^2 values in the mid 60% range (Albers, Janssen, and Mander 2008). Sathe et al. (2011) also found disagreement between boundary layer wind LIDAR and conventional anemometer measurements of atmospheric turbulence.

3 Observational Data Set

As part of the Crop-Wind Energy Experiment 2011 (CWEX-11) (Rajewski et al. 2012), the CU Windcube (version 1) LIDAR and a rental Windcube (version 1) LIDAR were deployed within an operating wind farm in the agricultural fields of central Iowa (Figure 5). Because summer wind roses from Iowa (Figure 6 & Figure 7) indicate strong southerly winds, we located the Windcubes south (north) of a turbine to intentionally sample turbine inflow (wakes). One Windcube (CU1) was approximately 165m south of a row of six modern multi-megawatt wind turbine generators (WTG) placed in a line running from west to east; the second Windcube (CU2) was located 250m directly north of the WTG row and the southern Windcube. In addition to the LIDARs, other equipment interrogated the effects of turbine wakes on the agricultural crops in the vicinity. Collaborators in the Agronomy department at Iowa State University deployed an array of two surface flux stations south and north wind turbine row. The National Center for Atmospheric Research (NCAR) placed an Integrated Surface Flux System (ISFS) south of the turbine row and an additional three ISFSs north of the turbines (NCAR ISFS 2012). Surface flux data were recorded for the duration of the Windcube operational period.

The WTG observed in this study had an 80m hub height and 80m rotor diameter (40m to 120m AGL). The rotor blades begin to rotate at a cut in speed of 3.5 m/s, below which there is minimal power production. Electrical power production reaches a maximum at 12 m/s, the rated speed for the turbines. At speeds above rated, power production remains constant with increasing wind speed. However, at the cut out speed of 25 m/s the turbine rotor is locked so that it no longer rotates to prevent mechanical wear and tear in high wind conditions.

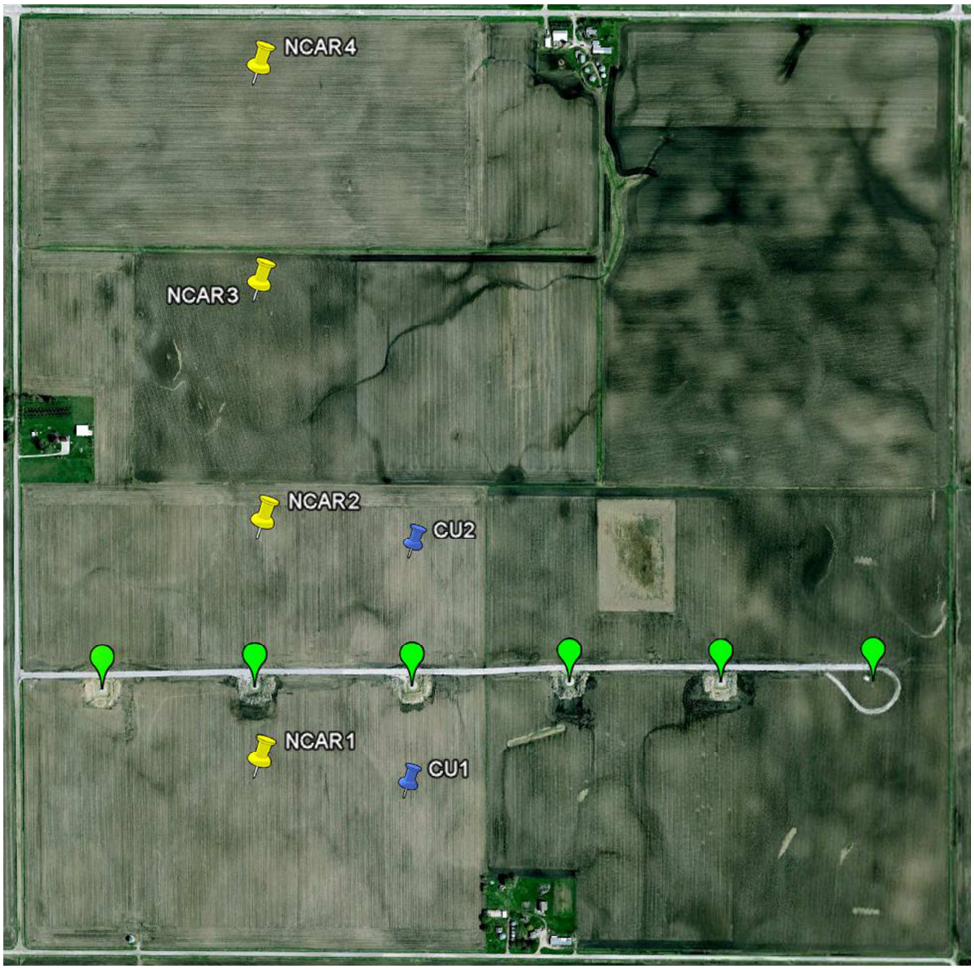

Figure 5: A map of the field site shows an East-West row of wind turbines indicated by green markers. Blue markers show the locations of each Windcube LIDAR system and yellow markers are the locations of surface flux stations.

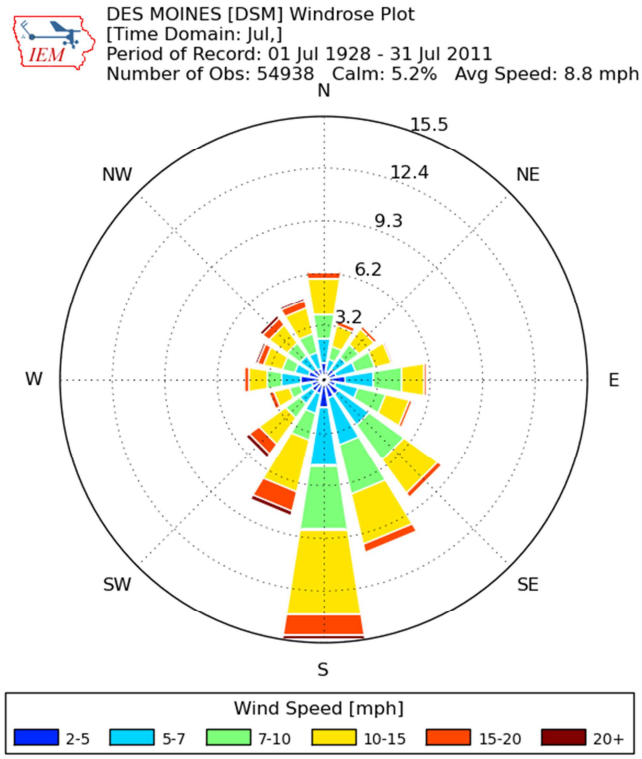

Figure 6: Surface wind rose for the month of July from the years 1928 through 2011 in central Iowa.

http://mesonet.agron.iastate.edu/onsite/windrose/climate/monthly/07/DSM_jul.png

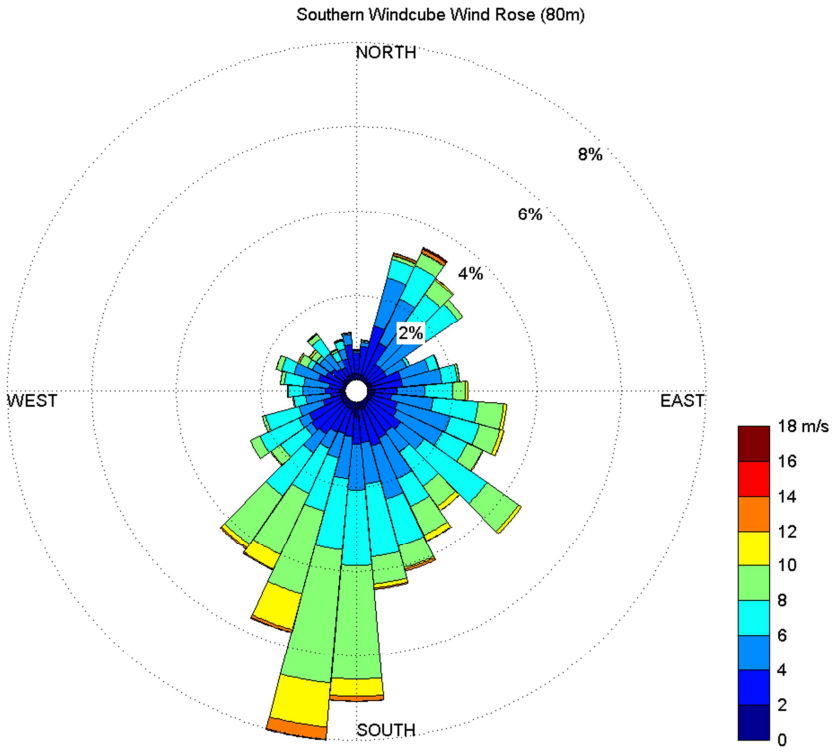

Figure 7: A wind rose from the southern Windcube measurments at 80 m AGL indicate a predominant southerly flow. Data from the entire observational period are included.

The row of WTGs pictured in Figure 5 is on the southern end of a larger utility sized wind farm at an elevation of approximately 335 m above sea level. Each WTG has a hub height of 80m AGL and a 3 bladed rotor diameter of 80m. The landscape surrounding the study site is primarily composed of soybean and corn agricultural fields with portions of the fetch interrupted by farm and homesteads. Corn is the primary crop surrounding the Windcube and wind turbines, however there are soybean fields located to the north and east of the Windcube measurement site. The closest homesteads are approximately 600 m to the Northwest and South-southeast from the Windcube. Running parallel to the row of wind turbines is a 10m wide gravel access road. The LIDAR observational period began on 30 June, 2011 and concluded on 16 August, 2011. Approximate sunrise occurred between 0430 and 0515 Local Standard Time while sunset ranged from 1915 to 2000 LST.

The Windcube records data every two minutes for each specified height based on the average of all return signals during the two-minute period. Any data that does not meet the carrier to noise ratio threshold

of -22dB is omitted from the recorded two-minute average. To determine the effect of wind turbine wakes on the wind profile, the two-minute Windcube data is used. Values for wind speed shear, directional shear, turbulence intensity, vertical turbulence intensity, and total kinetic energy are calculated based on the two-minute data from the measured wind speed components, wind direction, wind speed variance, and measurement height. Time periods during precipitation events (as measured at the local ISFS stations) were ignored due to observed increases in vertical wind speed sustained through an entire precipitation event (Aitken, Rhodes, and Lundquist 2012).

3.1 Windcube Inter-comparison

The first two days of the 2011 observational campaign were used to quantify any differences in measurement between the two Windcube units. Both units were co-located at the CU1 site (Figure 5) approximately three meters away from each other. For the duration of the inter-comparison period, winds ranged from calm to 20 m/s and wind directions were mostly out of the south-southwest; wind profiles were therefore unaffected by any turbines. Figure 8 shows an example of the wind speed comparison between the two Windcube units based on two-minute averages. The slope is near unity and the y-intercept of the best fit is close to zero. A high coefficient of determination, 0.985, shows a strong relationship between the data from each Windcube indicating that they were sampling essentially the same volume of air and recording the same measurements of wind speed and wind direction. R^2 values between the Windcube units were compared for wind speed and direction at all available heights; the results are summarized in Figure 9. Both wind speed and wind direction data is highly correlated between the two Windcubes at all heights for the inter-comparison period. After the inter-comparison period, WC 68 (ordinate from Figure 8) remained at the CU1 site (Figure 5) while WC 49 (abscissa from Figure 8) was relocated to the CU2 site (Figure 5) to capture wind turbine wake data.

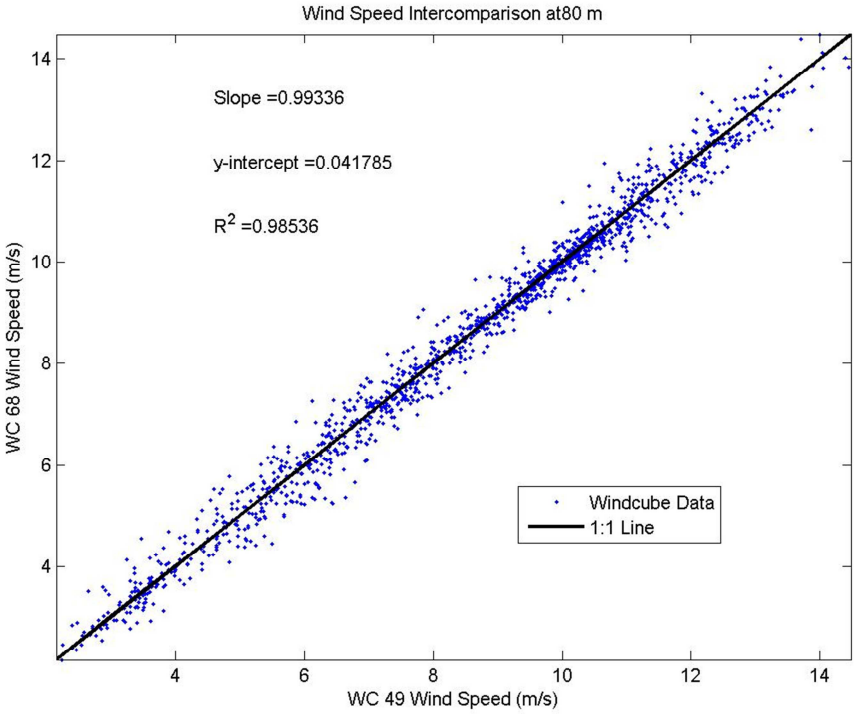

Figure 8: Hub height wind speed comparison for the two Windcube units.

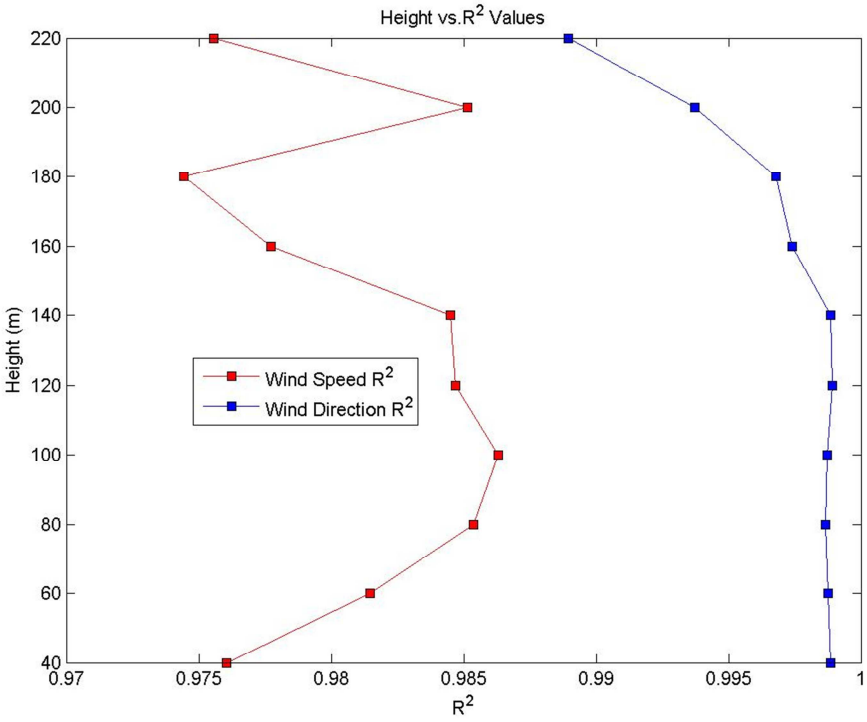

Figure 9: Height versus coefficient of determination for both wind speed and direction.

3.2 Wake Definition

For the purposes of the CWEX-11 study, time periods where the downwind Windcube sampled wake conditions need to be identified. The wake is defined by the hub height wind directions falling within a cone of wind directions where the wind turbine's wake is expected to impact the Windcube measurement profile. The wind direction cone incorporates a wake expansion value that Barthelmie et al. (2010) found in offshore wind farm data. Based on Barthelmie et al.'s analysis, we determined that wind directions lying between 167° and 195° should place a wind turbine wake directly over the northern Windcube. Other wind directions will also produce wakes from other turbines; the analysis here focuses only on wakes from the turbine located directly between the two LIDARs. As a proxy for wind turbine operation, Windcube hub height wind speed must be in excess of three m/s, consistent with the power curve for this turbine (which may not be identified due to pending nondisclosure agreements). Data were also removed for periods of measureable precipitation based on the ISFS surface station data set.

3.3 Wake Properties' Dependence on Wind Speed

One approach to analyzing the waked region behind a turbine is to compare the difference between upwind and downwind based on inflow wind speed and height. Two minute differences of horizontal wind speed and turbulence intensity data were categorized based on the inflow wind speed at the time of the difference measurement. Each upwind wind speed bin was limited to 0.5m/s increments from 0m/s to 20m/s, which covered the available range of wind speeds observed throughout the seven-week study period. Maximum, minimum, and mean statistics were calculated for each variable at every available wind speed bin and height. Examination of these figures shows that there is a dependence on wake properties with upwind wind speed.

3.3.1 Wind Speed difference

A deficit of wind speed in the turbine wake (Högström et al. 1988; Chamorro and Porté-Agel 2010, among others). The magnitude of this deficit varies with both altitude within the wake and with the speed of the flow entering the turbine rotor disk. We can consider both the maximum wake deficit within a given wind speed bin as well as the mean deficit. As seen in Figure 10**Error! Reference source not found.**, at hub

height (80m), the maximum deficit increases with upwind wind speed until 11.5-12 m/s bin. At inflow wind speeds greater than 12 m/s, which is rated wind speed for this turbine model, the deficit actually decreases related to inflow speed. Similarly, the same limiting behavior is seen at 100m, although the limit is reached at the 13-13.5 m/s bin. The maximum difference is greater than 5 m/s at all altitudes.

Similar behavior appears when the mean wind speed deficit is considered, although the values of the mean wind speed deficit are much lower than the maximum values. As seen in Figure 11, the average wake deficit exhibits largest values at or just above hub height (80m to 100m), and at wind speeds just below rated speed. Above rated speed, the deficit actually decreases until relatively high wind speeds are reached. There is also a positive slope to the largest difference values between 7 – 11 m/s upwind wind speed and for heights between 60m and 120 m, which means different heights of the rotor interact with the inflow differently at the same time. The momentum deficit is always present at hub height, but the magnitude of the deficit depends on the upwind wind speed. The maximum deficit occurs at wind speeds just below rated speed, near where the turbine power coefficient reaches a maximum value.

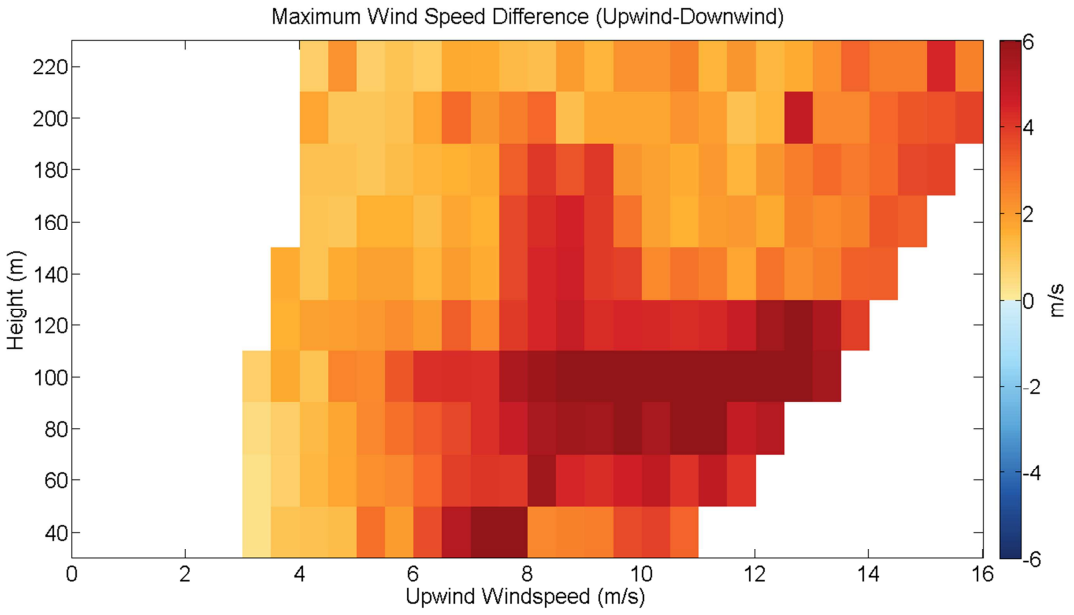

Figure 10: Upwind wind speed-height contours of maximum wind speed differences (upwind - downwind)

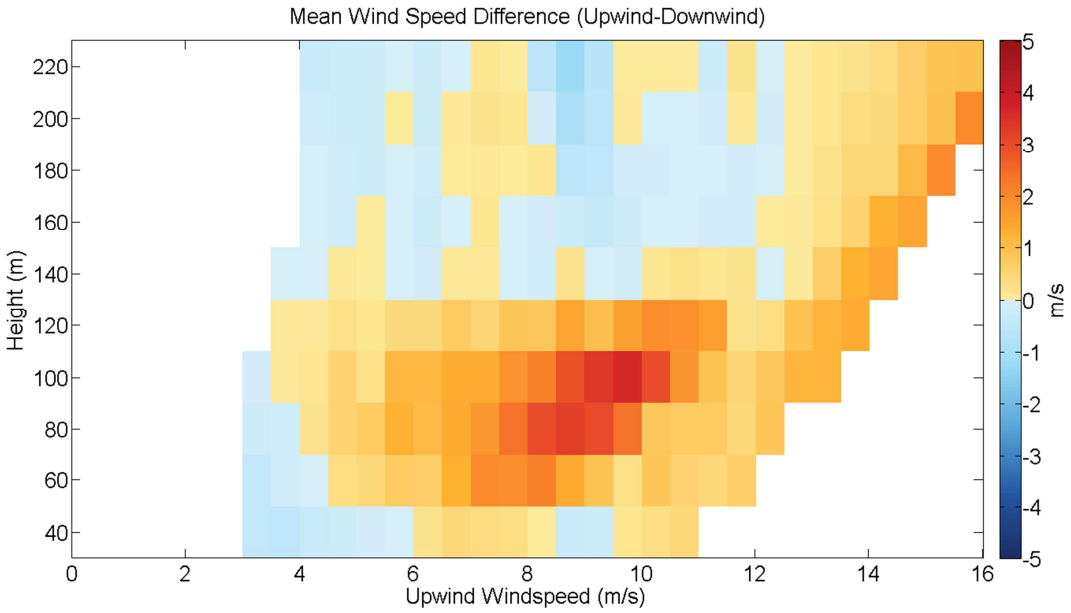

Figure 11: Upwind wind speed-height contours of mean wind speed differences (upwind - downwind)

3.3.2 Turbulence Intensity Difference

Previous investigations have observed enhanced turbulence intensity in the wake. Here, turbulence intensity is calculated from

$$I = \frac{\sqrt{\sigma_u^2 + \sigma_v^2}}{U}$$

where σ_u^2 and σ_v^2 are the u and v component wind speed variances and U is the mean horizontal wind speed (Chan 2008). Not only do the present observations show enhanced turbulence in the wake, but also that this enhancement depends on inflow wind speed. Plots of turbulence intensity differences (Figure 12) demonstrate a distinct region of turbulence enhancement at turbine hub height. (Turbulent kinetic energy behaves in a similar fashion though not shown here.) When considering the extreme values of turbulence intensity difference, as in Figure 13, we see that the most extreme differences occur near hub height or below (40m to 80m) for winds speeds of 10m/s, which is less than rated speed for this turbine (11 m/s). Similarly, for mean turbulence intensity difference, negative differences exist at hub height and speeds as in the minimum figure, however, the magnitude of the difference is smaller. Both these plots show negative

differences, which indicates that there was larger turbulence intensity near rotor height downwind of the turbine.

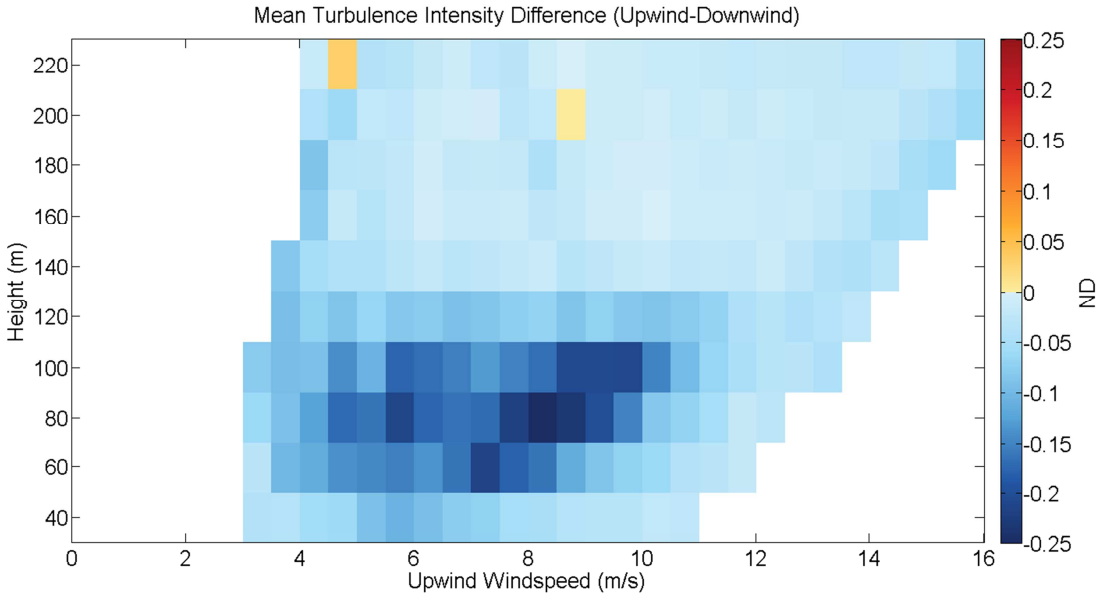

Figure 12: Upwind wind speed-height contour of mean turbulence intensity differences (upwind - downwind)

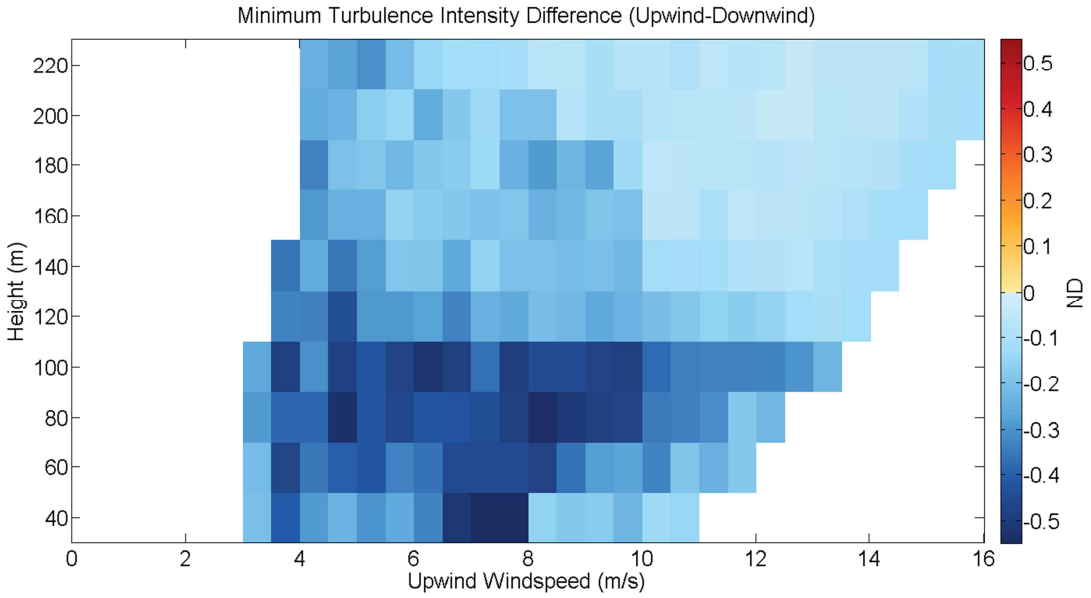

Figure 13: Upwind wind speed-height contour of minimum turbulence intensity differences (upwind - downwind)

4 Behavior of turbine wake over an averaged or "canonical" day

It is expected that turbine wake characteristics may vary over the course of a day as atmospheric stability varies. To synthesize these characteristics and how they vary over a diurnal cycle, the LIDAR data have been aggregated into a "canonical day" in the following fashion. All of the times and heights where data are available for both Windcube systems are identified. From this set of data, we isolate the southerly flow cases as above, using only wind directions between 167° and 195° following the 5-degree wake expansion observed by Barthelmie et al., (2010). For these cases, the CU1 site is upwind of the wind turbine row and CU2 is directly in the wake of one turbine. Data at each time and height coordinate is then averaged with all others in the data set with the same time of day and height above ground. To increase data availability through the full 24 hour cycle, averaged periods of 20 minutes are used for analysis. Furthermore, periods when data are available at reduced frequencies relative to the maximum data availability are masked with a cross-hatch to indicate data coming from only one particular day instead of multiple days. In the following description of the canonical day, "non-waked" refers to observations by the upwind wind cube during conditions that fit the wake definition. Similarly, "waked" refers to observations by the downwind Windcube that are in the turbine wake.

4.1 Data availability

The number of available data points at each time and height coordinate for the canonical study reveal that there are consistent variations throughout an average 24 hour cycle. In Figure 15, we can see that reduced data availability exists during the morning and evening transition periods, which may be caused by the transition in boundary layer structure near sunrise and sunset. To denote these periods of reduced data availability, a hatching appears over heights and times that represent data from less than 40% of the maximum available data (55 data points, denoting 5.5 days reporting data at that time/height). This level of hatching ensures each non-hatched data point reflects at least two days' worth of data. Hatching was chosen in place of complete omission since the data that was recorded is still real and useful information.

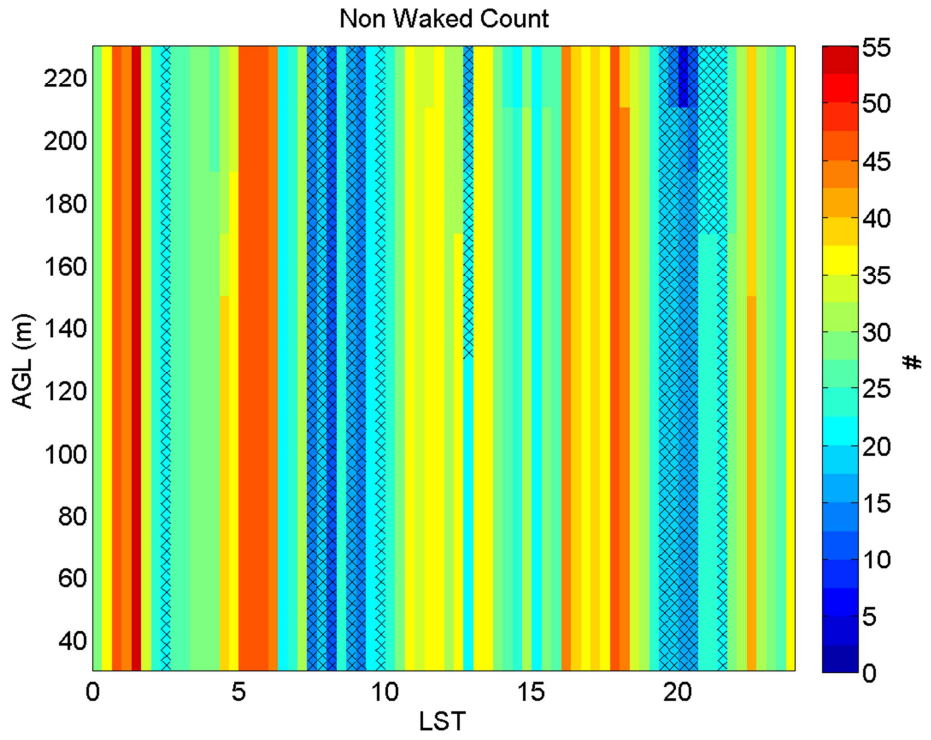

Figure 14: Number of available data points at CU1 for the canonical case study.

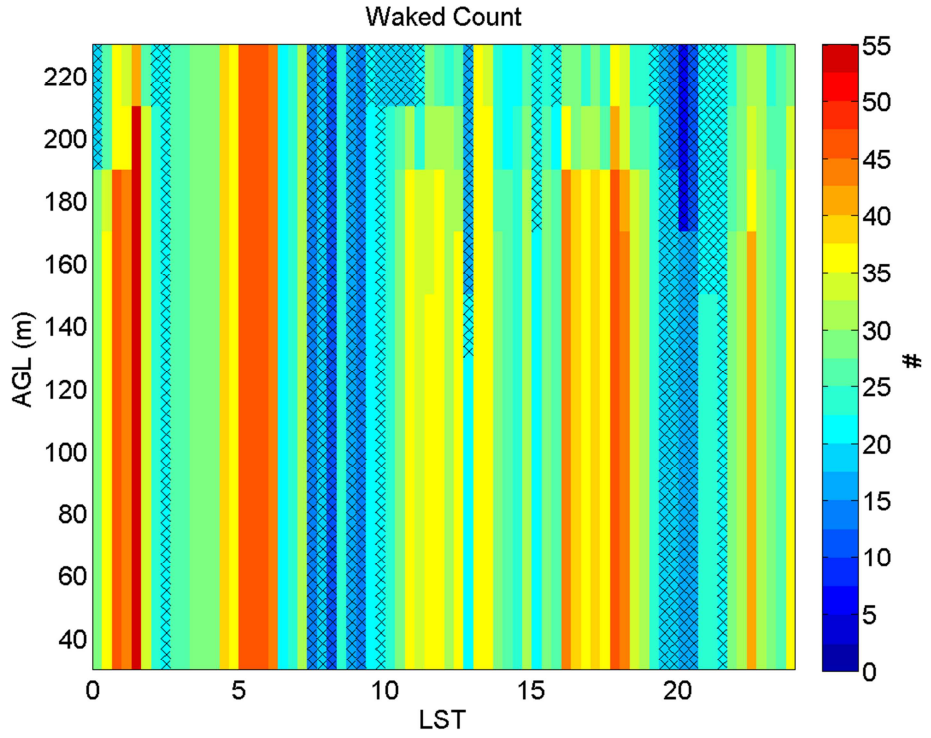

Figure 15: Number of available data points at CU2 for the canonical case study.

4.2 Wind speed difference

Horizontal wind speed measured by both Windcubes show similar average daytime behavior aloft (Figure 16, Figure 17): strongest winds occur in the first half of the morning and then redevelop later in the afternoon. The strongest wind speed difference between waked and non-waked, as expected from the presence of the turbine, is found in the altitudes of the rotor disc (40 m to 120 m). Greater velocity deficit is generally found in the rotor region during the night under more stable conditions. Unstable conditions associated with daytime convection likely enhance the mixing of higher-momentum air into the wake, thereby reducing the persistence of the wind turbine wake in the rotor disc region. The strongest velocity deficit found in waked flow exceeds 4 m/s at approximately 2300 local time and in the top half of the rotor disc altitude region. It is interesting to note in Figure 18 that a wind speed surplus exists downwind of the wind turbine during the nighttime portion of the 24 hour cycle at 40 m AGL, at the bottom of the rotor disk. Co-located surface flux station wind speed data at 10m also exhibit this speed-up below the rotor disk (Rajewski et al. 2012).

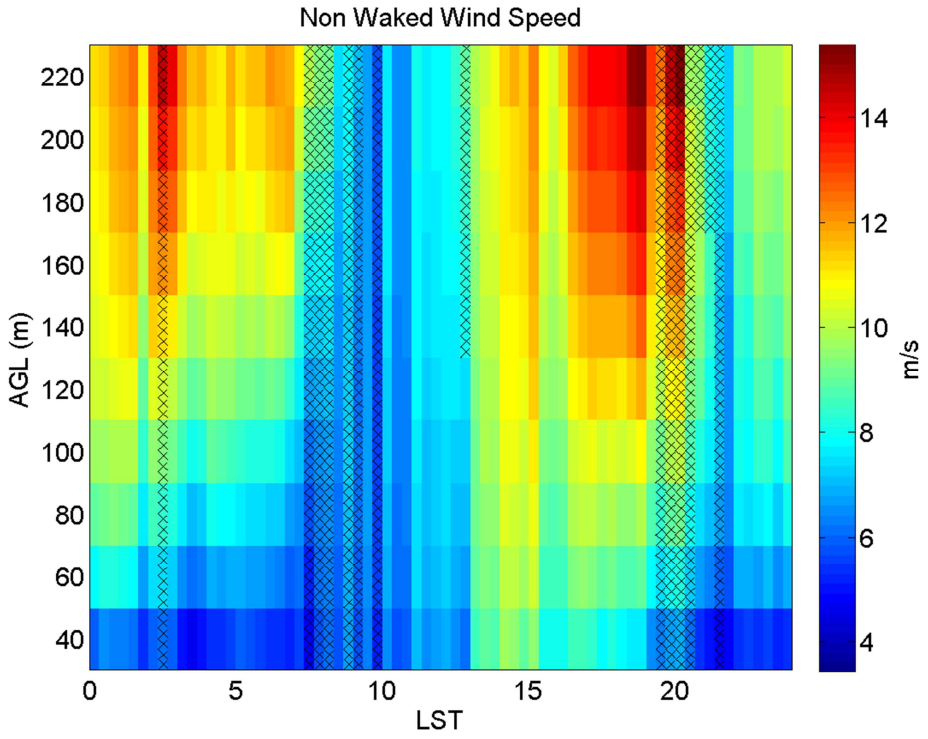

Figure 16: Canonical time-height contour plots of upwind horizontal wind speed

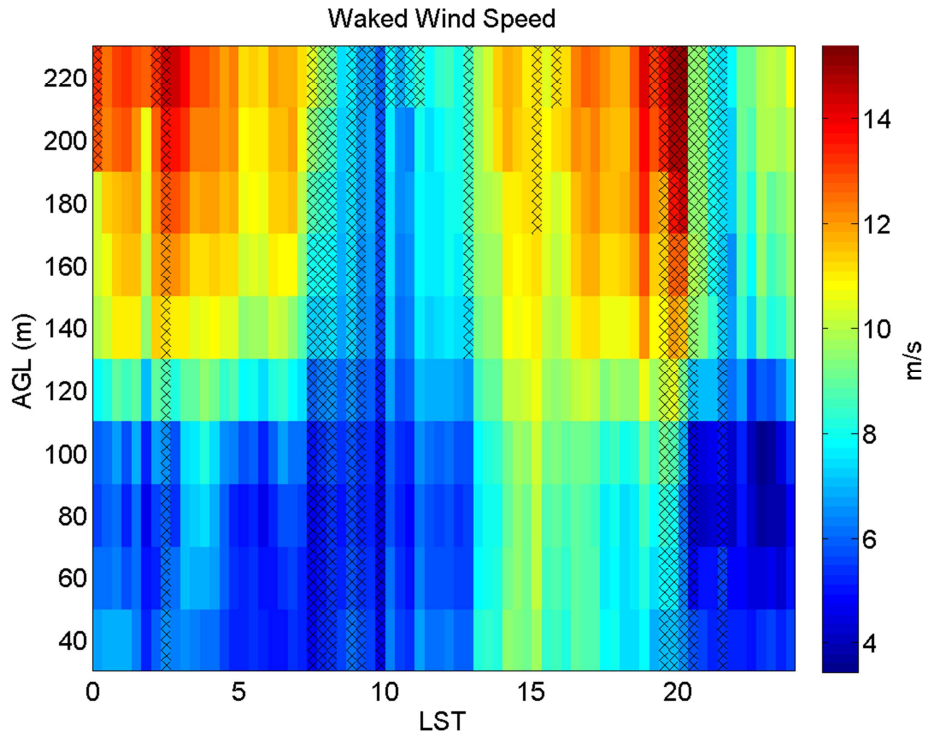

Figure 17: Canonical time-height contour plots of downwind horizontal wind speed

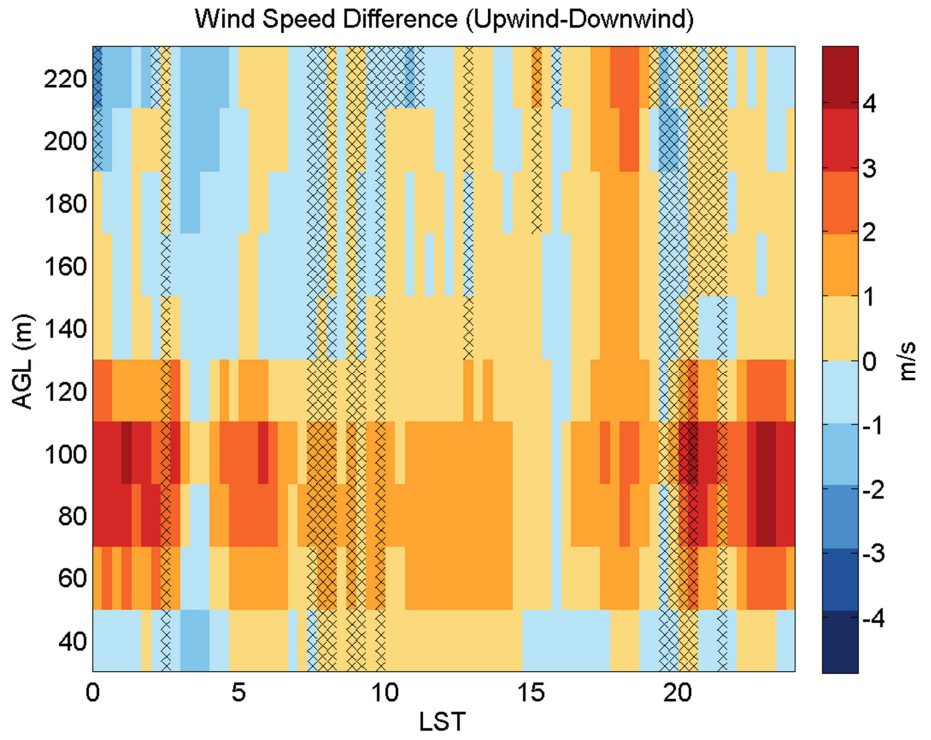

Figure 18: Canonical time-height contour plots of upwind - downwind horizontal wind speed differences

4.3 Wind Direction difference

The physical alignment of the two Windcube systems to true North was not the same for the duration of the CWEX11 deployment. To correct for this offset, wind direction data from multiple wind directions not experiencing turbine wakes and at heights above the wind turbine rotors were compared. An offset of 1.5° was found between the two Windcube systems; all subsequent analysis incorporates the direction offset so that there is no virtual offset between the two data streams.

LIDAR measurements of wind direction indicate veering (changing wind direction with height in an anti-cyclonic direction) with height throughout the full 24 hour period under both wake and non-wake conditions as would be expected in an atmospheric boundary layer. The majority of time and heights show upwind and downwind differences of five degrees or less; Windcubes are accurate to 1.5° for wind direction. Considering that other researchers have found that turbine wakes are not axisymmetric (Chamorro and Porté-Agel (2010)) , these subtle differences probably reflect that the averaging required for this canonical analysis has eroded any meaningful difference in wind direction.

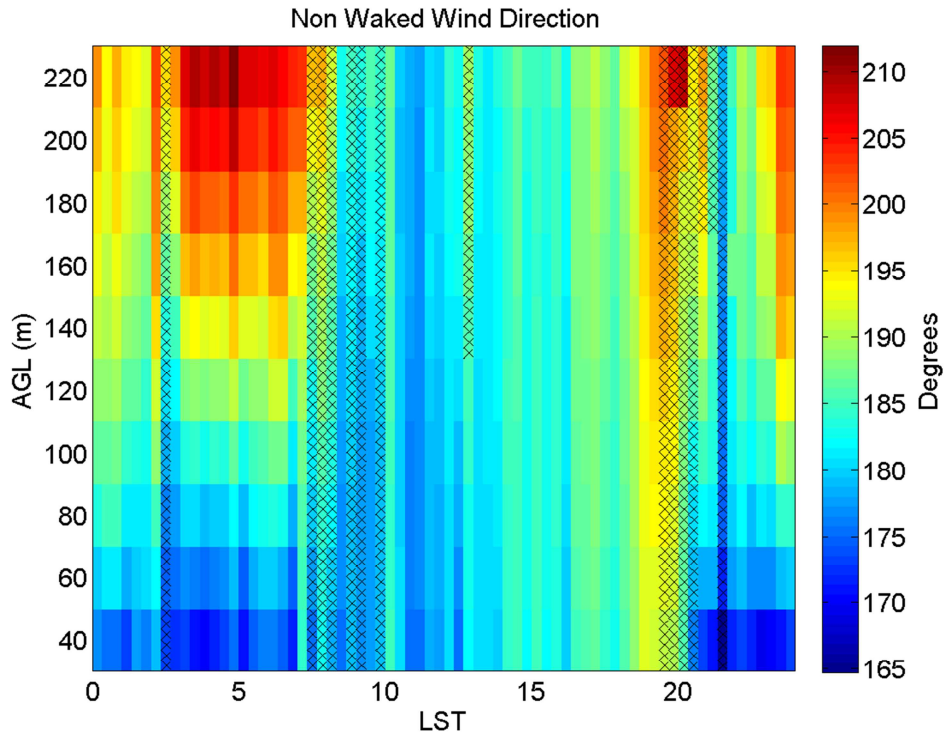

Figure 19: Canonical time-height contour plots of upwind wind direction

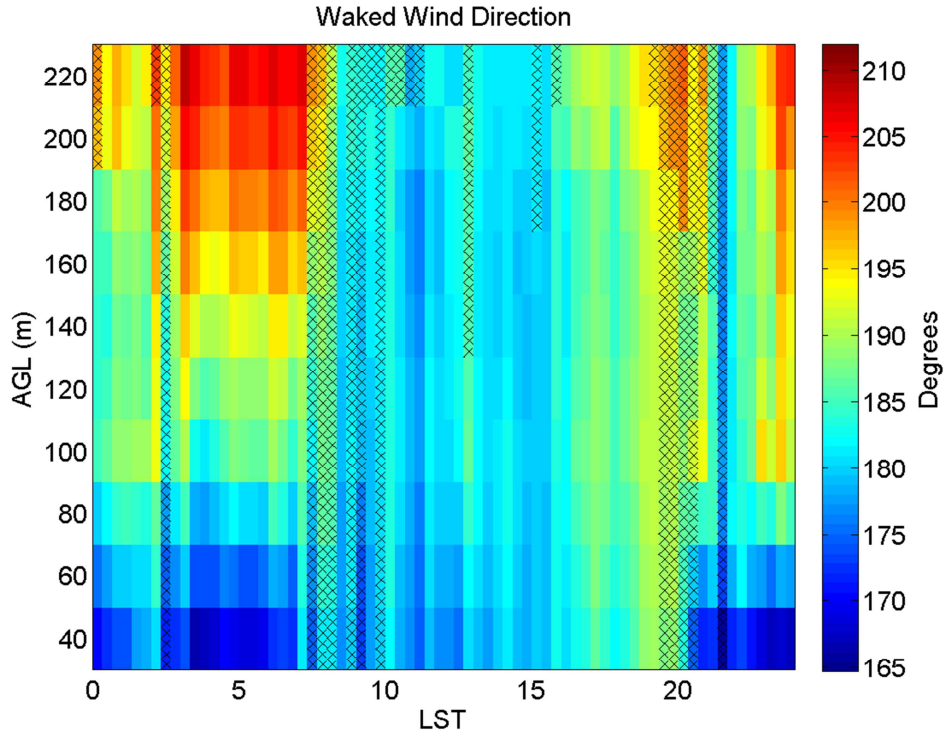

Figure 20: Canonical time-height contour plots of downwind wind direction

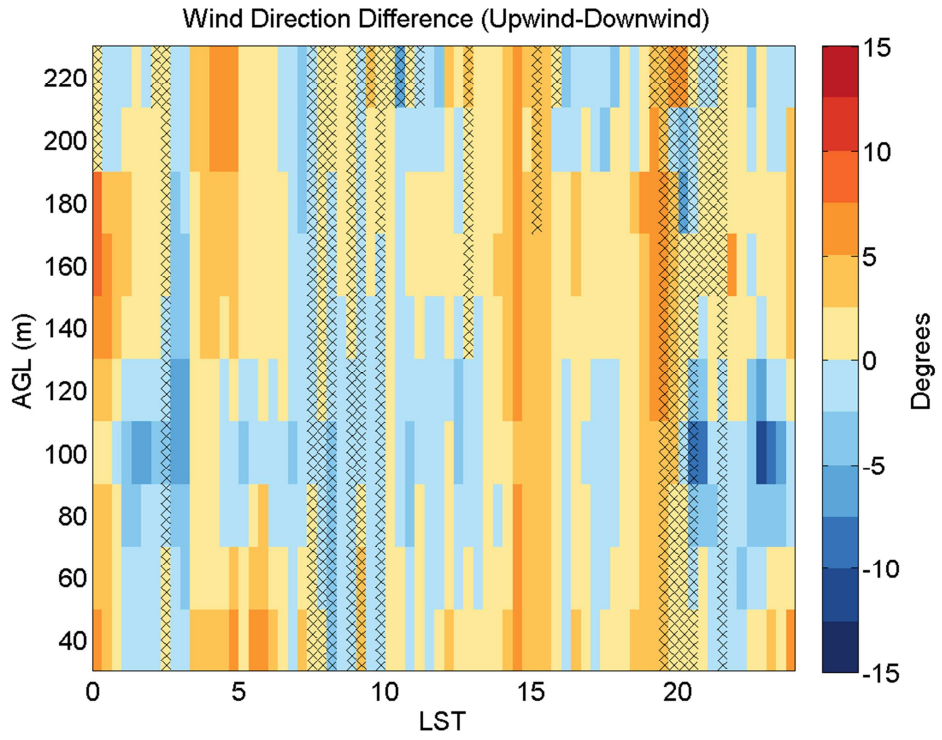

Figure 21: Canonical time-height contour plots of upwind - downwind wind direction differences

4.4 Wind speed shear

Wind speed shear is defined by the difference in wind speed at different heights. The definition of wind speed shear incorporates the change in component-wise values (u and v) with height (h) (Stull 1988).

$$\text{Wind Speed Shear} = \left[\left(\frac{u(h_{i+1}) - u(h_i)}{h_{i+1} - h_i}\right)^2 + \left(\frac{v(h_{i+1}) - v(h_i)}{h_{i+1} - h_i}\right)^2\right]^{0.5}$$

Wind shear measured upwind of the turbines shows a distinction between daytime and nighttime conditions (Figure 24). Upwind data (Figure 22) primarily have higher wind shear near the surface and during stable conditions. Conversely, daytime convective conditions inhibit the development of shear conditions. The same trends exist for the downwind (Figure 23) as seen in the upwind; however, differences (Figure 24) exist at and slightly above the rotor disc. From 100m up to 140m wind speeds increase with height consistently through the 24 hour period but especially so during the nighttime stable conditions. Heights from 60 m up to 100 m indicate diminishing wind speeds with greater height. Again more extreme shear values exist under

stable flow conditions. The turbine rotor induces a maximum wind shear at the 120 m during nocturnal stable conditions.

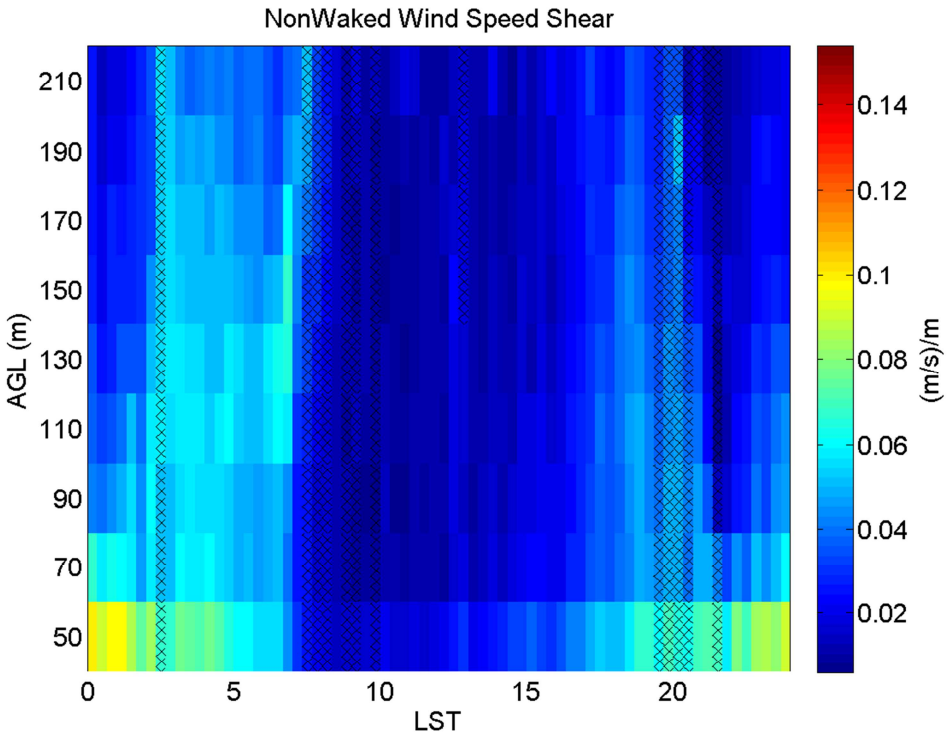

Figure 22: Canonical time-height contour plots of upwind horizontal wind shear

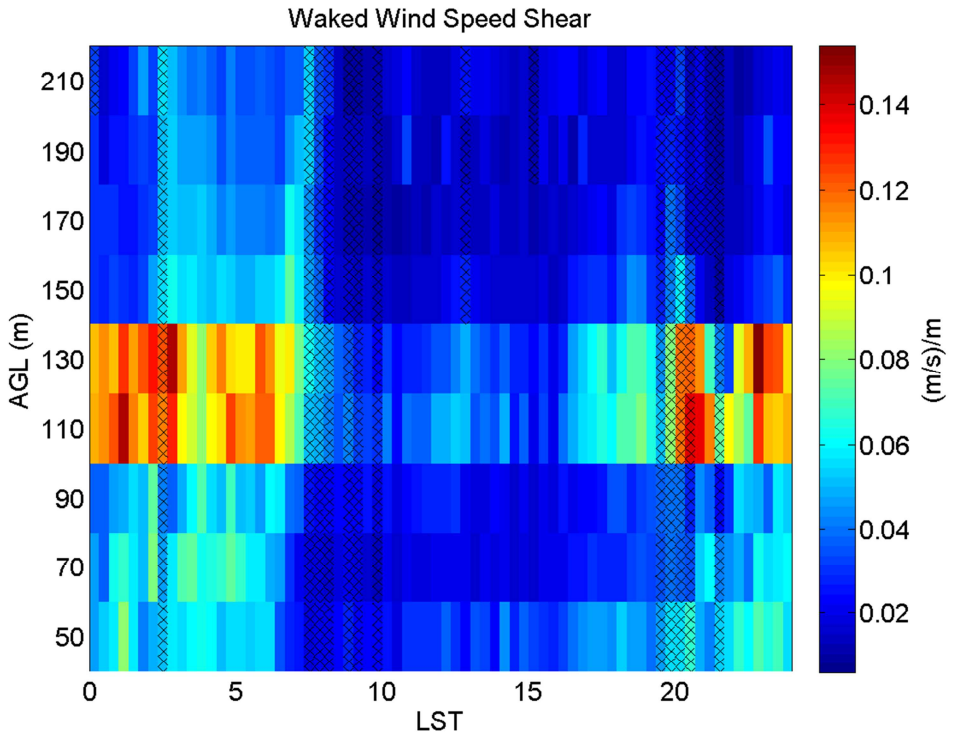

Figure 23: Canonical time-height contour plots of downwind horizontal wind shear

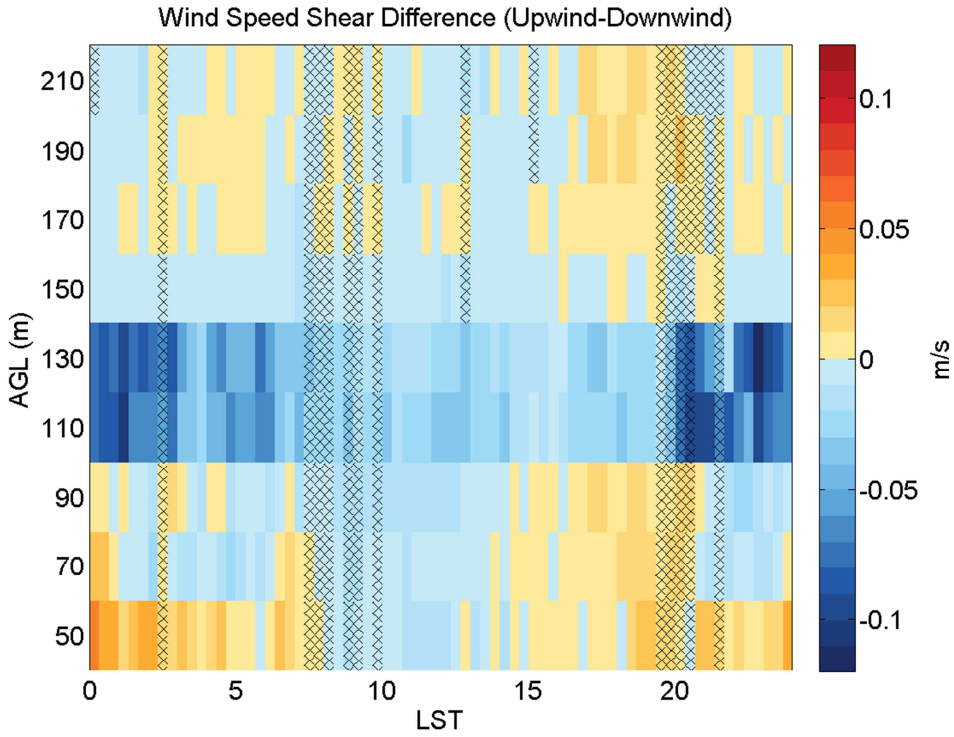

Figure 24: Canonical time-height contour plots of upwind - downwind horizontal wind shear differences

4.5 Power law coefficient, alpha

Alpha is the exponent required to satisfy the power law ($U_{i+1}/U_i = (z_{i+1}/z_i)^{\alpha}$). Alpha is commonly used in the wind energy industry not because it is an accurate portrayal of the true wind profile, but because it captures information about wind shear that is easily comparable between multiple geographic locations (Schwartz, Elliott 2006). Larger values of alpha indicate a steeper gradient of wind speed change per change in height. Upwind data (Figure 27) indicates strong wind shear from 40 – 60 m, but a rather uniform alpha value of zero exists for all other time and heights. Waked conditions show negative alpha values between 40 – 60 m when compared to the upwind data. The negative alpha values result from the velocity deficit created by the wind turbine that reverses the wind shear because the wind below the rotor disc now has a greater speed than the wind in the rotor disc region.

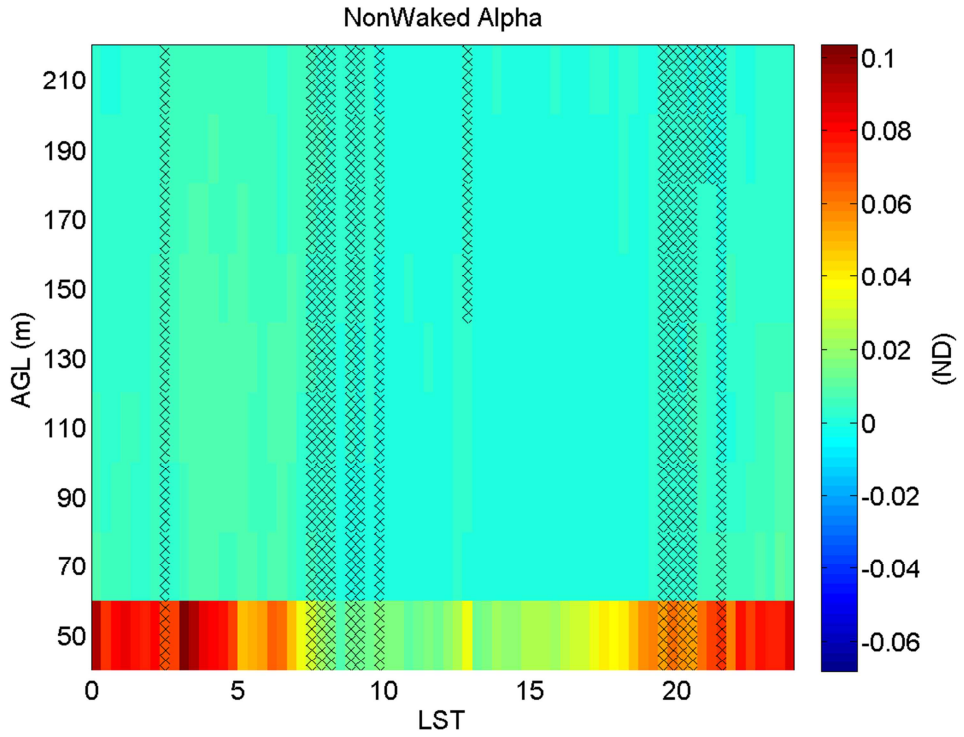

Figure 25: Canonical time-height contour plots of upwind alpha, the power law coefficient

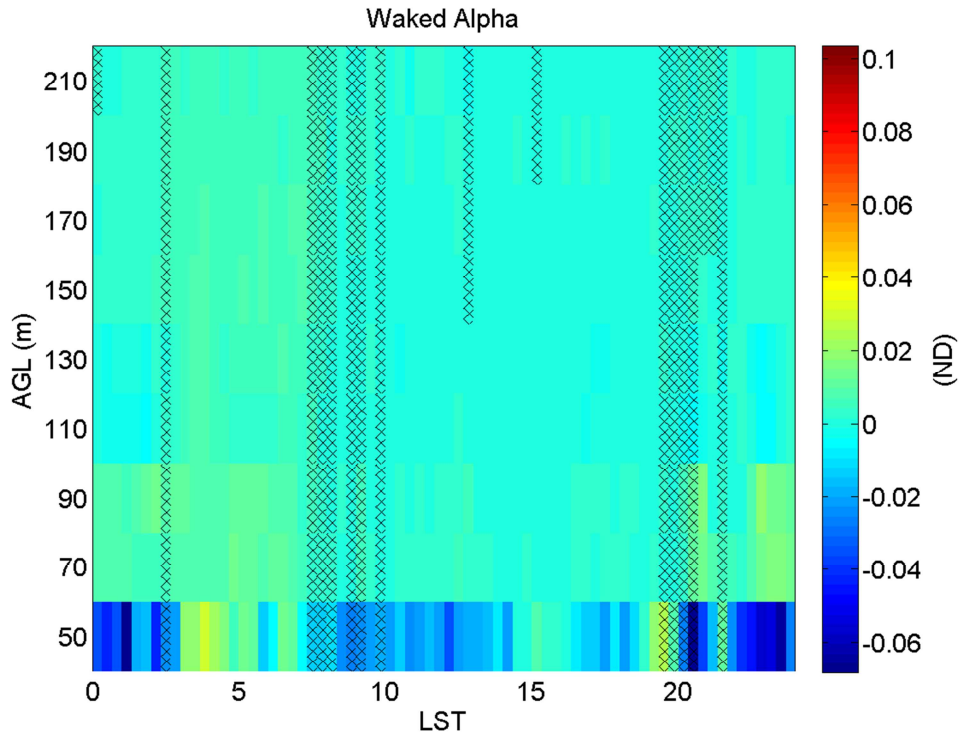

Figure 26: Canonical time-height contour plots of downwind alpha, the power law coefficient

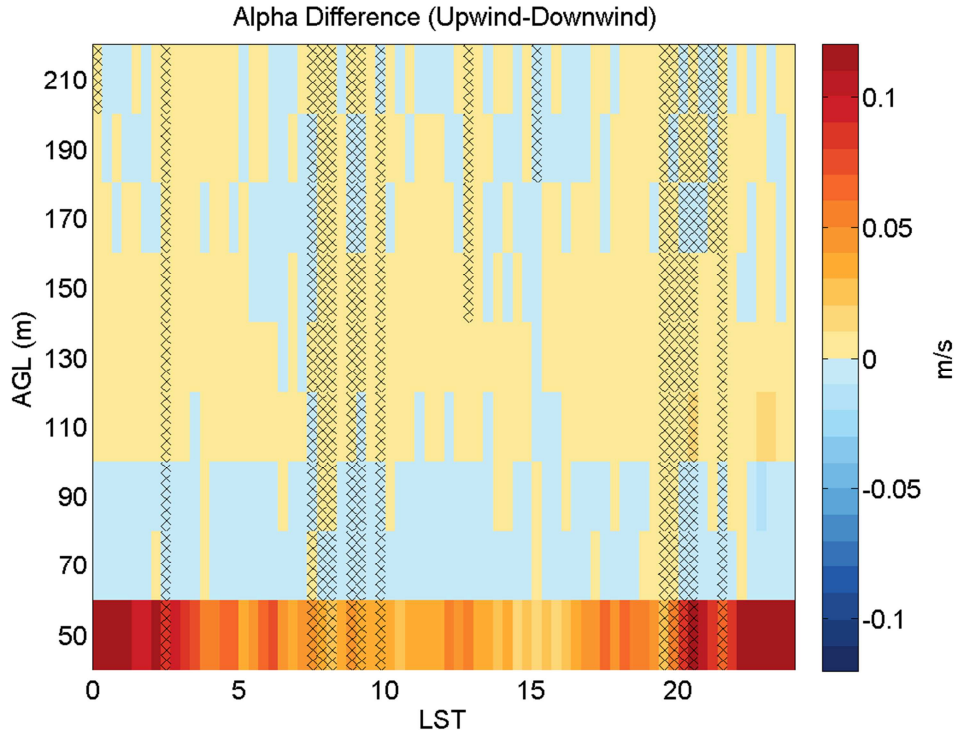

Figure 27: Canonical time-height contour plots upwind - downwind alpha differences

4.6 Vertical Velocity

Windcube measurements of upwind vertical wind speed show primarily slight subsidence through all heights and times as seen in Figure 28. One exception exists in the upper portion of the rotor disc region during the daytime convective heating. Downwind, however, data clearly shows the impact of a wind turbine on vertical wind velocities. Vertical winds show strong upward movement across the entire rotor disc through the full 24 hours. From the top of the rotor disc to 170m, waked conditions induce downward motion of air through the entire day with a larger and more persistent downward motion from 800 to 1400 LST that can extend up to 220m. The switch in direction of vertical wind speed creates a convergence zone along the top of the rotor disc and a divergence zone at the bottom of the rotor.

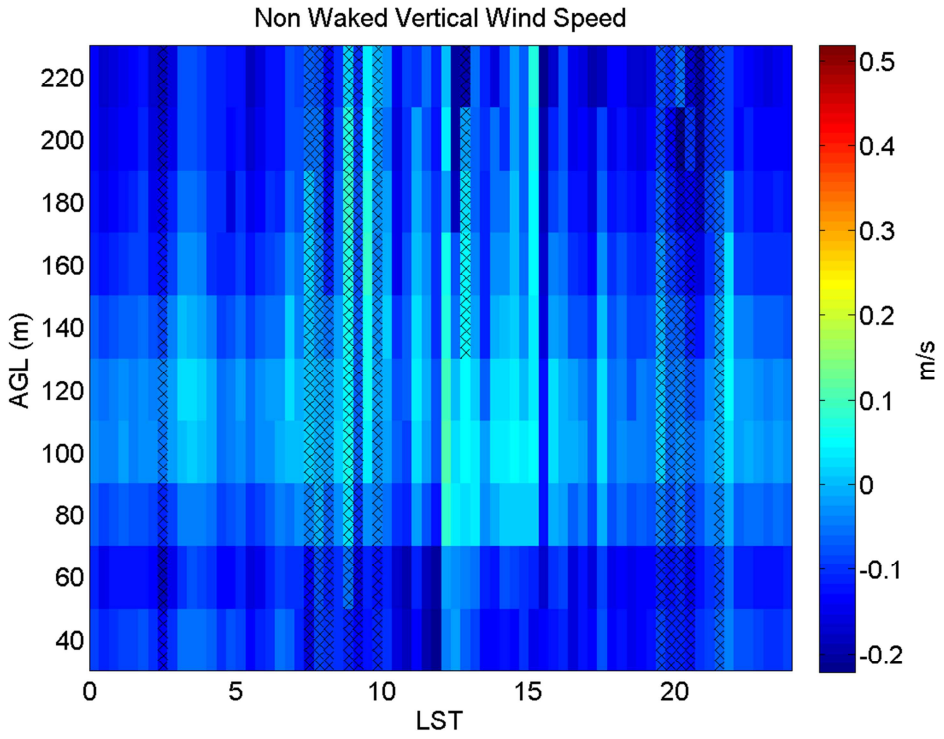

Figure 28: Canonical day time-height contour plots of upwind vertical wind velocities

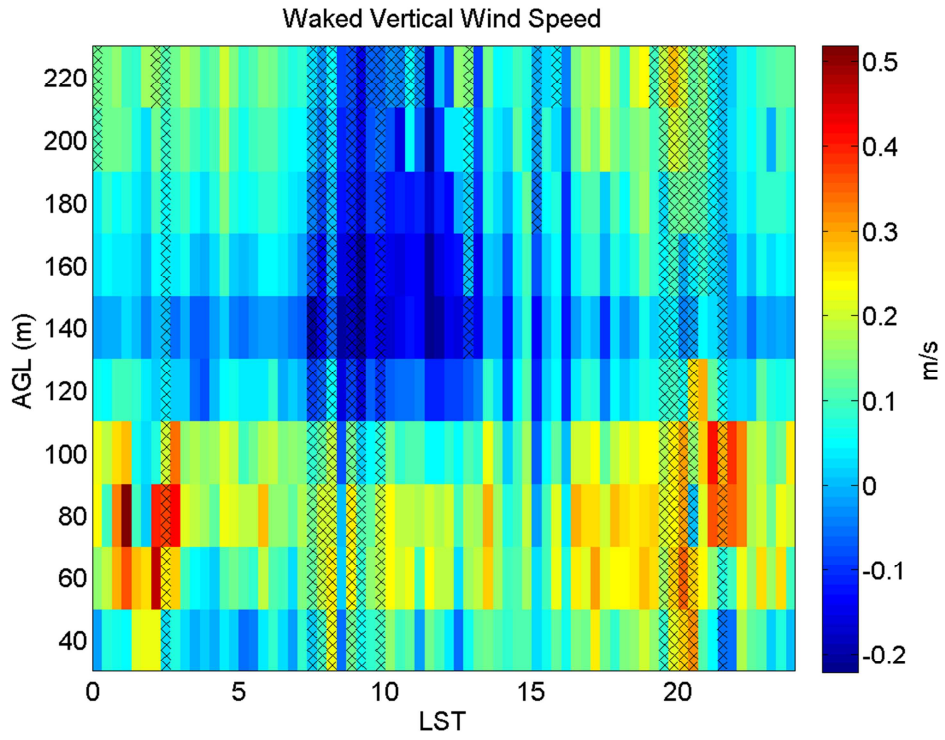

Figure 29: Canonical day time-height contour plots of downwind vertical wind velocities

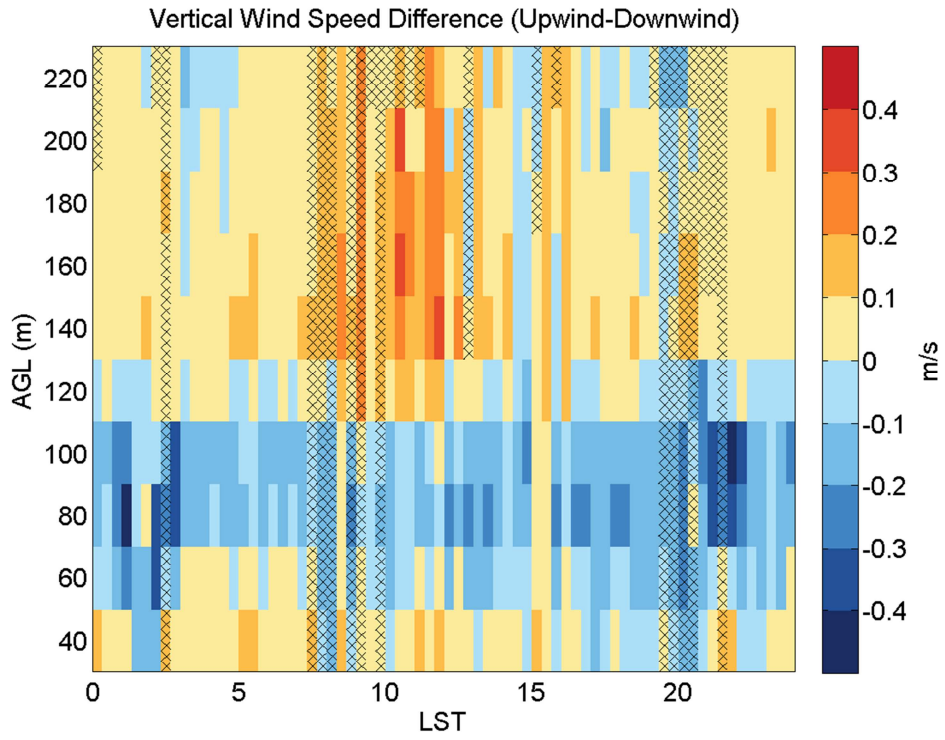

Figure 30: Canonical day time-height contour plots upwind - downwind vertical wind velocity differences

4.7 Horizontal Turbulence Intensity

Turbulence intensity, I, frequently used by the wind power industry includes only the variation of the horizontal wind speed instead of considering the individual horizontal components. Studies show that both mean wind speed and turbulence intensity play important roles in determining the power output of a wind turbine (Wharton and Lundquist 2011). As expected, both upwind and downwind flow (Figure 33) show increased I values at all heights during convective conditions. The diurnal cycle of the atmospheric boundary layer is characterized by turbulent convection during the day due to surface heating, and stable conditions at night. Typically, sunrise induces a rapid rise in turbulent values whereas sunset is characterized by a more gradual decline in turbulence (Stull 1988). The upwind Windcube has stronger turbulence intensity during the day as compared to at night, as expected. The same trend is captured for the waked flow, however the turbulence intensity increases for all times of the day in the rotor disc region as well. The strongest differences between upwind and downwind (Figure 33) exist at hub height (80 m) but the effect is seen across the whole rotor disc.

The time series of turbulence intensity (Figure 34) at individual heights illustrate the differences seen between upwind ('Non-wake') and downwind ('Wake') conditions. The 40m and 80m heights show a consistent increase in turbulence intensity of approximately 0.05 in the waked data over the non-waked values. Both the 120m and 160m levels, outside the rotor disc, have nearly identical turbulence intensity values throughout the entire 24 hour period. At all four levels, the largest difference between upwind and downwind I values exist in the 2 hours either side of midnight.

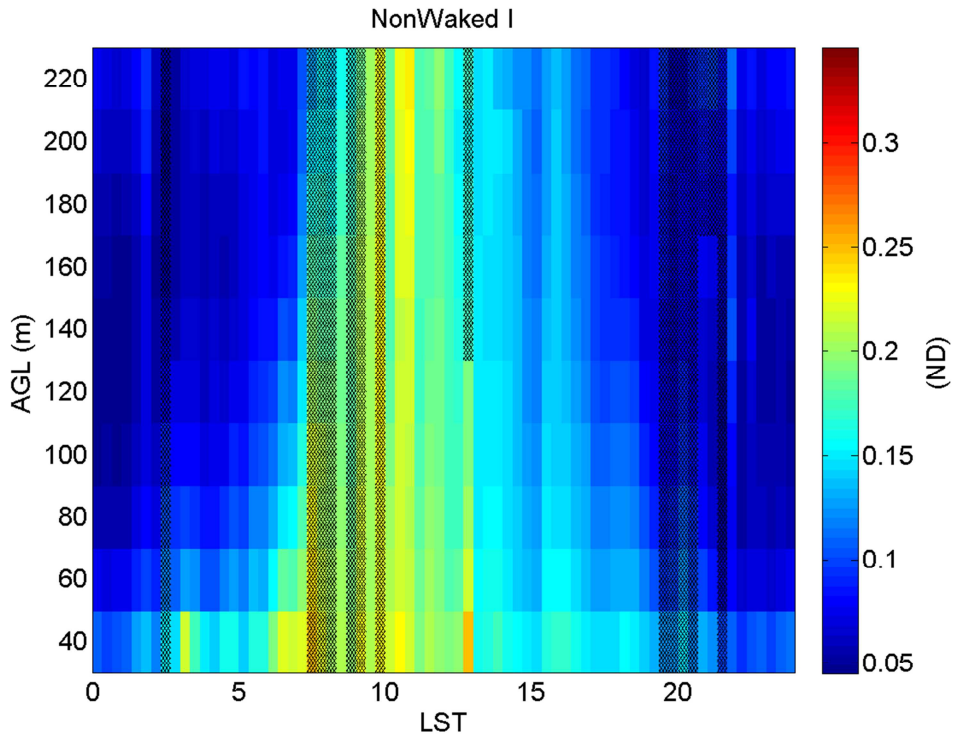

Figure 31: Canonical time-height contour plots of upwind turbulence intensity

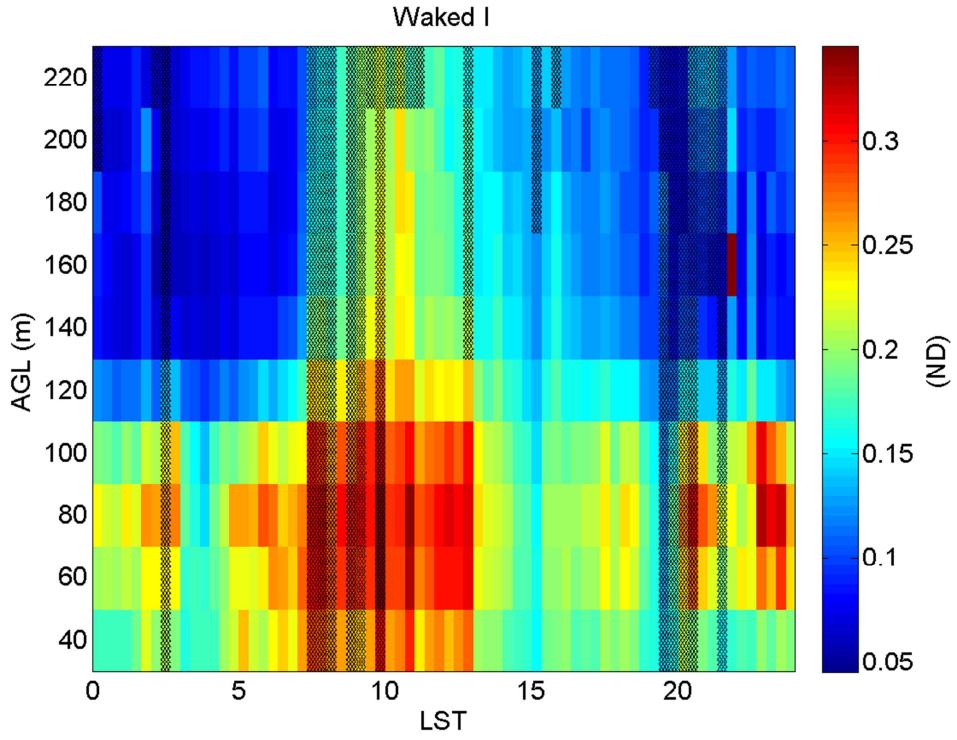

Figure 32: Canonical time-height contour plots of downwind turbulence intensity

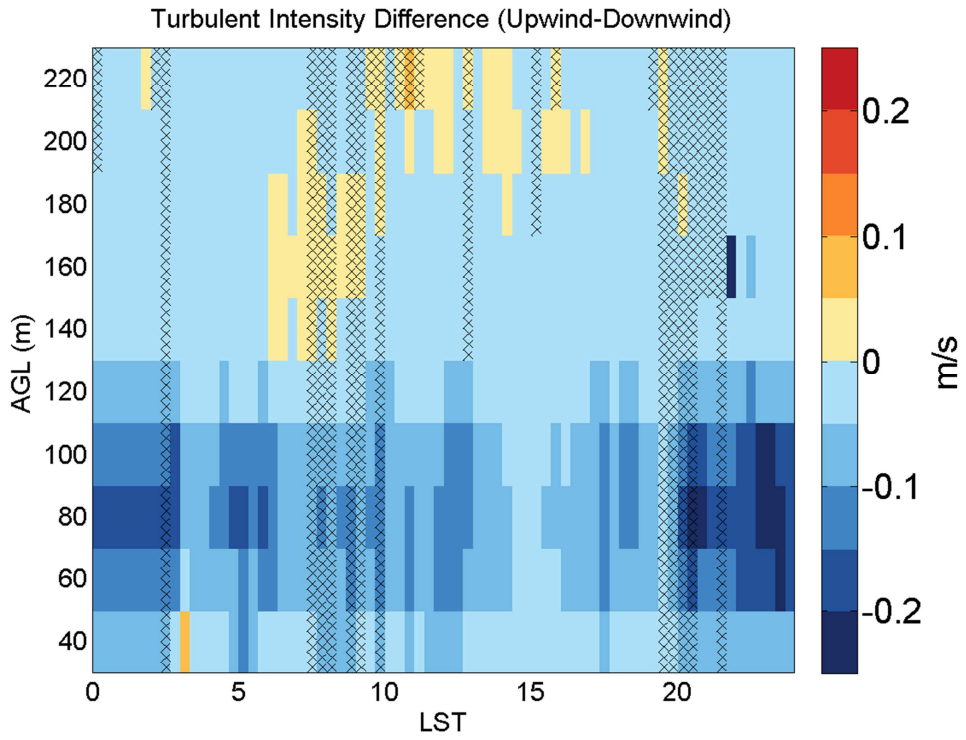

Figure 33: Canonical time-height contour plots of upwind – downwind turbulence intensity differences

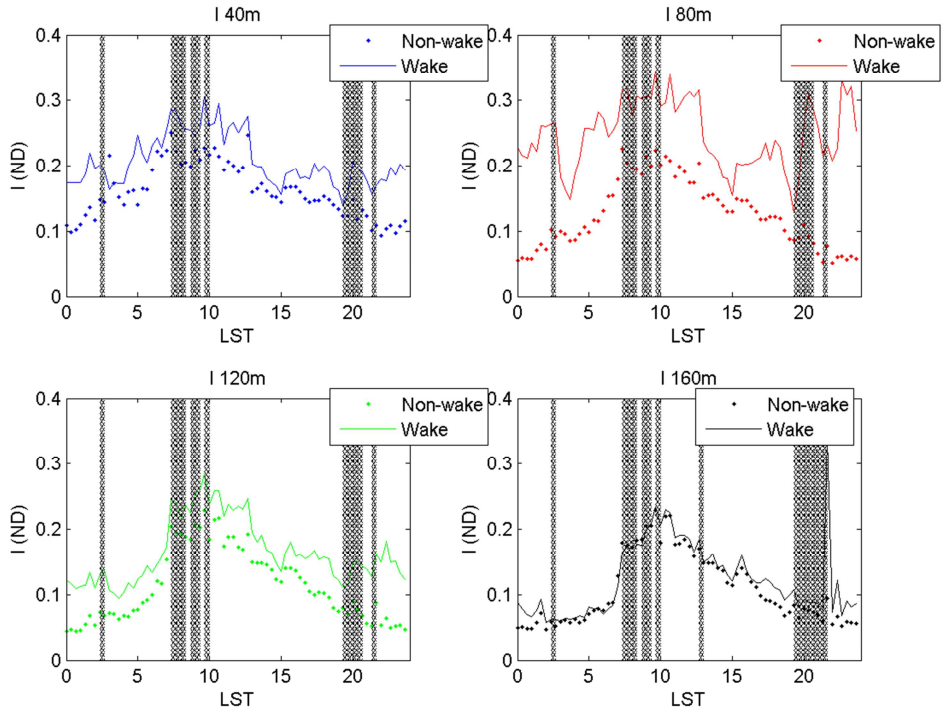

Figure 34: Time series plots of I at the bottom of the rotor disc, hub height, top of the rotor disc, and 40m above the rotor disc for waked and non-waked flow

4.8 Vertical turbulence intensity

Boundary layer wind speeds are often reduced during the day due to the interference of convection on the larger scale forcing. The same daytime turbulence is responsible for the increased variability of the vertical wind speed values, where σ_w^2 is the variance of vertical velocity and U is the mean horizontal wind speed.

$$I_w = \frac{\sigma_w^2}{U}$$

Vertical turbulence intensity is rarely measured or used in the wind energy industry, but the advent of remote sensing instruments that can routinely measure vertical variances will likely change this trend since research shows the effect of vertical turbulence intensity on wind turbine power production (Wharton and Lundquist 2011). Similar to horizontal turbulence intensity, vertical turbulence intensity has increased values through the convective portion of the day due to both the reduced horizontal wind speed and increased vertical wind speed variance. The difference in vertical turbulence intensity (Figure 37) between upwind and downwind is similar in structure for horizontal turbulence intensity, but all times and heights show greater values in the downwind flow when compared to the upwind conditions.

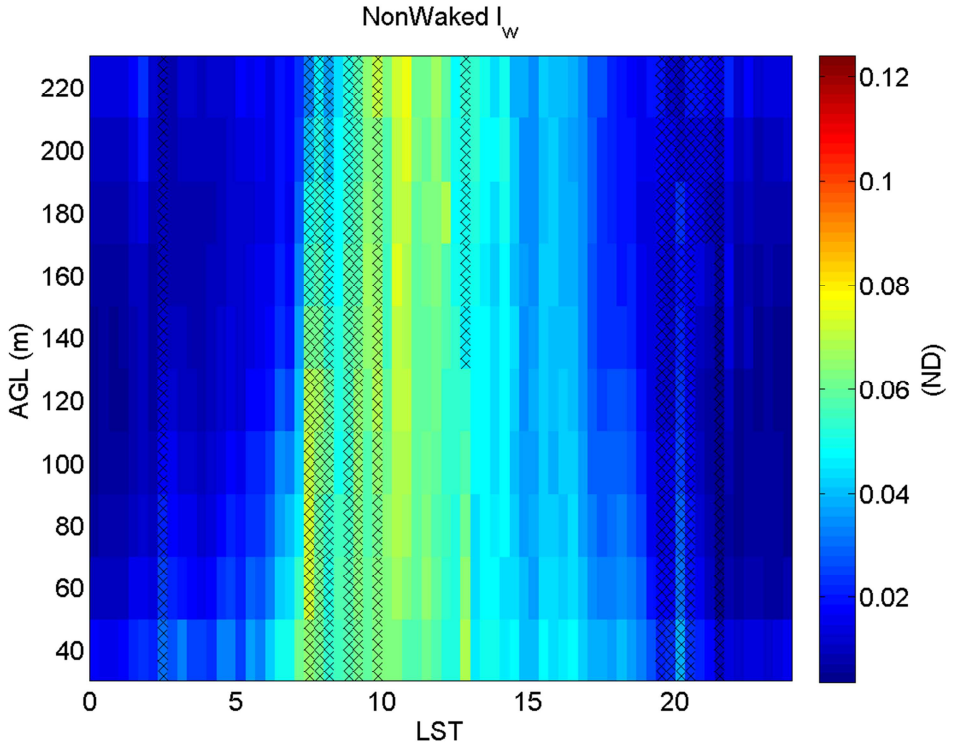

Figure 35: Canonical time-height contour plots of upwind vertical turbulence intensity

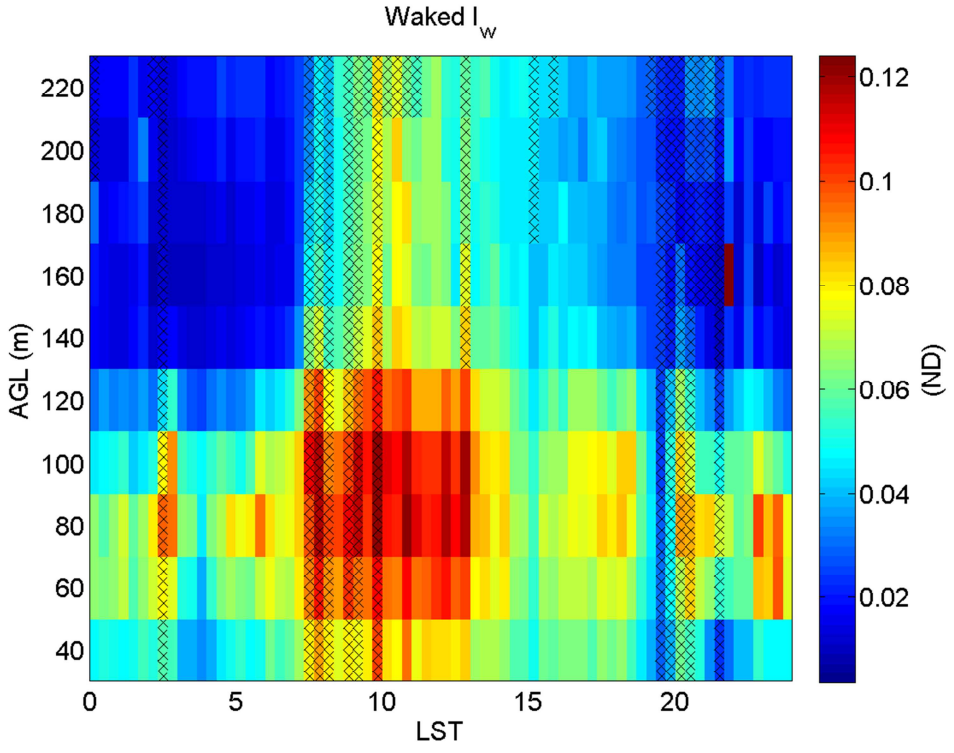

Figure 36: Canonical time-height contour plots of downwind vertical turbulence intensity

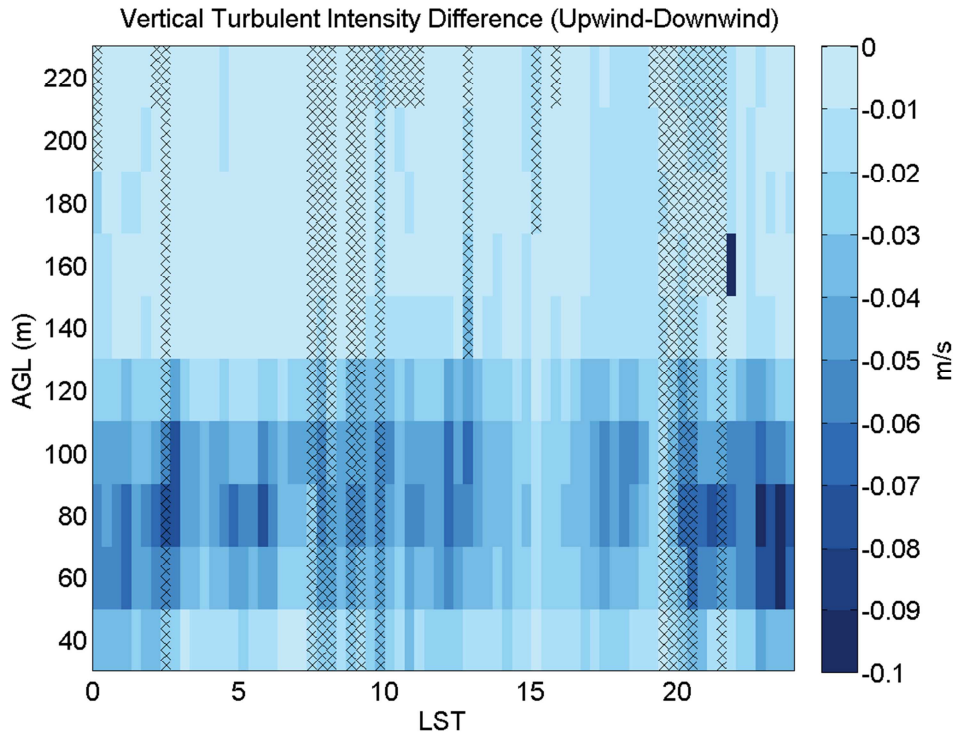

Figure 37: Canonical time-height contour plots of upwind - downwind vertical turbulence intensity differences

4.9 Turbulence Kinetic Energy

A final measure of turbulence is turbulent kinetic energy (TKE). TKE incorporates both horizontal and the vertical component in to its definition (Stull 1988).

$$TKE = \frac{\sigma_u^2 + \sigma_v^2 + \sigma_w^2}{2}$$

Upwind flow in Figure 38 indicates higher levels of TKE under daytime convective conditions; furthermore, TKE increases with height during daytime convection as well. Nighttime TKE remains low at all heights when conditions are stable. Downwind flow shows a strong increase of TKE in the rotor region during the day and more subtle increases during the night and aloft. While Sathe et al. (2011) question the ability of a LIDAR system to measure TKE, the difference plot reveals useful information about the influence of a wind turbine on atmospheric turbulence.

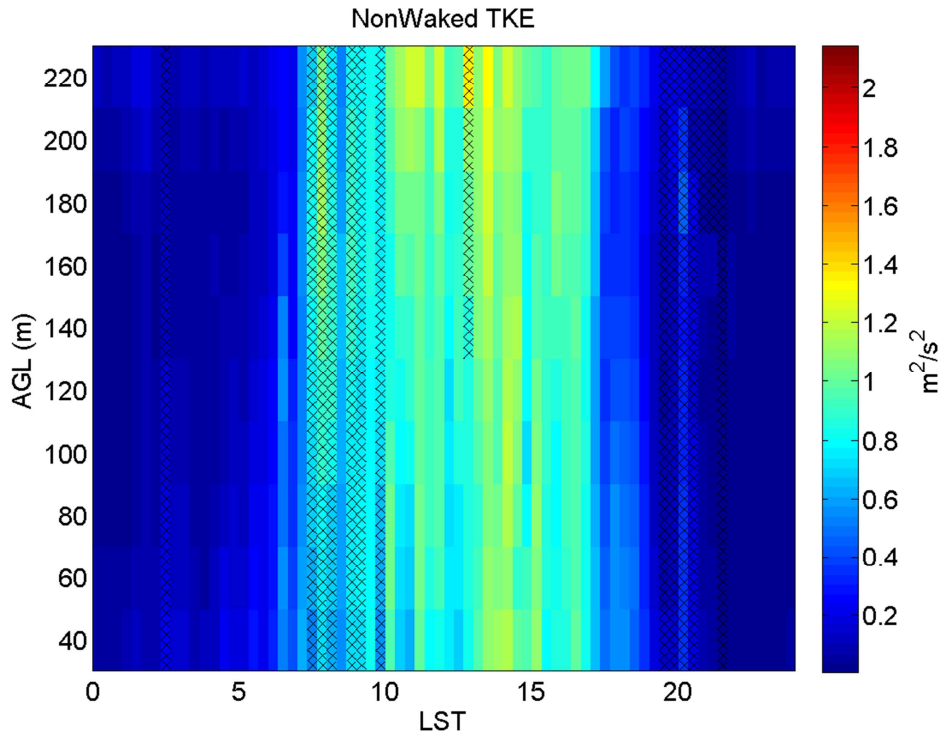

Figure 38: Canonical time-height contour plots of upwind turbulent kinetic energy

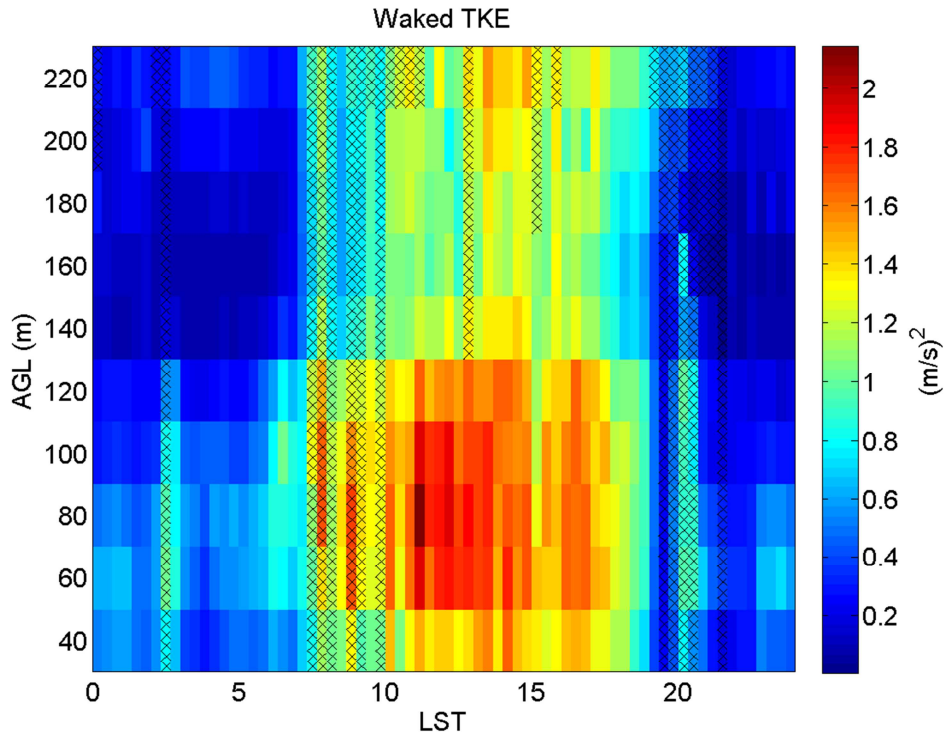

Figure 39: Canonical time-height contour plots of downwind turbulent kinetic energy

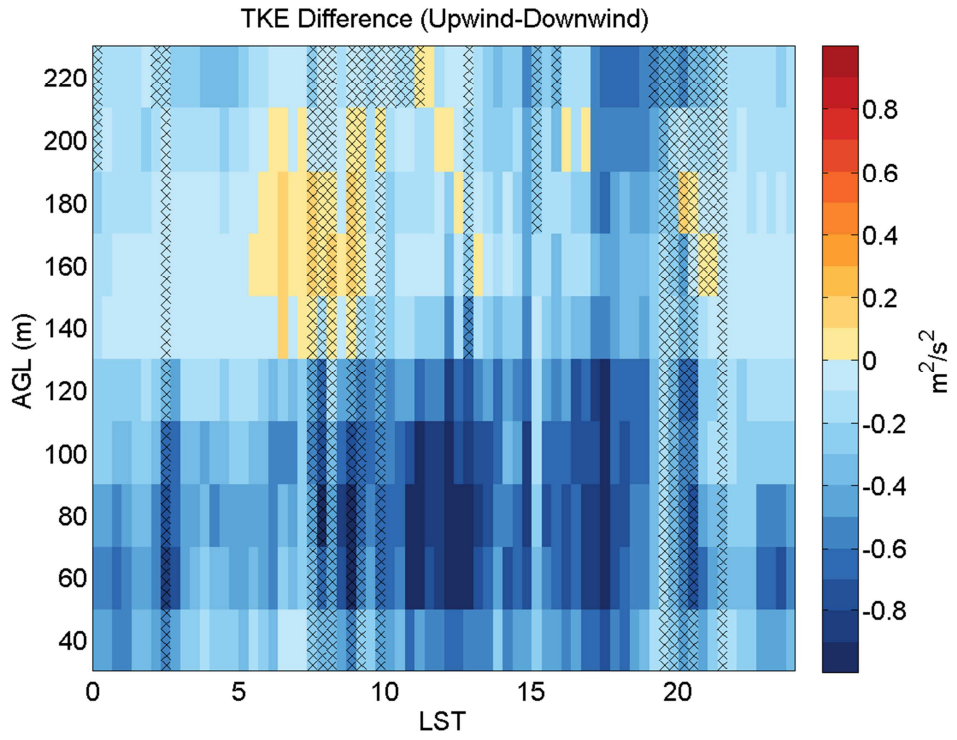

Figure 40: Canonical time-height contour plots of upwind - downwind turbulent kinetic energy differences

4.10 Summary of upper-air wake impacts as seen through the "canonical day" analysis.

Nearly all comparisons between the canonical upwind and downwind cases show that the primary differences between the two locations exist in the rotor disc region that extends from 40m from 120m. Additionally, the difference plots reveal that the effects of the turbine on the downwind flow differ based on time of day and convective or stable conditions (Chamorro and Porté-Agel 2010). Some of these wake characteristics that extend over the span of the rotor disc include decreases in horizontal wind speed, increases in vertical velocity, increases in both horizontal and vertical turbulence intensity, and increase in turbulent kinetic energy. Additionally, effects of the rotor disc are present for wind speed shear, directional wind shear, and the alpha parameter, though not all these effects are present across the entire rotor disc.

5 Case Studies

To ensure that the canonical day analysis is representative of shorter time scales, we examine two case studies with consistent wind speeds and wind directions that fit the wake definition applied in section 3.2. The first case study occurs through the night, which is representative of stable boundary layer conditions. The second case study begins in the mid afternoon and concludes immediately after evening twilight. Surface heating during the day creates a well-mixed and uniform atmospheric boundary layer that prevents wind turbines wakes from dominating atmospheric conditions downwind when compared with stable conditions, when there are larger wind turbine impacts on the surface than daytime convective cases (Kelley et al. 2004; Baidya Roy 2011).

5.1 Case Study 1: Stable Nighttime

The nocturnal case study began around 21:00 local time on July 16, 2011 and concluded at 07:00 on July 17, 2011. Weather conditions during the event consisted of southerly flow at wind turbine hub height with wind direction variations from 170° to 195° as seen in Figure 41. Average hub height wind speeds were about 9m/s and decreased throughout the night to 7m/s with some variation. Synoptically, Iowa was situated between a blocking high to the east and a weak low pressure to the northwest that resulted in the light southerly winds in Iowa observed at hub height.

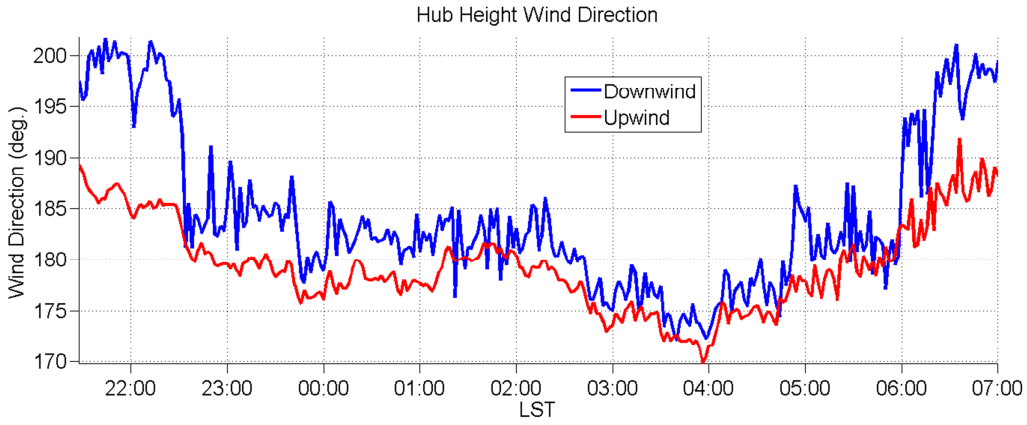

Figure 41: Upwind and downwind hub height wind directions for the stable condition case study

5.1.1 Wind Speed

The wind speed deficit during the nighttime case study (Figure 44) shows the effect of the wind turbine on horizontal wind speed. From 22:30 until 02:30 the maximum wind speed deficit is strongest at 100m, not at hub height, but rather in the top half of the rotor disk. Wake deficit exists between 40m and 140m. The reduced wind speeds above the rotor at 140m, is evidence of a vertically expanding turbine wake, extending beyond the top of the rotor disk at 120m. Beginning at 03:00 and concluding near 05:00, the wind direction shifted from southerly flow to more South-Southeasterly flow. With this change in flow direction, the downwind wind speed deficit was reduced, though still present. The result in the wind direction shift is that the Windcube LIDAR begins to detect the edge of the wake or even a region of the atmosphere unaffected by the wind turbine, thus there is a reduction in the wind speed deficit at and below hub height.

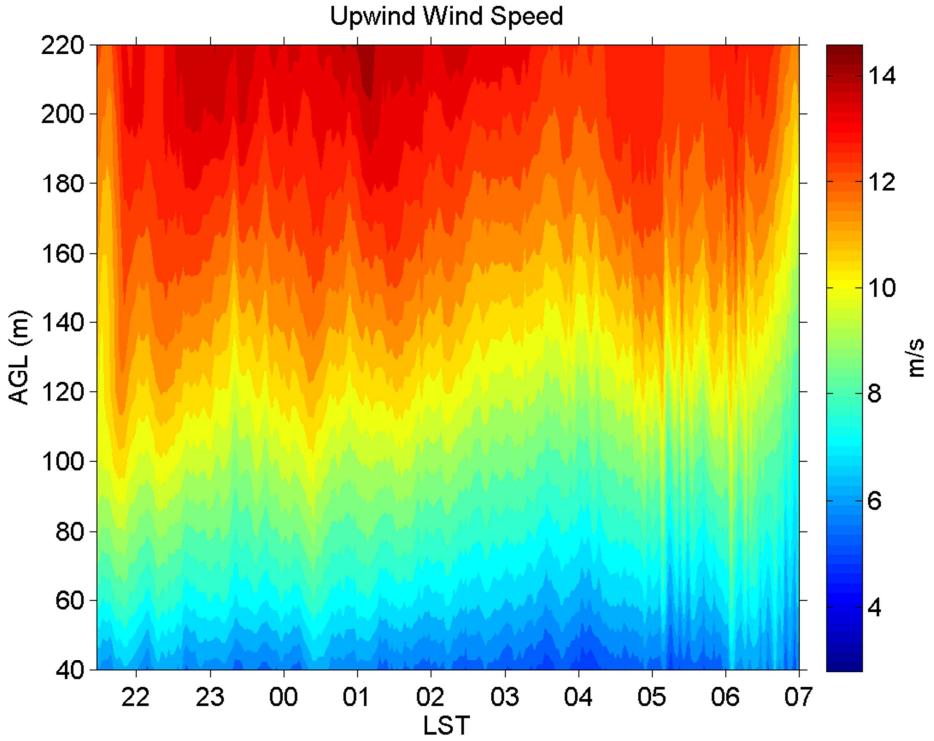

Figure 42: Time-height contours of upwind horizontal wind speed

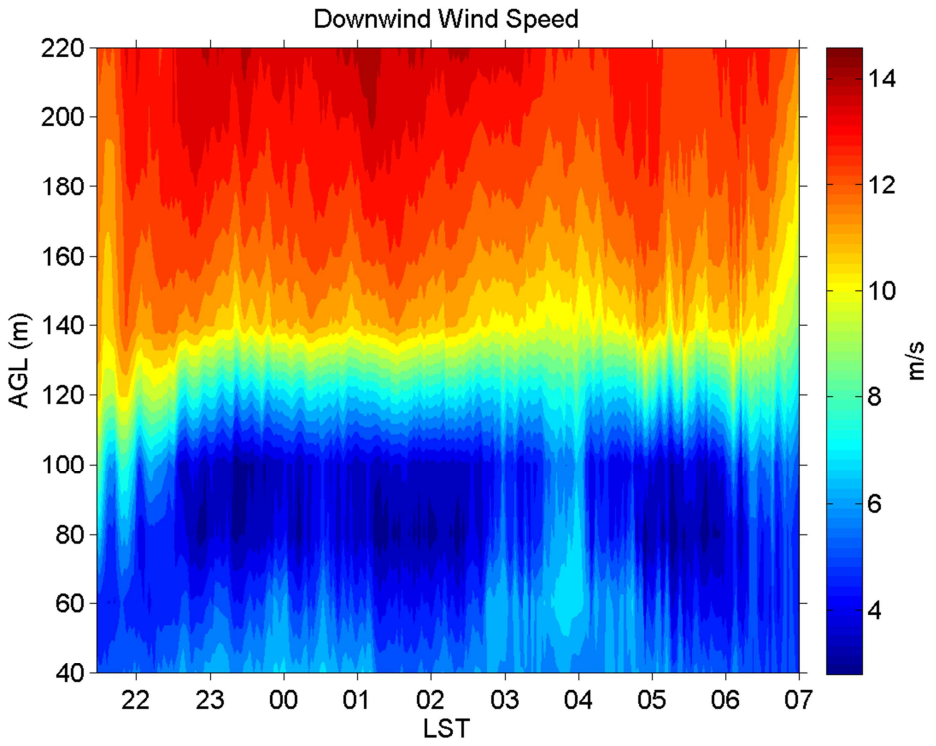

Figure 43: Time-height contours of downwind horizontal wind speed

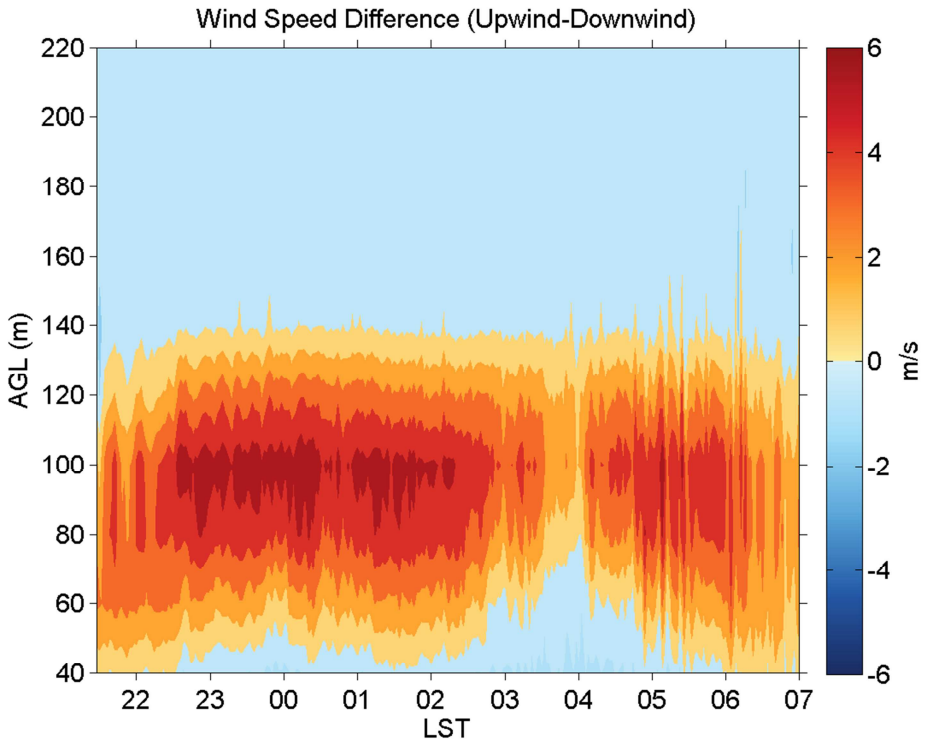

Figure 44: Time-height contours of upwind - downwind horizontal wind speed differences

5.1.2 Vertical Wind Speed

The wind turbine wake also impacts vertical velocities during the stable nocturnal case. To understand the vertical winds detected by the LIDAR, we must carefully consider the upwind wind direction as we expect to see vertical winds of differing signs on opposite sides of the wind turbine wake because half the wake has upward motion while half the wake has downward motion (Chamorro and Porté-Agel 2010). Upwind directions between 185° and 190° (21:30-22:30) show downward motion of approximately 0.2m/s at and below hub height; conversely, speeds of 0.8m/s upward are reached in the top half of the rotor disc (Figure 47). Wind directions between 175° and 185° (22:30-02:45 and 04:45-6:15) tend to show upward motions across the entire rotor disc reaching speeds of 0.8m/s at hub height and smaller magnitude further away from hub height in either direction. The shift in wind direction, to values less than 175° (02:45-04:45), show consistent downward motion across much of the rotor. Based on our analysis of wake properties, the Windcube is very likely not sampling wake flow for this wind direction, but flow outside of the wake could still be affected by the presence of the wake.

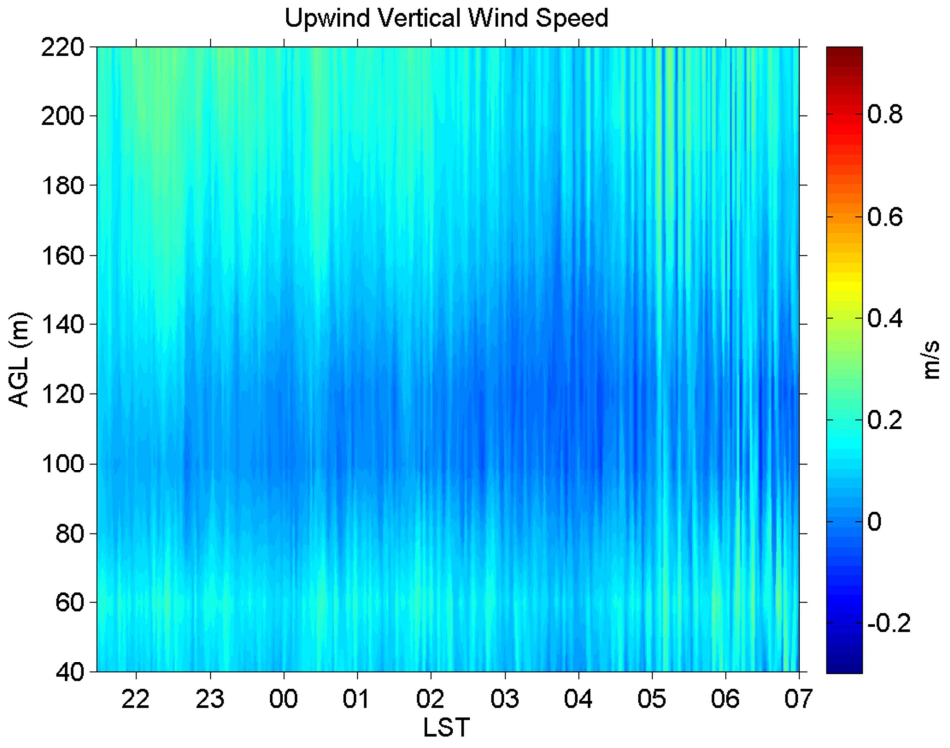

Figure 45: Time-height contours of upwind vertical wind speed

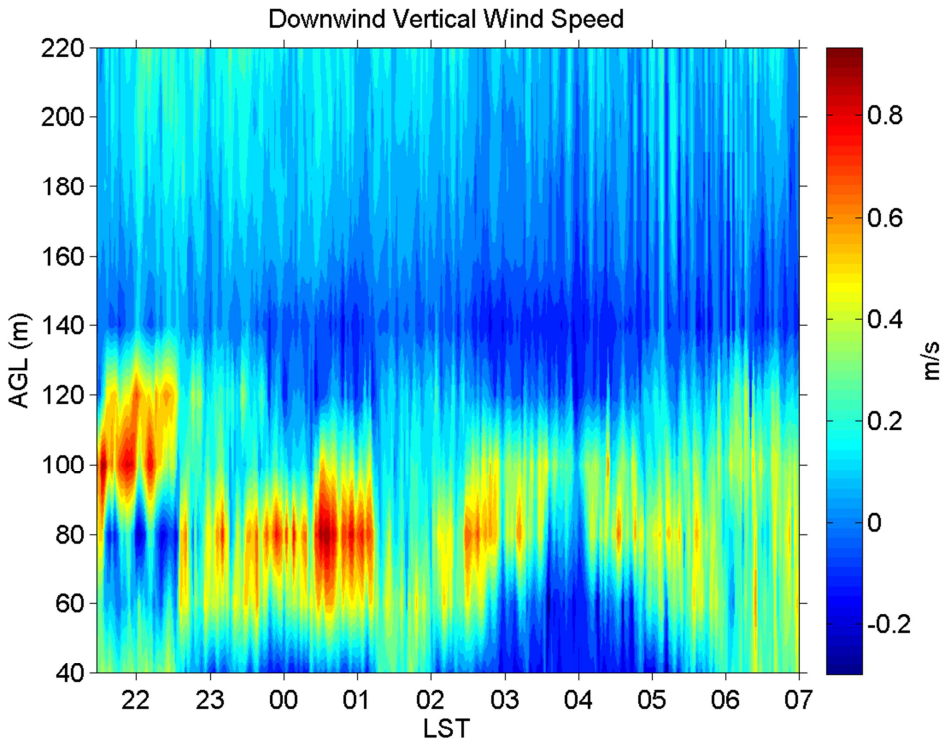

Figure 46: Time-height contours of downwind vertical wind speed

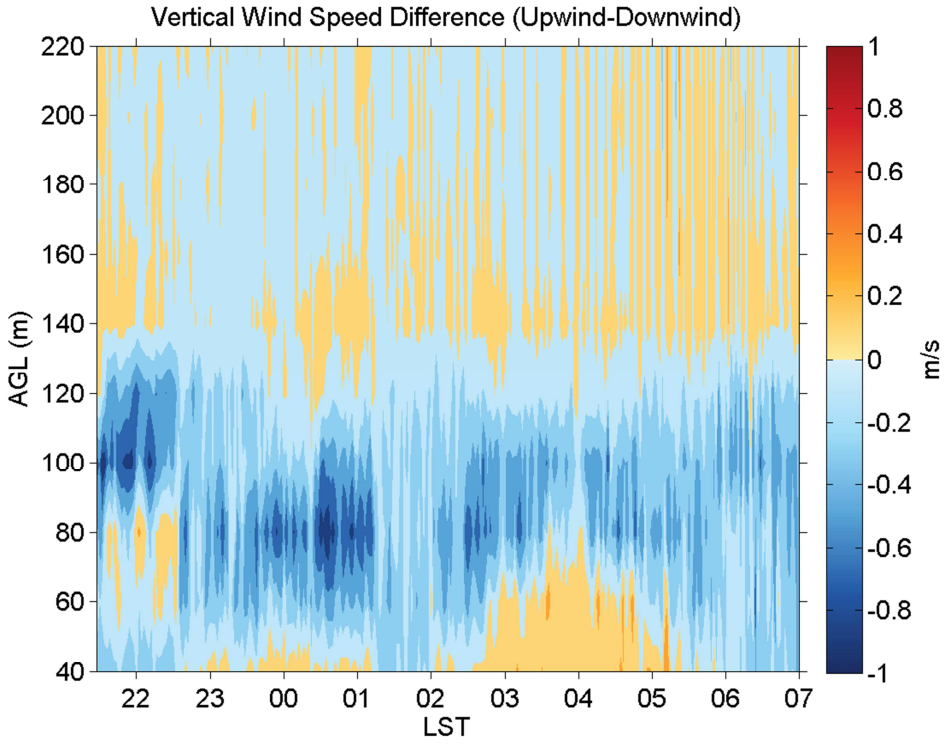

Figure 47: Time-height contours of upwind - downwind vertical wind speed differences

5.1.3 Turbulence Kinetic Energy

At nearly all times during the night, upwind TKE is limited to values less than 0.5 m^2/s^2 for all heights; TKE only begins to increase in magnitude near sunrise at 06:00 (Figure 50). TKE downwind of the turbine has a range approximately five times larger than as seen upwind; these elevated levels persist throughout the night. The large increase of TKE beginning shortly after 06:00 is due to development of daytime convective conditions. For this time period, the larger values of TKE are primarily below 100m and in the rotor disc region. When the wind direction shifted to the southeast at (02:45-04:45), the height of stronger TKE increased to around 120m, which is consistent with wind tunnel observations (Chamorro and Porté-Agel 2010).

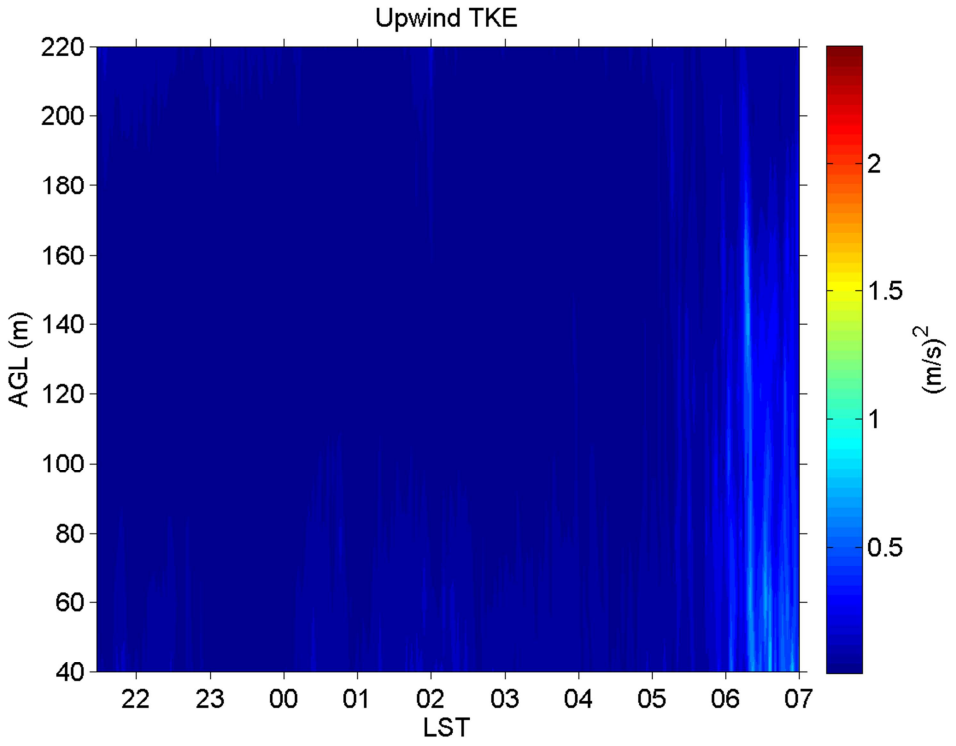

Figure 48: Time-height contours of upwind TKE

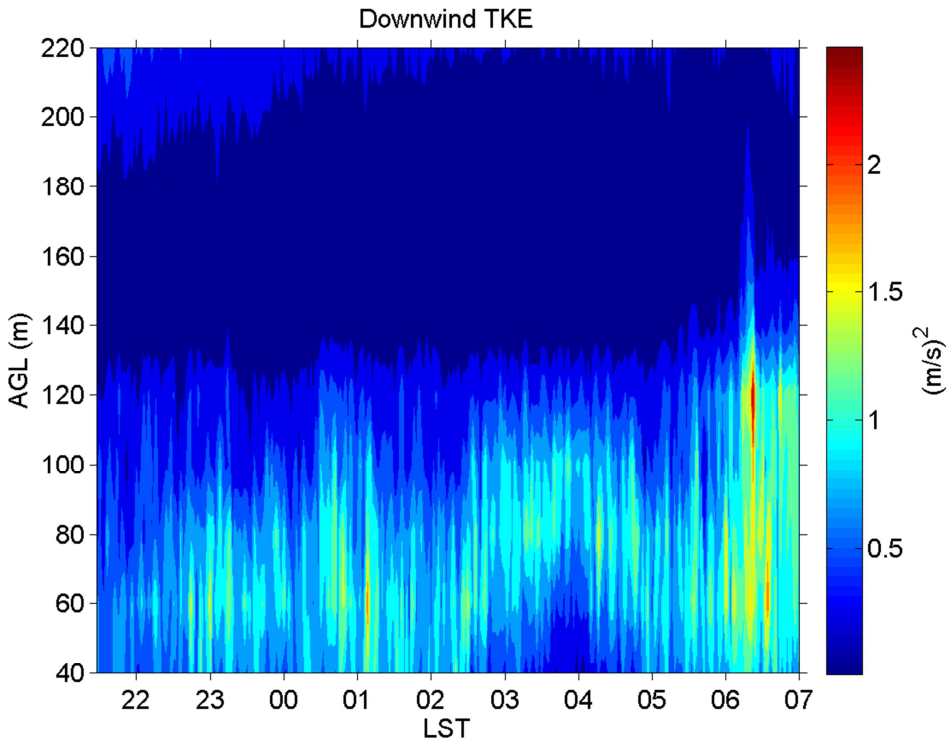

Figure 49: Time-height contours of downwind TKE

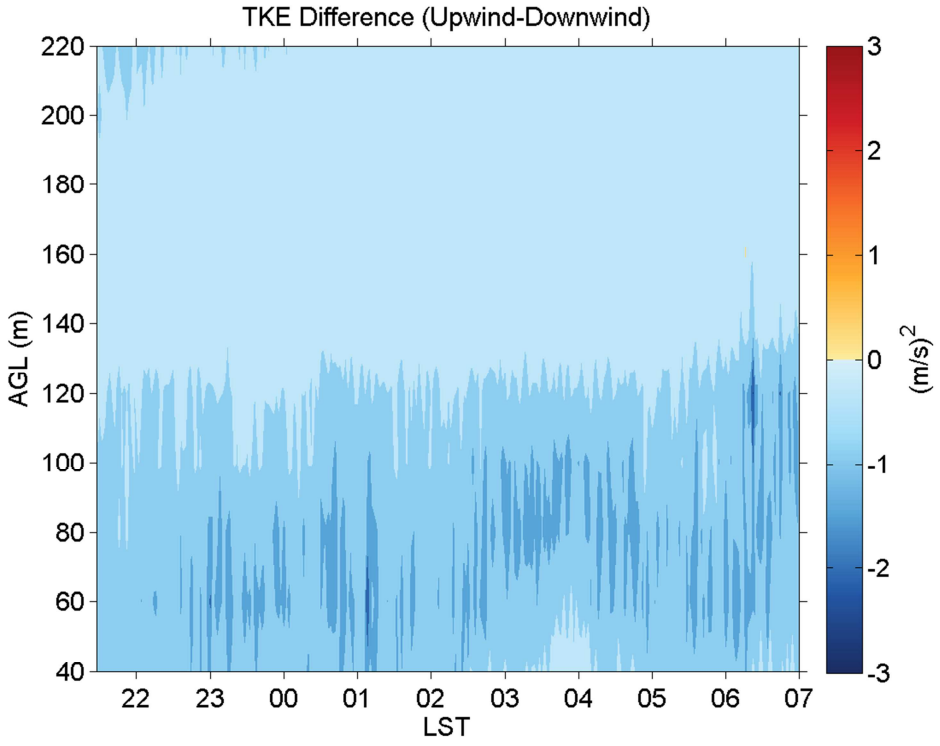

Figure 50: Time-height contours of upwind - downwind TKE differences

5.1.4 Turbulence Intensity

Much like TKE, turbulence intensity values increase in the lee of a wind turbine rotor due to increased turbulent flow in the wake. The upwind turbulence intensities (Figure 53) are small at all heights throughout the night and only begin to increase at sunrise. However, the downwind turbulence intensity in the rotor disc region remains large throughout the night. We can see that for wind directions between 185° and 190° (21:30-22:30), turbulence intensity increases in the lower half of the rotor disc between 40m and 80m. Then from 22:30 until 03:00 with winds from 170° to 175°, the largest values of turbulence intensity exist at the 80m level with high values throughout the entire rotor. Observations during the wind shift at (02:45-04:45) to 175° still show increased turbulence intensity, though the magnitude is smaller than when the flow was more southerly. After sunrise we see evidence of a further deepening of the turbulent layer in both the upwind and downwind data sets, though the largest values of turbulence intensity downwind are still in the rotor disc area.

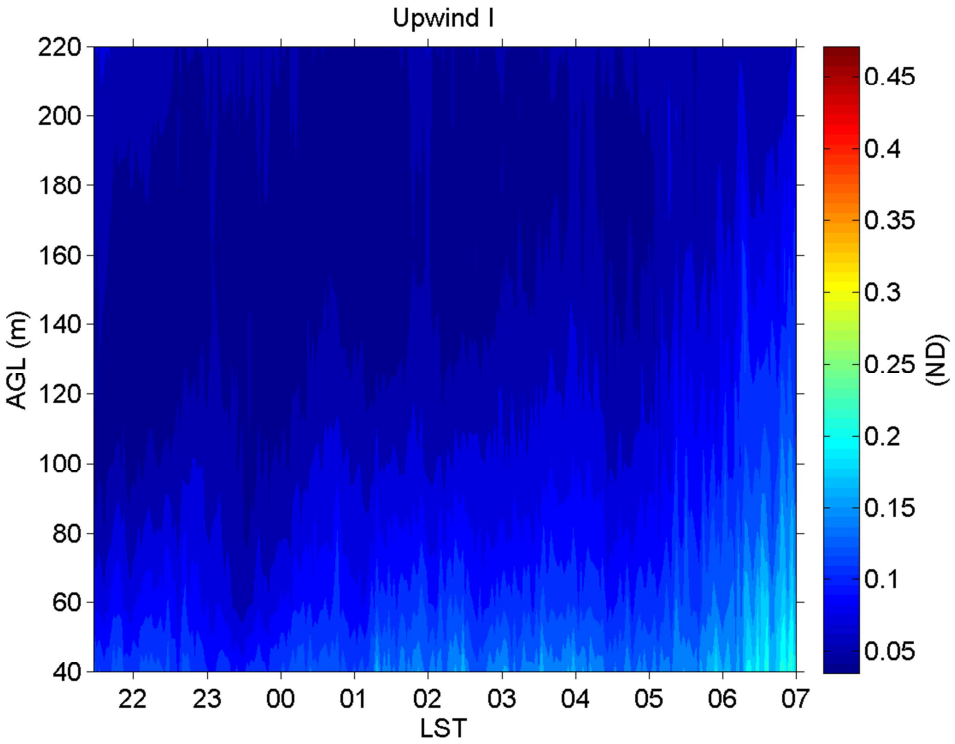

Figure 51: Time-height contours of upwind turbulence intensity

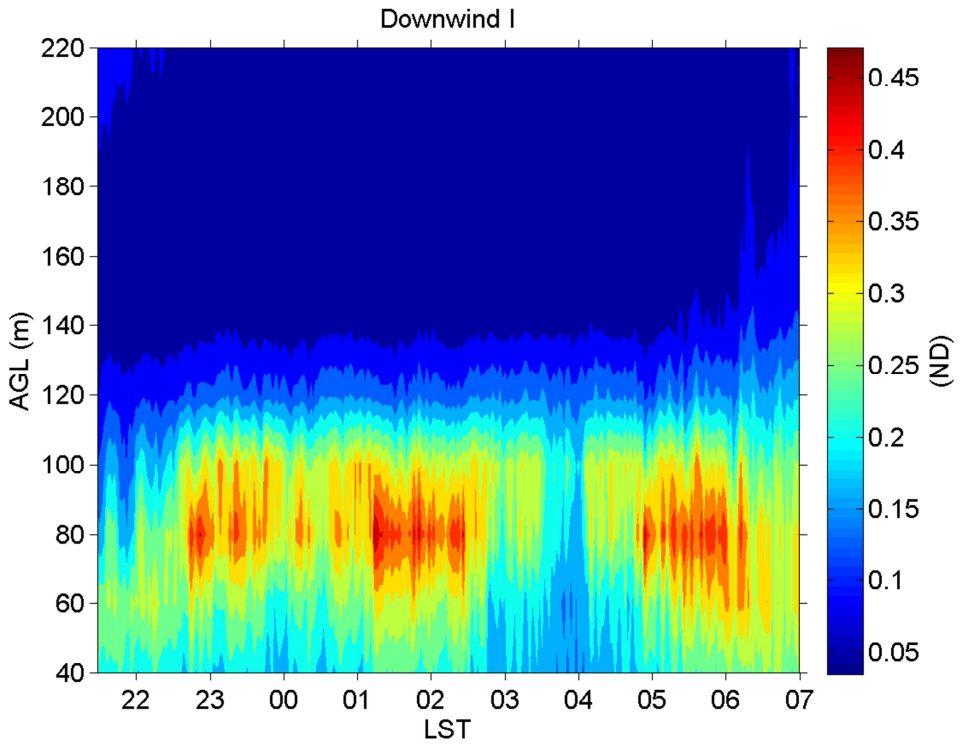

Figure 52: Time-height contours of downwind turbulence intensity

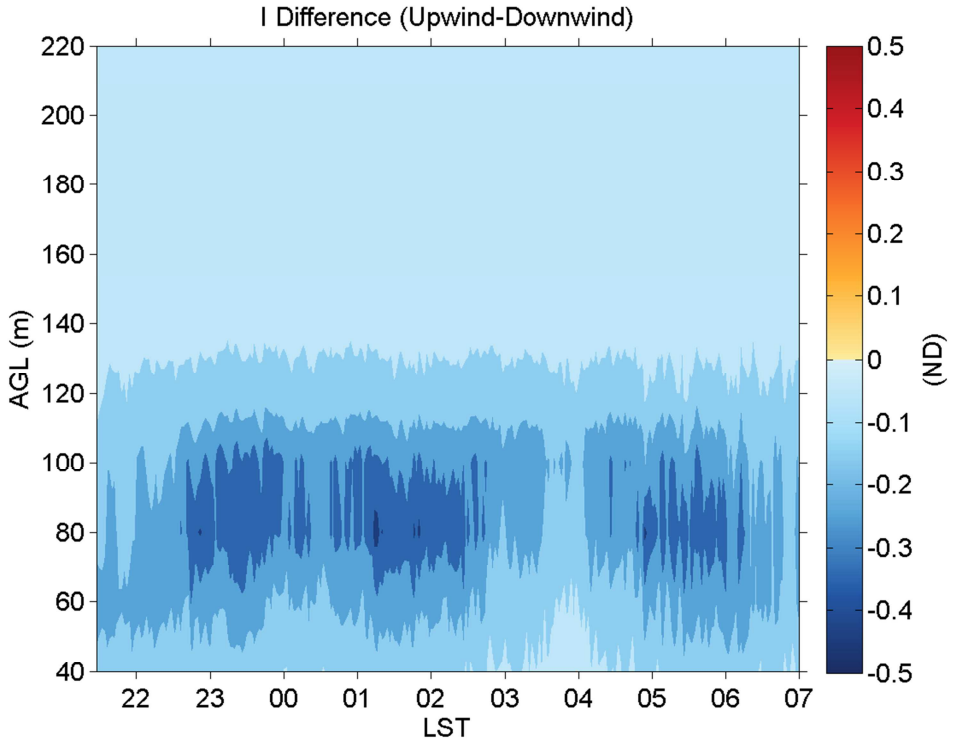

Figure 53: Time-height contours of upwind - downwind turbulence intensity differences

5.1.5 Vertical Turbulence Intensity

Vertical turbulence intensity (Figure 56) behaves very similarly to horizontal turbulence intensity, so much of the previous discussion applies for this section. The main difference that vertical turbulence intensity shows is that the vertical extents of large values of vertical turbulence extend beyond the rotor disc by 10m to 20m both above and below, and the vertical variation of magnitude is more variable in height than for horizontal turbulence intensity. However, like horizontal turbulence intensity, the strongest vertical turbulence intensity exists at the hub height.

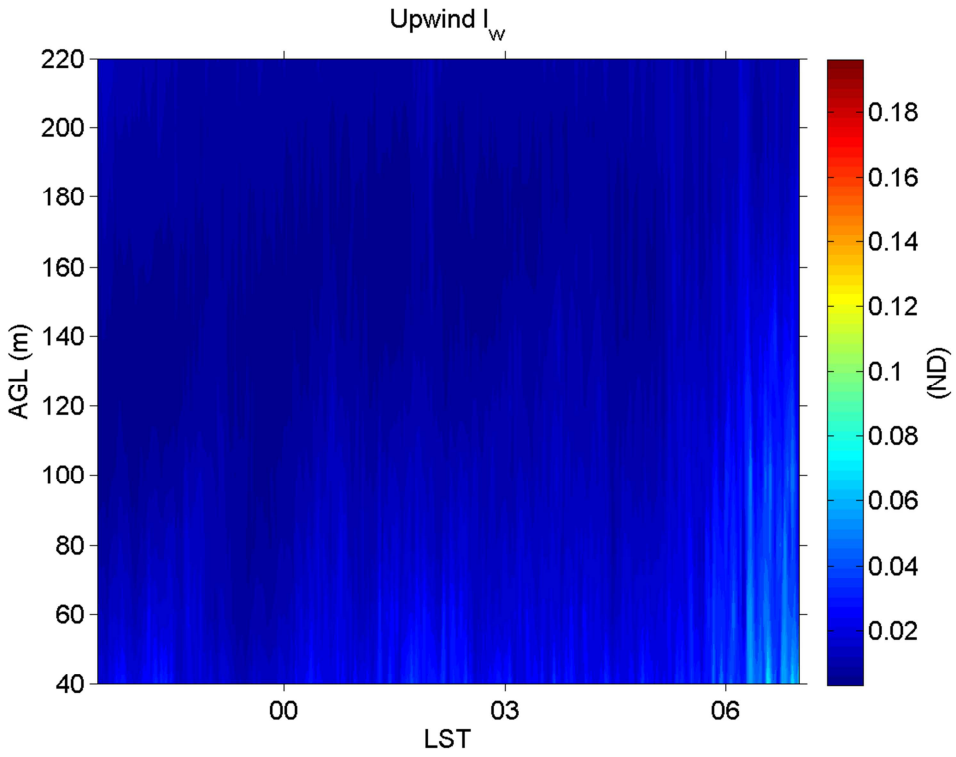

Figure 54: Time-height contours of upwind vertical turbulence intensity

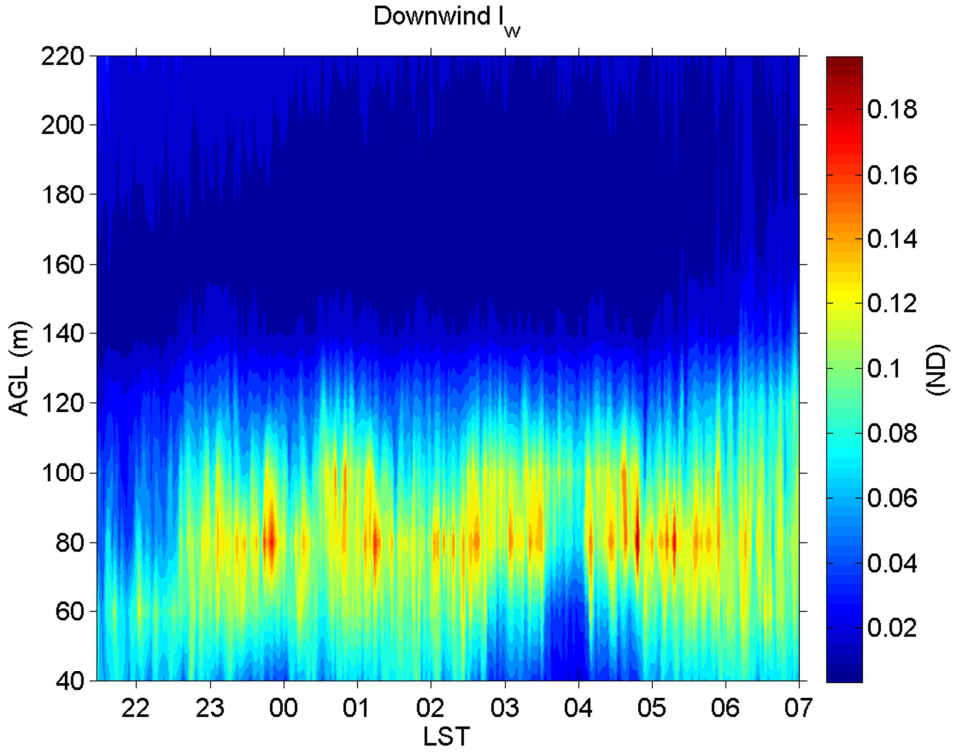

Figure 55: Time-height contours of downwind vertical turbulence intensity

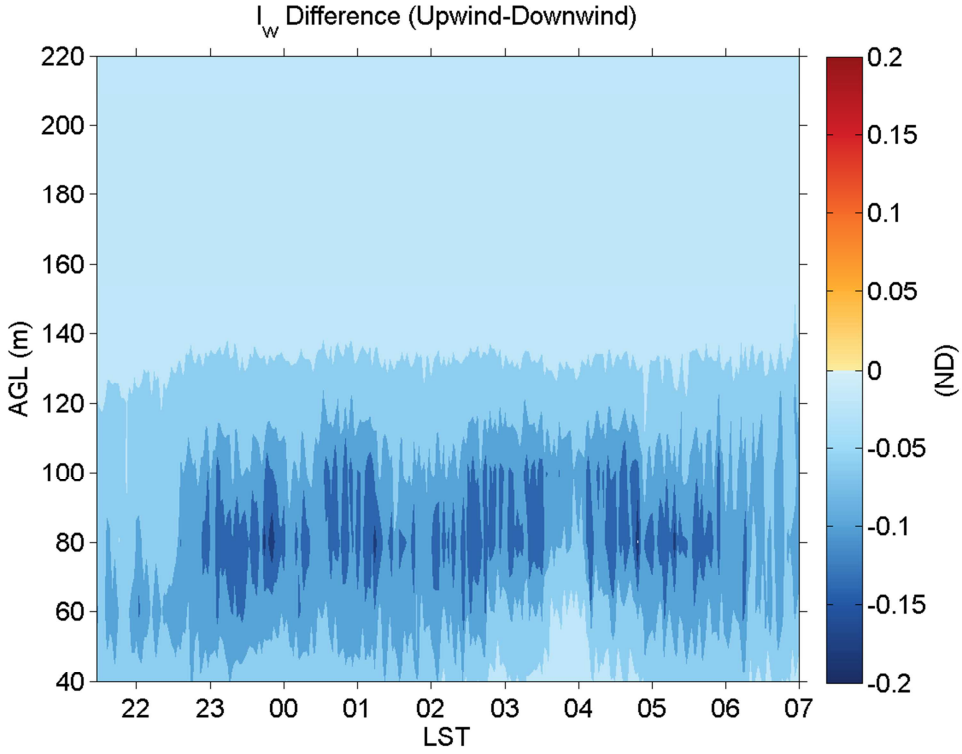

Figure 56: Time-height contours of upwind - downwind vertical turbulence intensity differences

5.1.6 Wind Speed Shear

Wind shear upwind of the turbine row (Figure 57) shows values below 0.1(m/s)/m at all heights with the largest values existing at the bottom of the LIDAR profile. Downwind wind speed shear (Figure 59) increases for nearly the entire night. For the waked observations, shear values in the lower half of the turbine rotor region, from 50m – 90m, are similar in magnitude to or even smaller when compared with the upwind observations. At the same time, the magnitude of shear above hub height is large with the greatest shear present between 120m and 140m. Increased wind speed shear has the potential to form coherent turbulence structures which can impact the operational lifetime and power production of wind turbines downwind (Kelley et al. 2004).

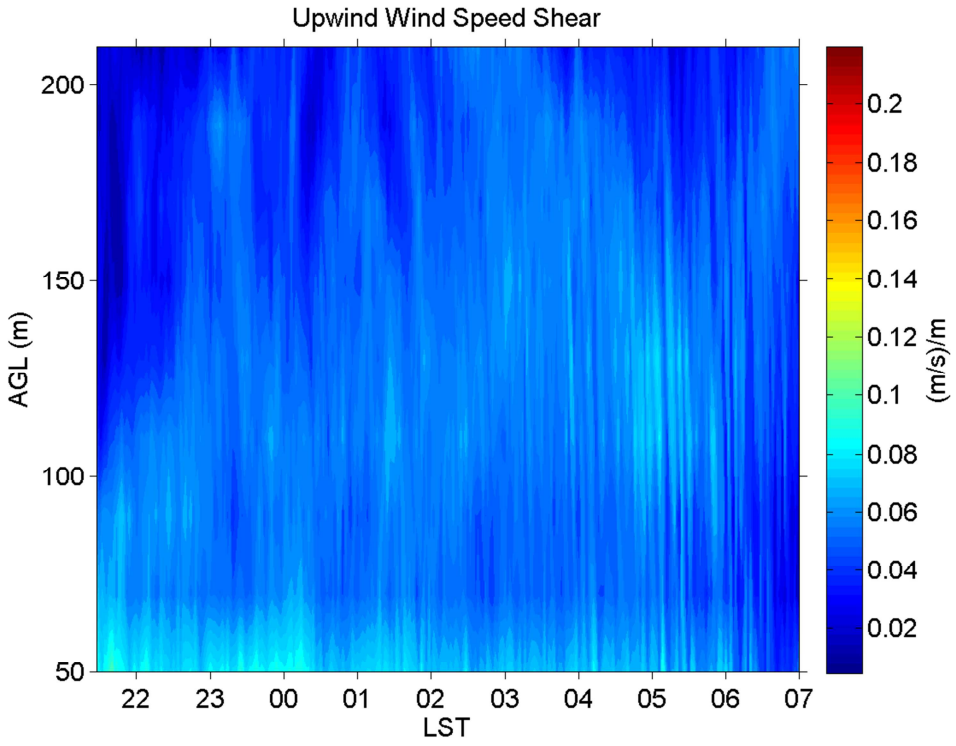

Figure 57: Time-height contours of upwind wind speed shear

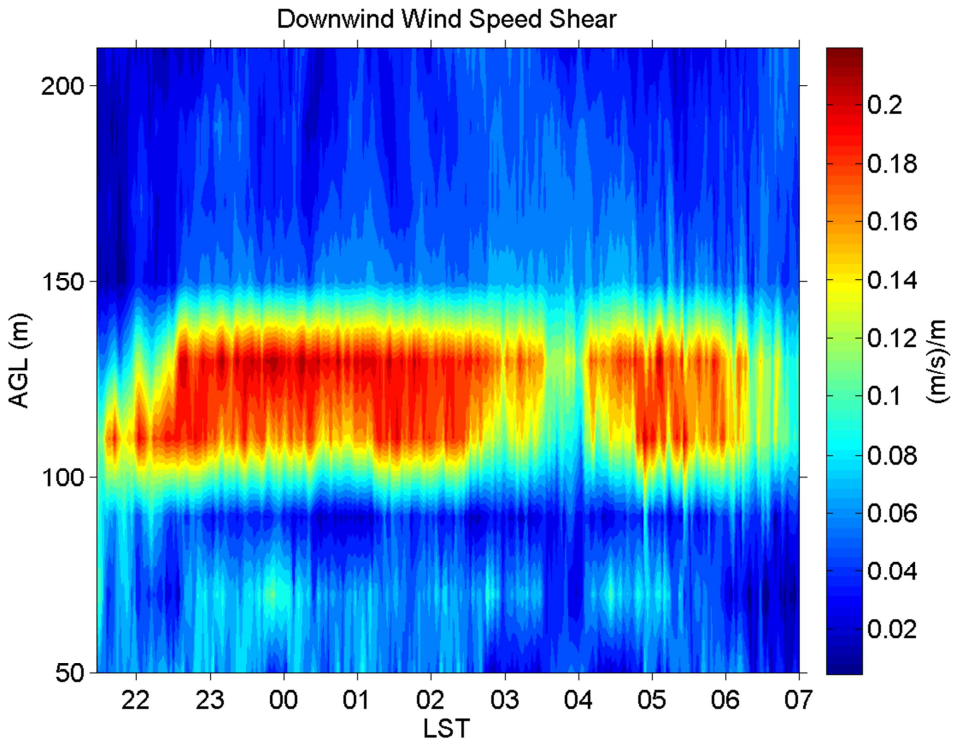

Figure 58: Time-height contours of downwind wind speed shear

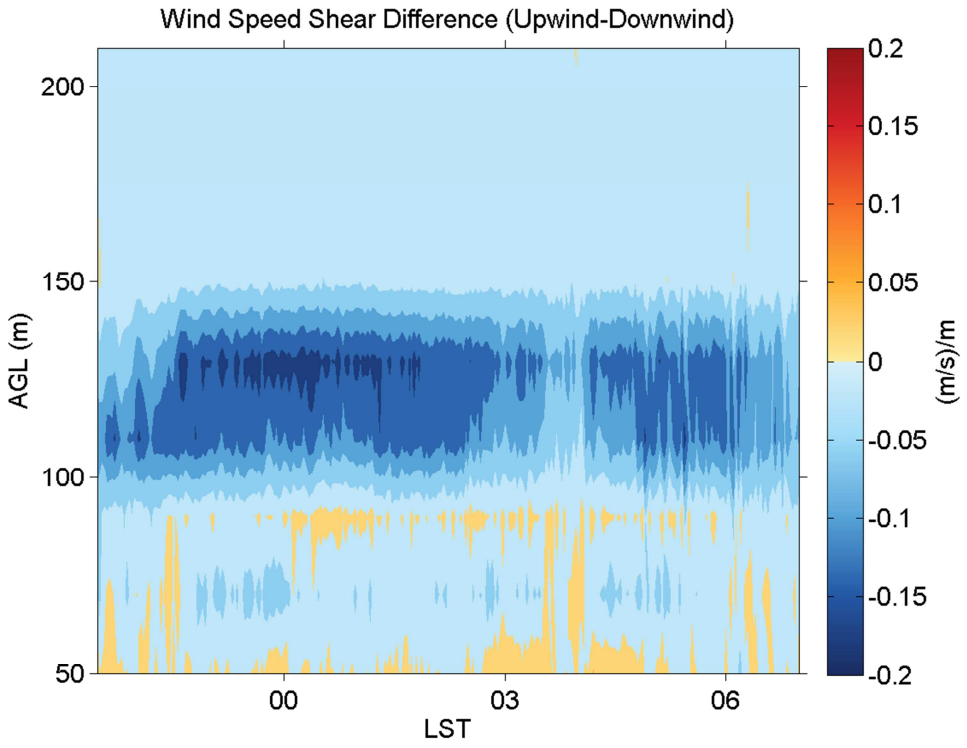

Figure 59: Time-height contours of upwind - downwind wind speed shear differences

5.1.7 Power law Coefficient, alpha

The power law coefficient profile for this case study resembles that of the canonical analysis. Upwind alpha (Figure 62) is near zero for much of the vertical extent, but below 70m alpha is between 0.02 and 0.08. Downwind, 50m to 70m alpha has negative values between -0.1 and -0.02 for 50m to 70m. Between 70m and 100m, alpha ranges from 0.02 to 0.04. From 100m to 140m, alpha is between -0.02 and 0. The exception to this downwind alpha trend is during the easterly wind shift around 03:00 to 05:00 where the values of alpha resemble values observed upwind of the turbine, and this reinforces our conclusion that at this time we are not sampling a turbine wake. Additionally, alpha's distinct sign change during a period where the wake is not being sampled shows how useful alpha is as a parameter for determining wake versus non wake conditions. We determined that evaluating the value of alpha is an easy and quick way to determine if the downwind LIDAR is in fact seeing a wake, and this can help refine our definition of waked conditions and understand how wakes spread based on inflow conditions.

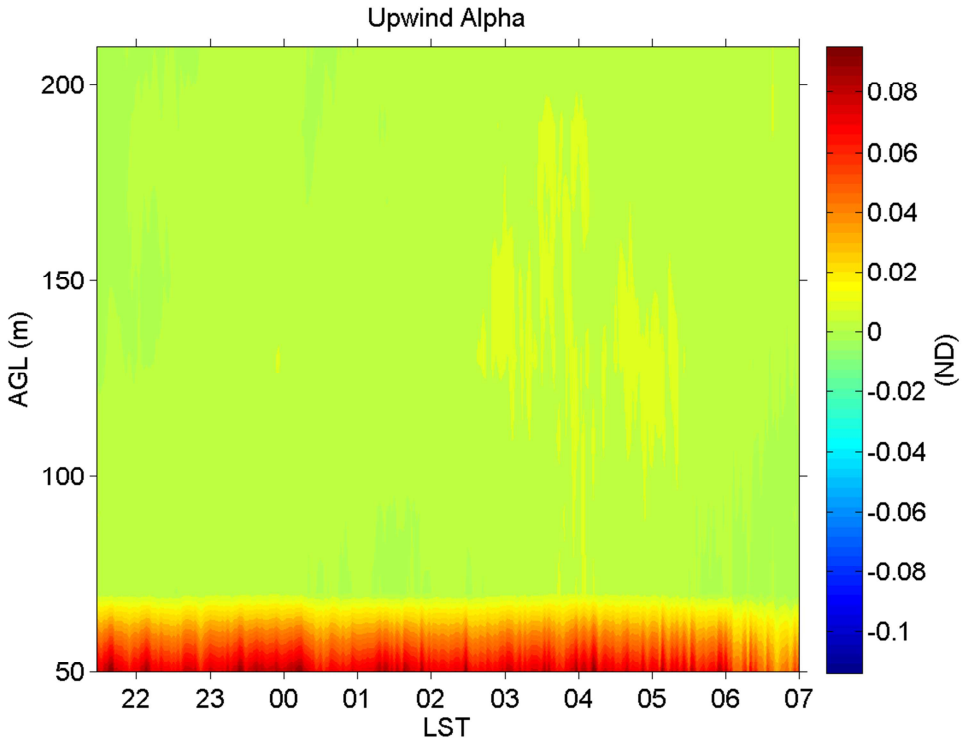

Figure 60: Time-height contours of upwind alpha, the power law coefficient

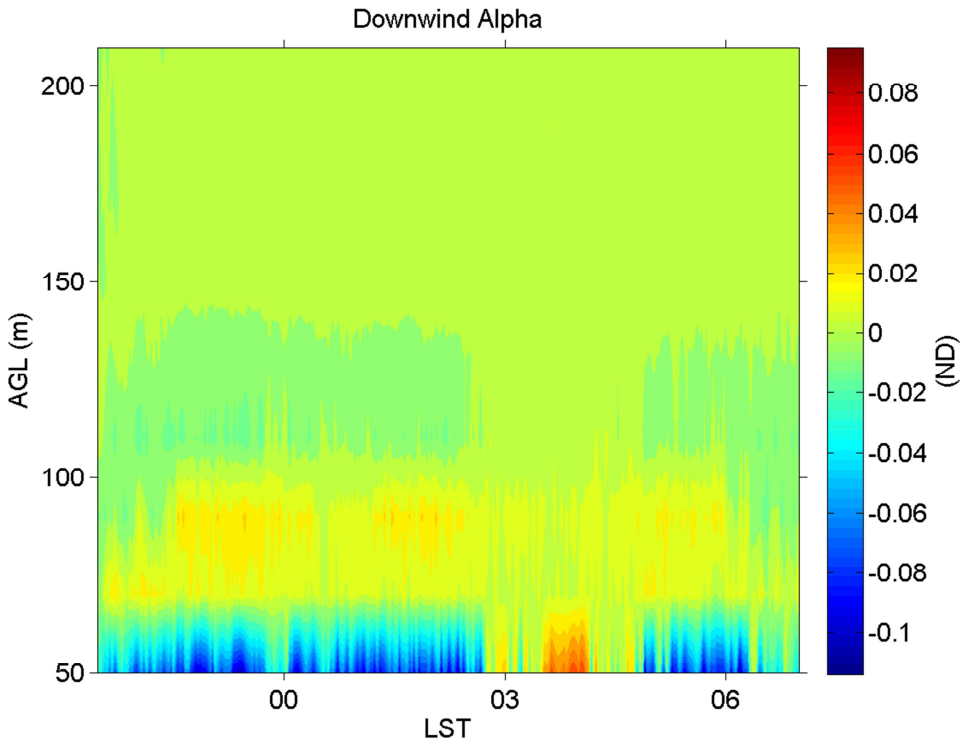

Figure 61: Time-height contours of downwind alpha, the power law coefficient

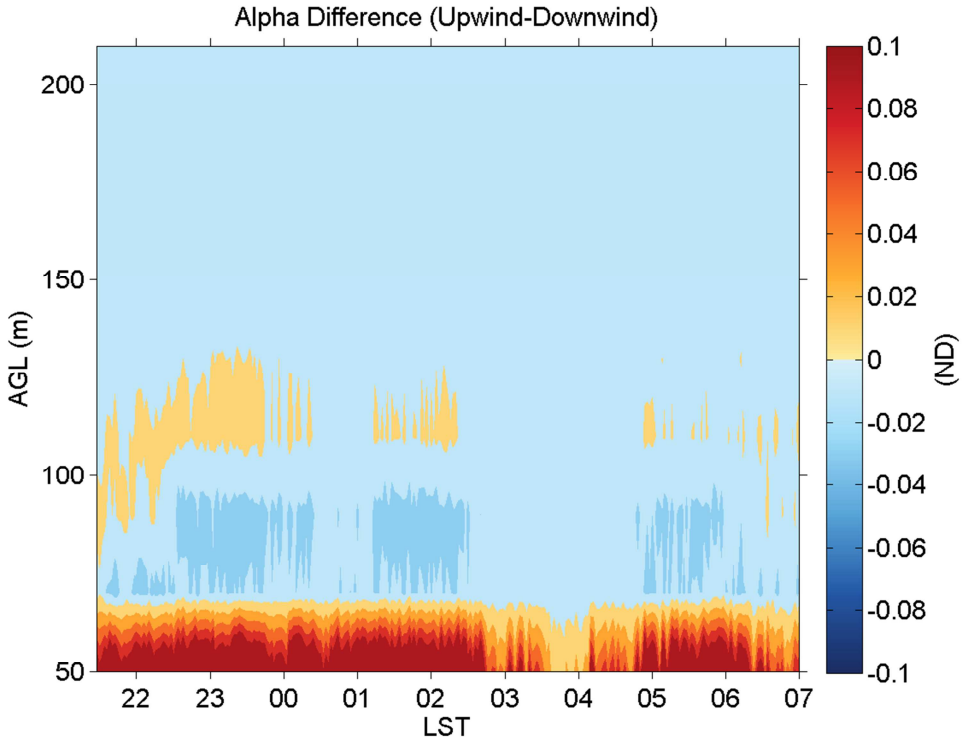

Figure 62: Time-height contours of upwind - downwind alpha differences

5.1.8 Wind Direction Shear

Upwind directional shear is positive at all heights and times with values ranging from approximately 0 to 0.03 (Figure 65). Downwind, shear varies in sign over the rotor height and is dependent on wind direction. Positive directional shear indicates that the flow is rotating clock-wise with height if viewed from above, conversely negative shear indicates counter clock-wise. Under normal undisturbed conditions, like those observed upwind, we expect to see positive directional shear due to viscous effects (Holton 2004). When the downwind LIDAR samples waked flow, a region of positive directional shear exists below a region of negative shear. At most times, the lower positive layer extends from 50m to about 90m, while the negative layer ranges from about 100m up to 140m. For southerly flow, the wind turbines at the field site rotate clockwise when viewed from the upwind LIDAR. Because we see negative shear, or counterclockwise rotation above the rotor in waked flow, the rotor must push the air above hub height to the east and air below hub height to the west. Previous observation and simulation studies indicate that wake rotation is contrary to rotor rotation direction, which conflicts with what the CWEX 2011 data show (Högström et al. 1988; Lee et al. 2012).

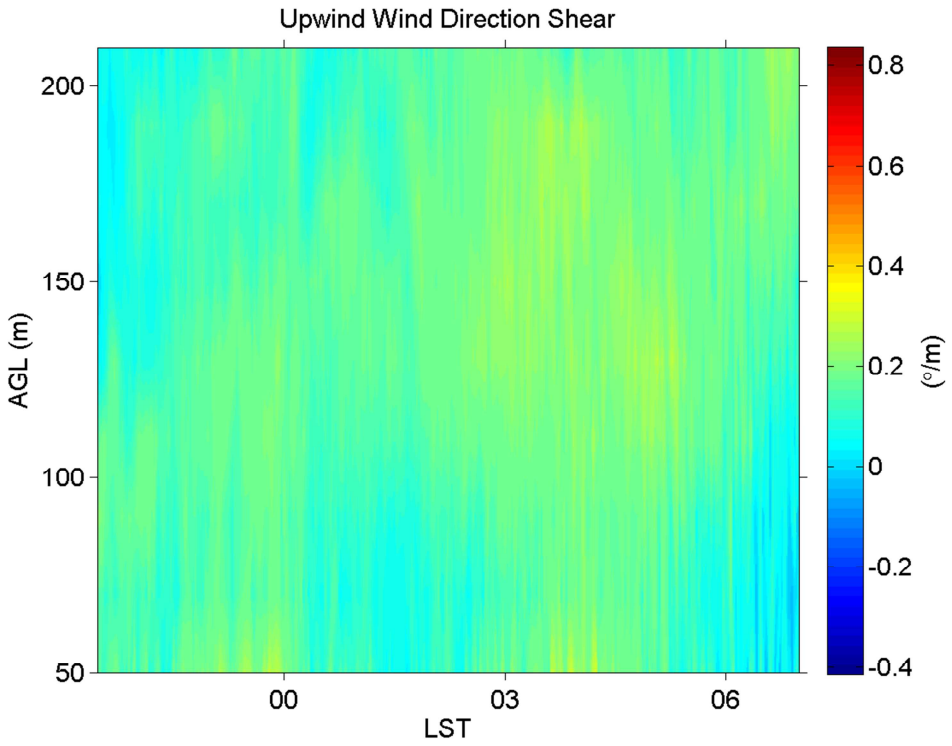

Figure 63: Time-height contours of upwind wind direction shear

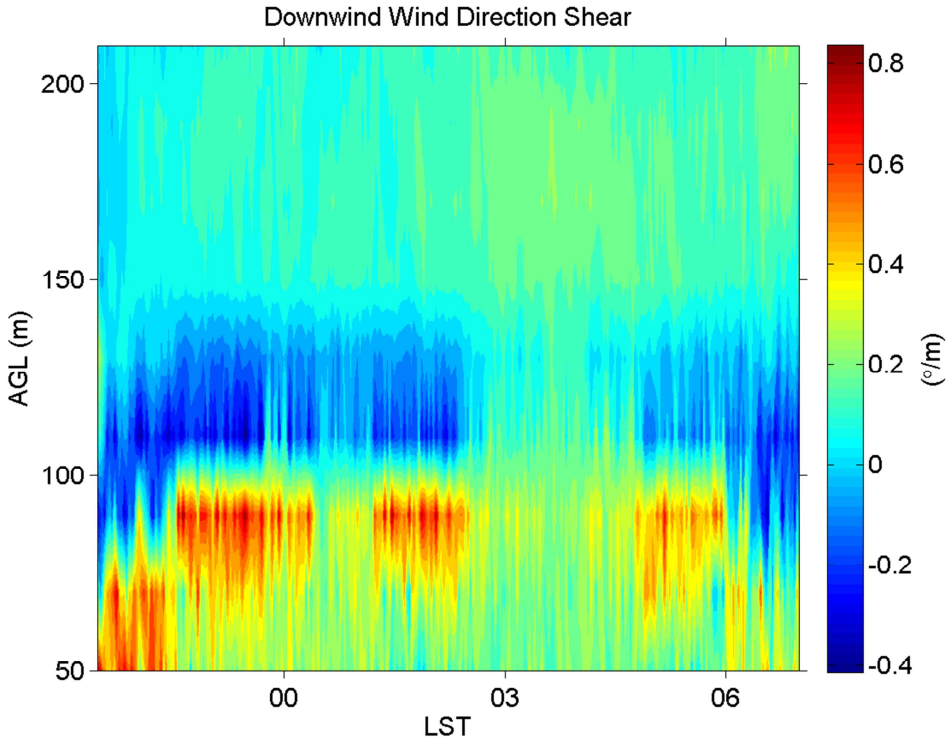

Figure 64: Time-height contours of downwind wind direction shear

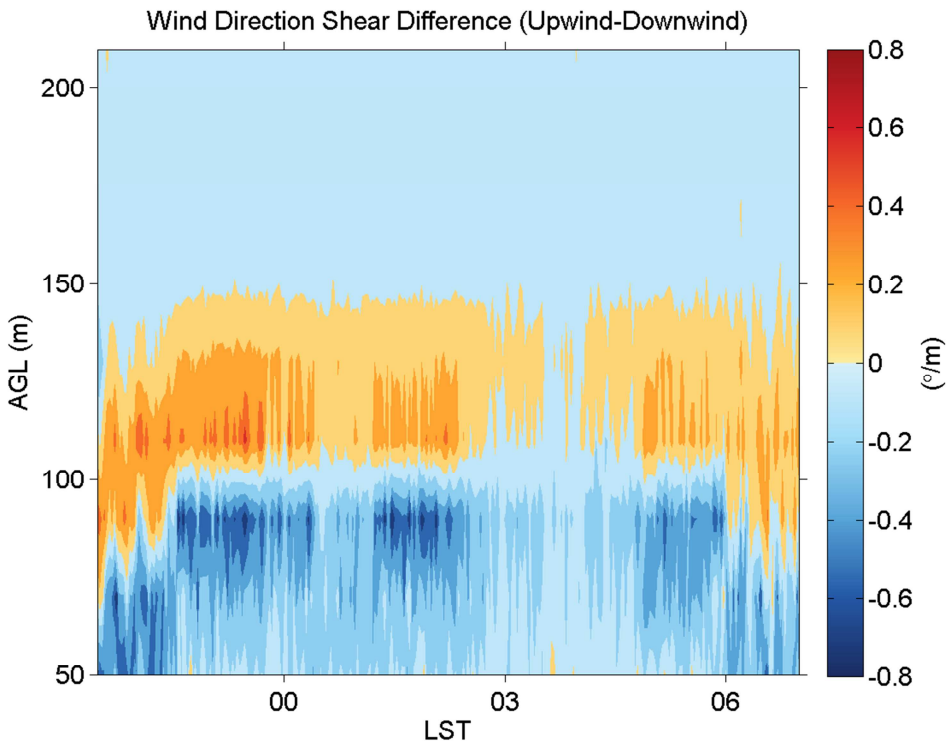

Figure 65: Time-height contours of upwind - downwind wind direction shear differences

5.2 Case Study 2: Convective / Evening Transition

The convective case study began around 16:00 local time on July 23, 2011 and concluded at 19:00 on July 23, 2011. Weather conditions during the event consisted of southerly flow at wind turbine hub height with wind direction variations from 170° to 195°. Average hub height wind speeds were about 9m/s and slowly decreased throughout the afternoon to 7m/s. Synoptically, a high pressure system moved slowly east from eastern Iowa into northern Illinois, and a low pressure system and stationary front moved in more rapidly from the central Nebraska-South Dakota border into central Iowa.

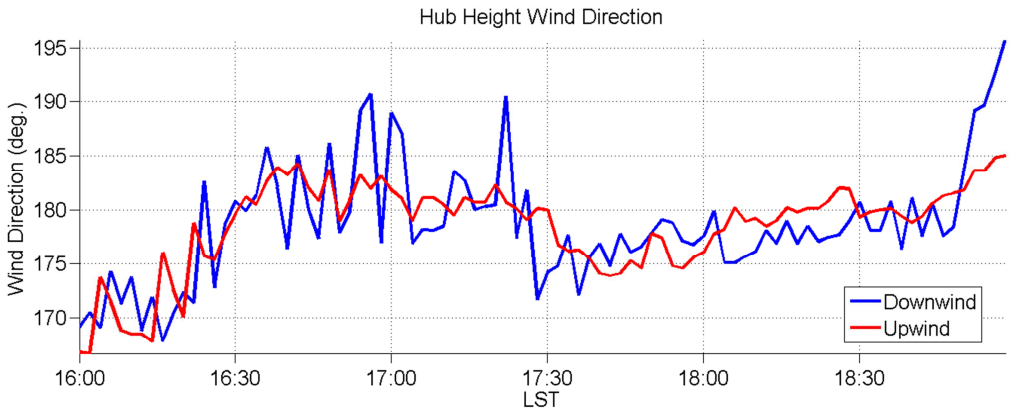

Figure 66: Upwind and downwind hub height wind directions for the convective condition case study

5.2.1 Wind Speed

Upwind wind speeds for the convective case study show increasing wind speed with height (Figure 69) as would be expected in a convective boundary layer. Downwind, wind speed is reduced by 4m/s at hub height with smaller reductions spanning the entire rotor disc. Shortly before 18:00 local time, there was a brief period where downwind speed nearly matched upwind values, but there is no change in wind direction that can explain this behavior. The primary difference between the day and night cases study for wind speed is variability of the wind speed deficit depth downwind of the turbine. Night time wind speed deficits maintained a nearly constant wake deficit between 50m and 140m with southerly flow. The convective case has more variability in the depth of the wake deficit, even during periods of nearly constant wind direction, perhaps due to convective rolls.

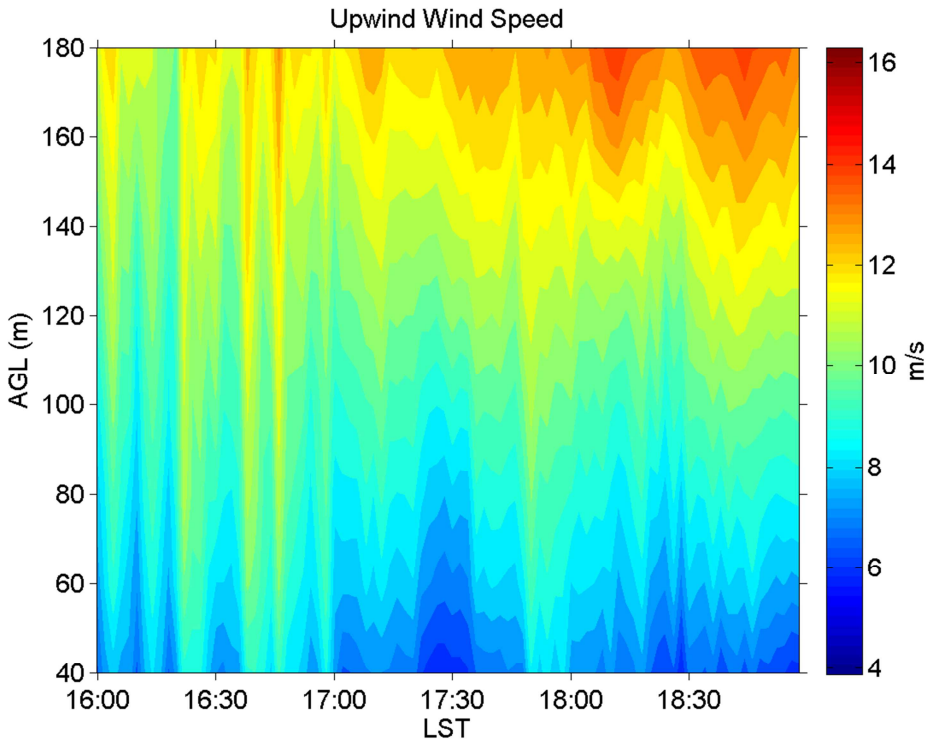

Figure 67: Convective time-height contours of upwind wind speed

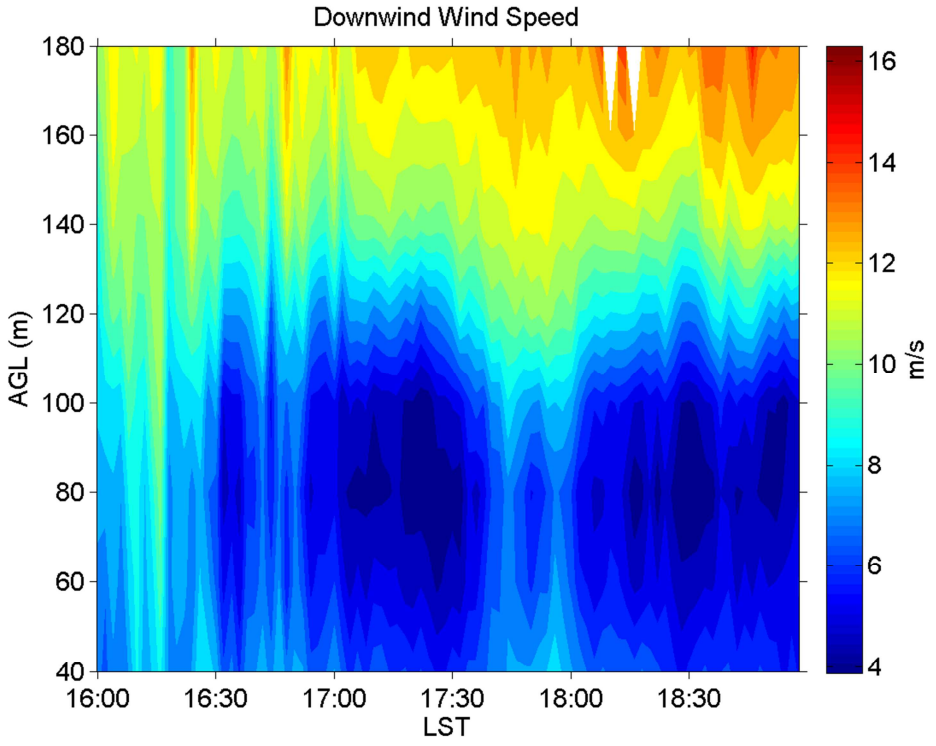

Figure 68: Convective time-height contours of downwind wind speed

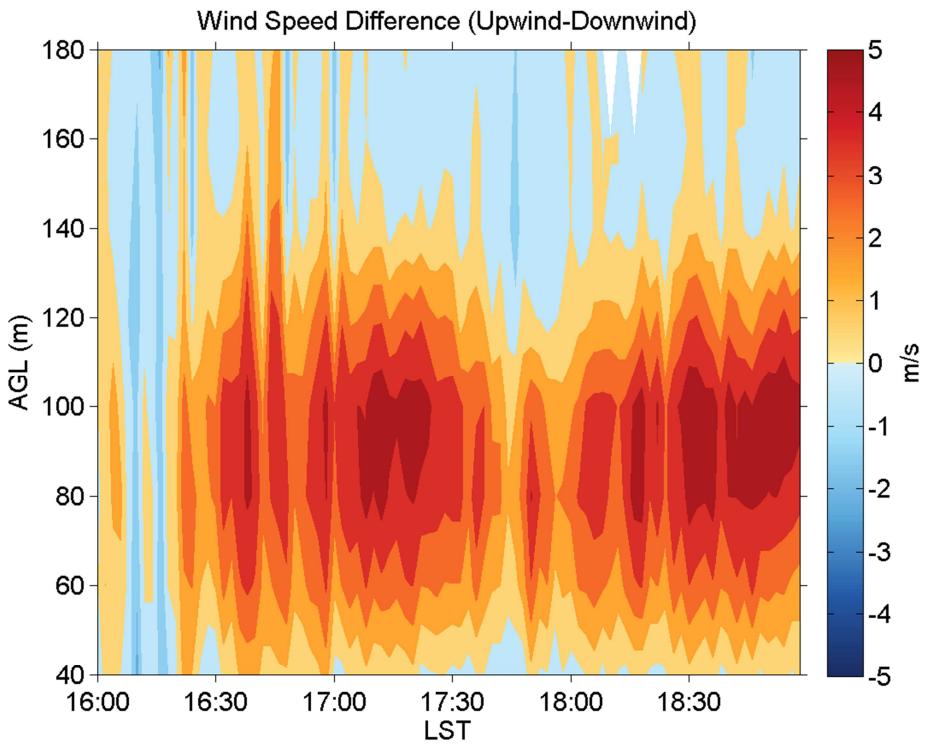

Figure 69: Convective time-height contours of upwind - downwind wind speed differences

5.2.2 Vertical Wind Speed

Upwind vertical wind speed (Figure 72) is positive for most the case study period, which indicates convective conditions. At a number of times there are upward speeds on the order of 0.25m/s, and occasional periods with downward motions of the same magnitude, consistent with large convection cells in the atmospheric boundary layer. Downwind vertical speeds show similar vertical velocities as compared with the upwind observations. The largest increase is in the rotor disc with values often near 0.75m/s. Areas immediately adjacent to the rotor disc tend to have downward motion. These results are similar to what is observed in the stable condition case study; however, we do not see the strong gradient in vertical wind speed for wind directions between 185° and 190°, likely indicating more mixing.

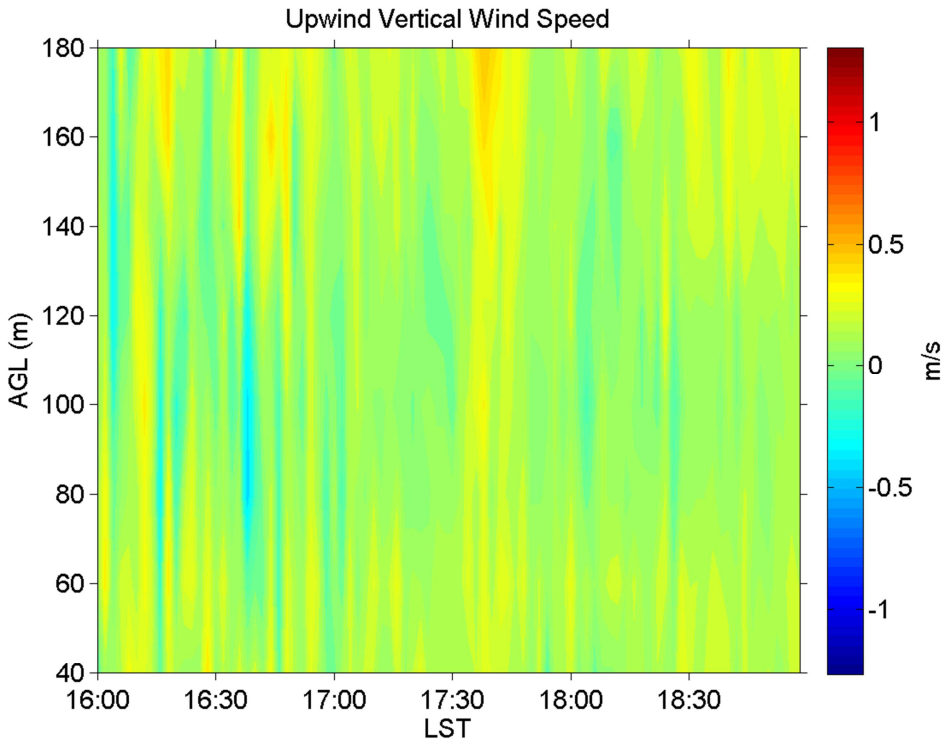

Figure 70: Convective time-height contours of upwind vertical wind speed

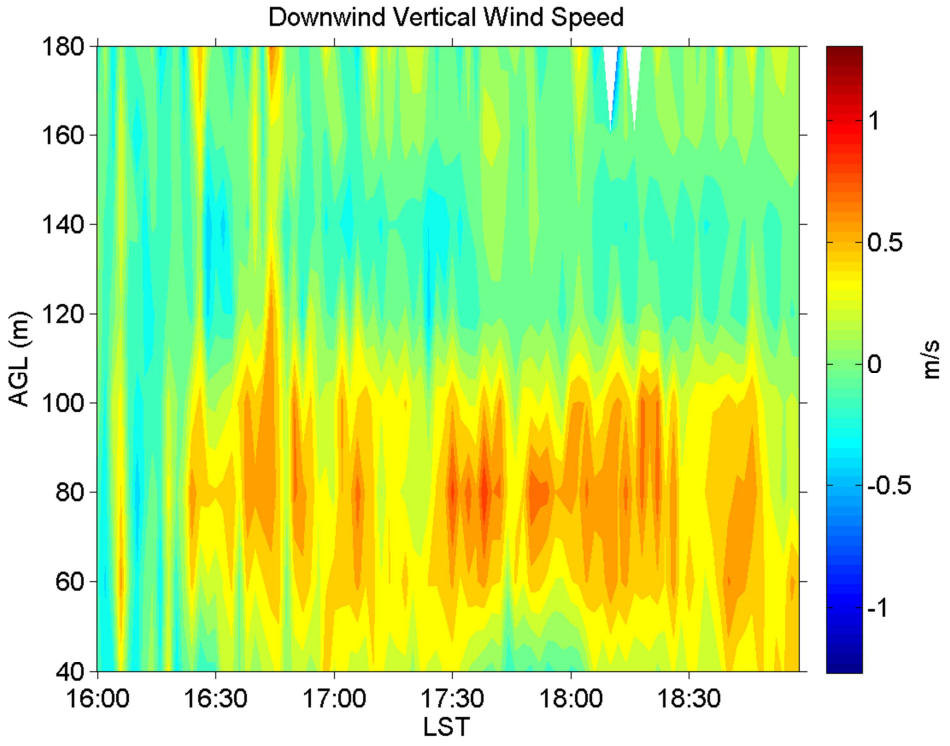

Figure 71: Convective time-height contours of downwind vertical wind speed

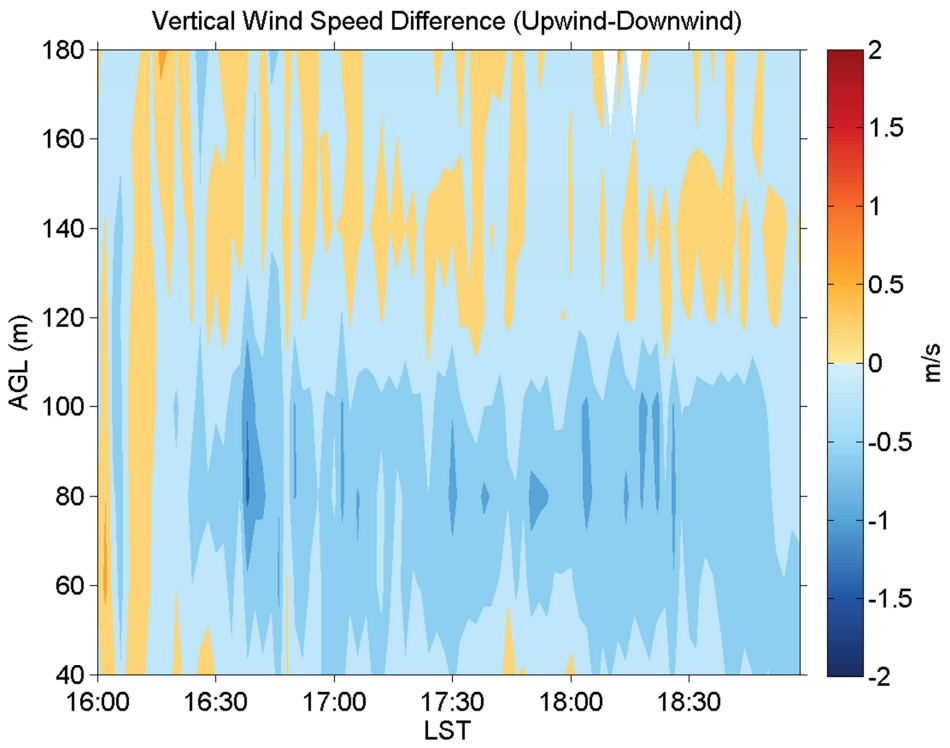

Figure 72: Convective time-height contours of upwind - downwind vertical wind speed differences

5.2.3 Turbulent Kinetic Energy

The first hour of the daytime case study shows expected TKE in convective conditions: strong positive values due to thermals from surface heating (Figure 75). The convective signature is amplified by approximately a factor of two over the upwind TKE for this hour. After 17:00, the upwind turbulence calms to levels of about 0.5 m^2/s^2, reflective of the onset of the evening transition of the boundary layer (Acevedo and Fitzjarrald 2001). The downwind TKE also decreases by nearly the same amount, yet is still elevated compared to upwind TKE. The magnitude of TKE for the daytime and nighttime cases are similar; however, the daytime case maintains increased TKE values across the entire rotor disc while the nighttime TKE extent was mostly limited to the lower half of the rotor disc with exception during more westerly wind flow.

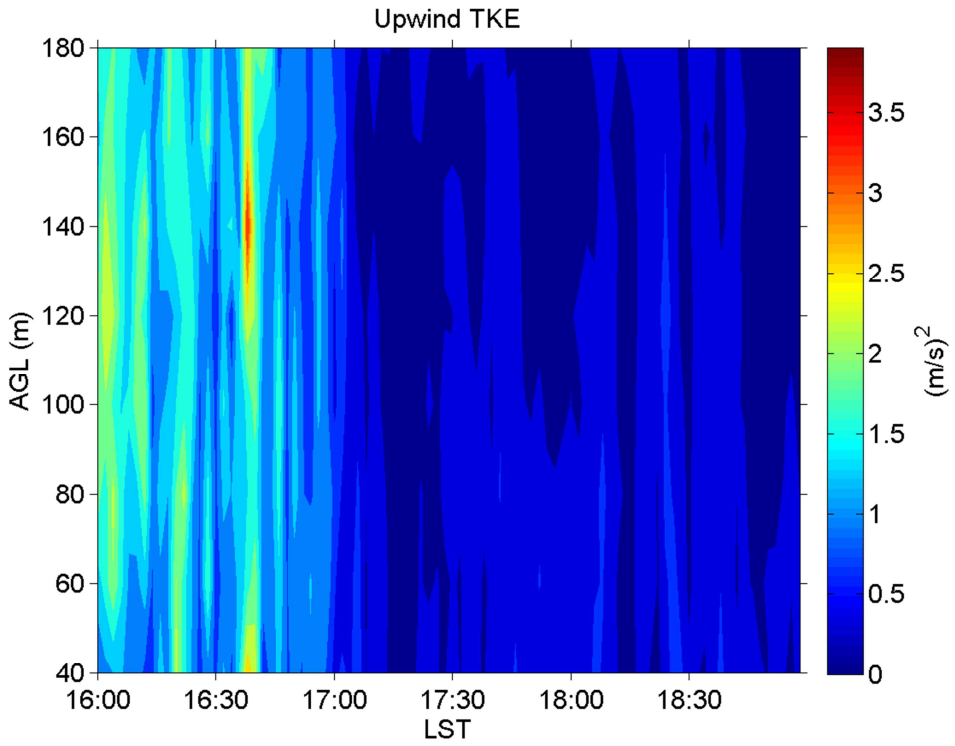

Figure 73: Convective time-height contours of upwind TKE

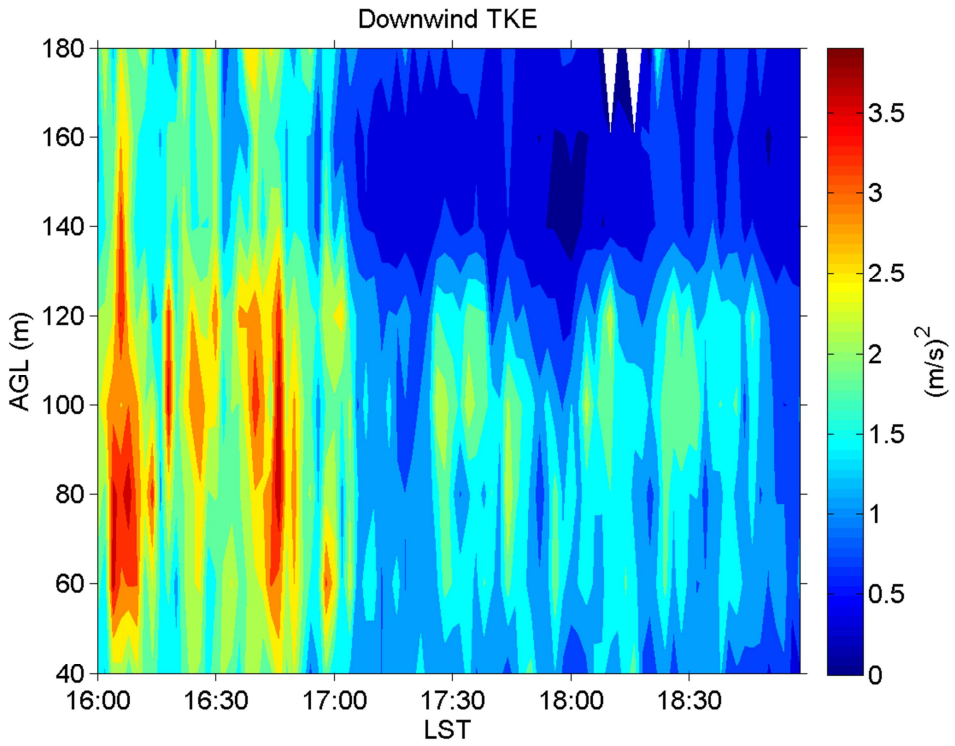

Figure 74: Convective time-height contours of downwind TKE

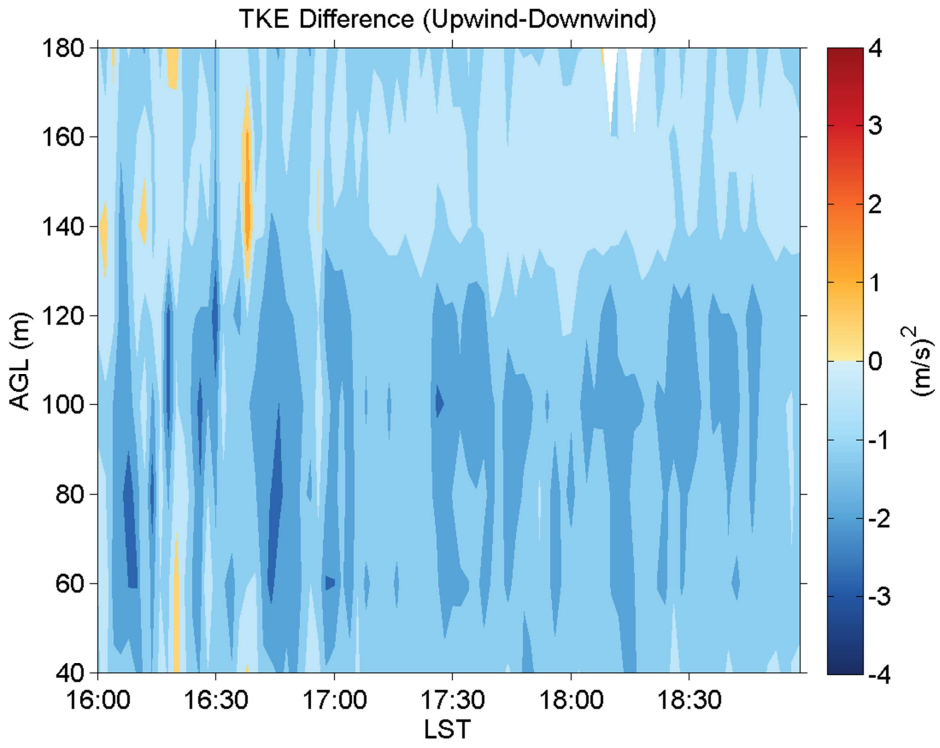

Figure 75: Convective time-height contours of upwind - downwind TKE differences

5.2.4 Turbulence Intensity

Much like TKE, turbulence intensity shows higher values during convective conditions than during stable conditions. Upwind turbulence intensity (Figure 78) decreases in magnitude above 100m after the first hour of the daytime period. Below 100m there are brief periods of turbulence intensity similar in magnitude to those found in the first hour of the case study. Unlike TKE, downwind turbulence intensity is not strongest during the first hour of the case study though the values are still amplified when compared with upwind values. Changes in downwind turbulence intensity do not seem to depend on upwind variations for convective conditions.

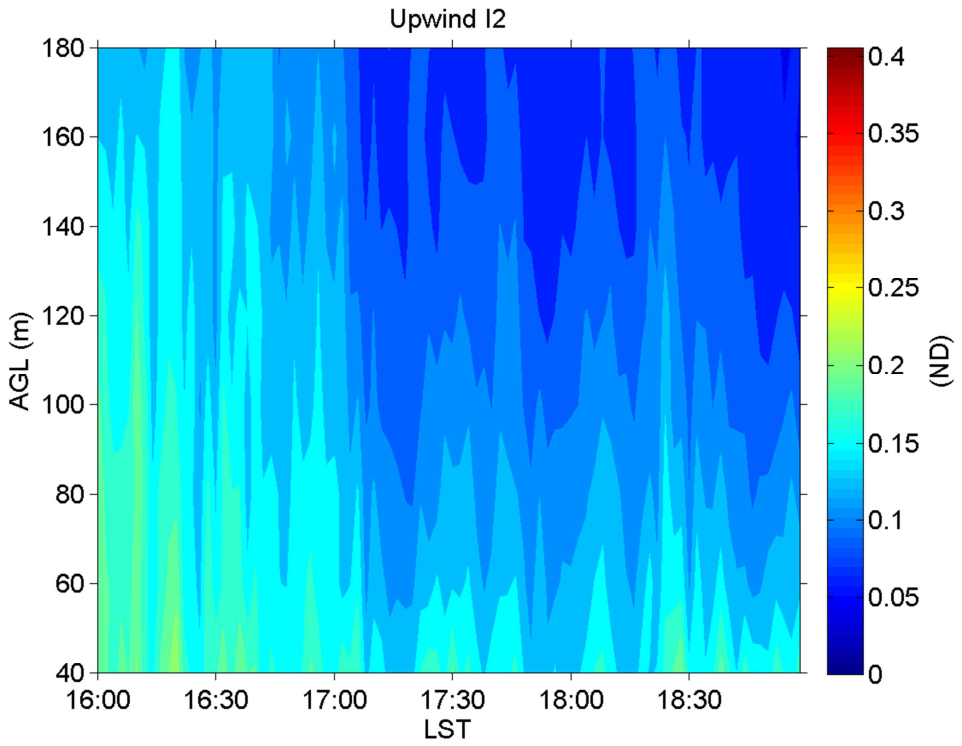

Figure 76: Convective time-height contours of upwind turbulence intensity

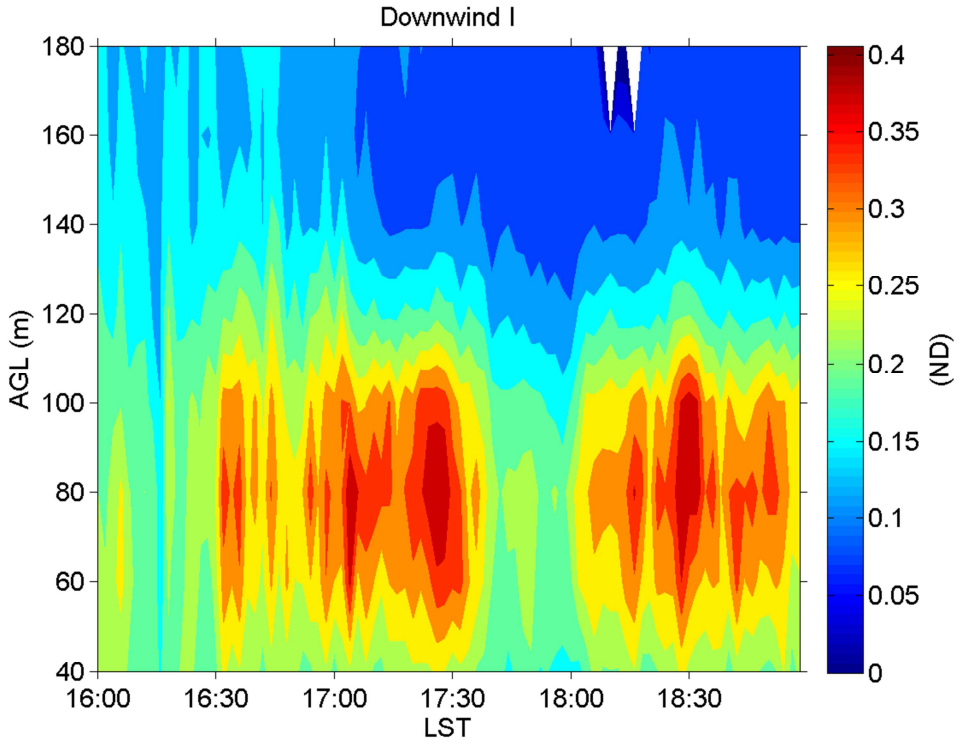

Figure 77: Convective time-height contours of downwind turbulence intensity

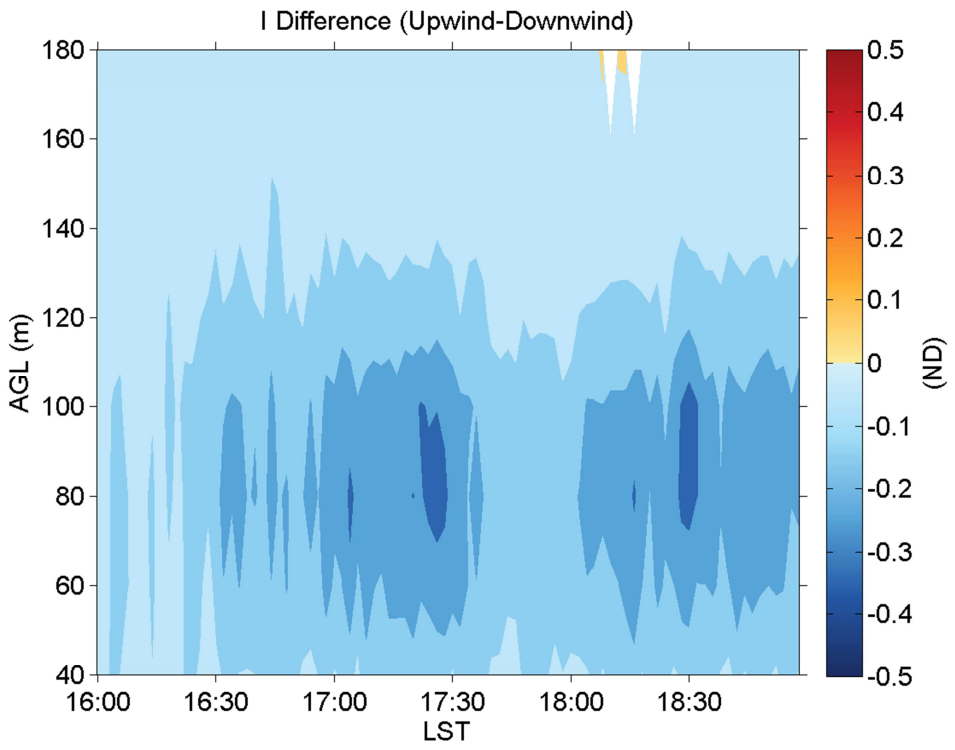

Figure 78: Convective time-height contours of upwind - downwind turbulence intensity differences

5.2.5 Vertical Turbulence Intensity

Vertical turbulence intensity under convective conditions behaves much like horizontal turbulence intensity both upwind and downwind (Figure 81) of the wind turbine and the previous discussion applies here as well. The main difference that exists between the horizontal and vertical definitions is that downwind vertical turbulence intensity is greatest at 100m, above hub height, whereas downwind horizontal turbulence intensity reaches a maximum at 80m hub height.

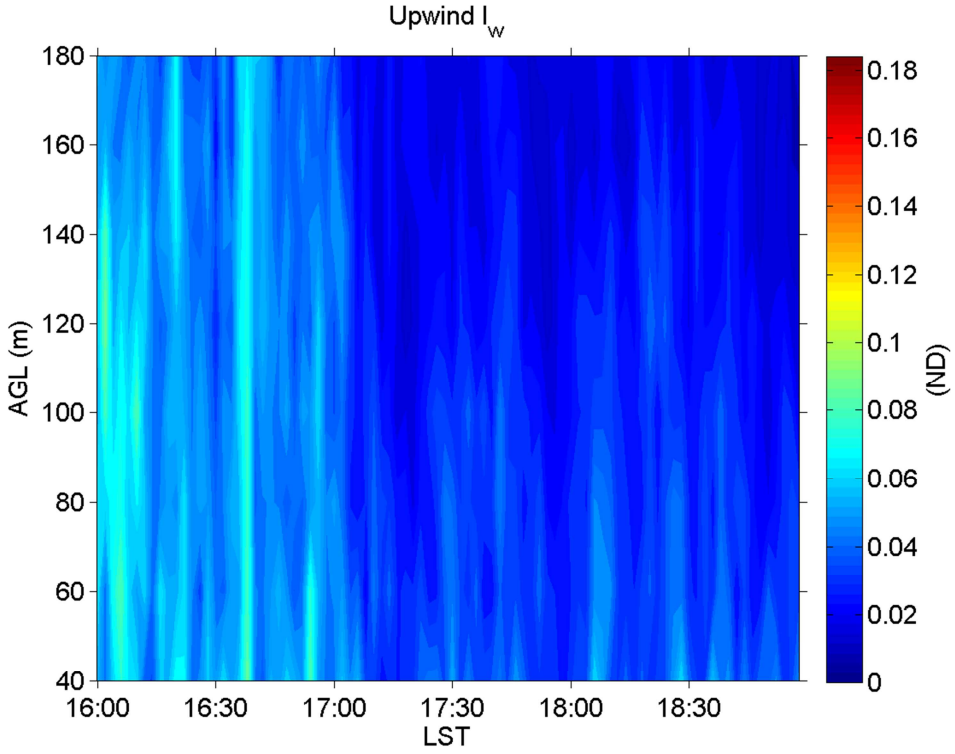

Figure 79: Convective time-height contours of upwind vertical turbulence intensity

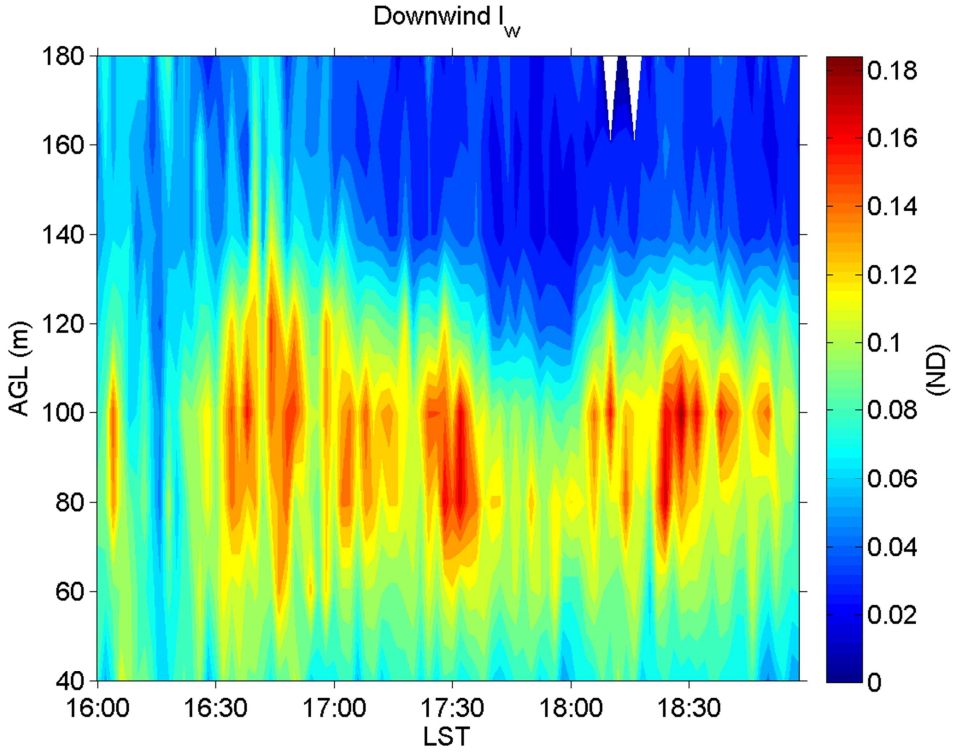

Figure 80: Convective time-height contours of downwind vertical turbulence intensity

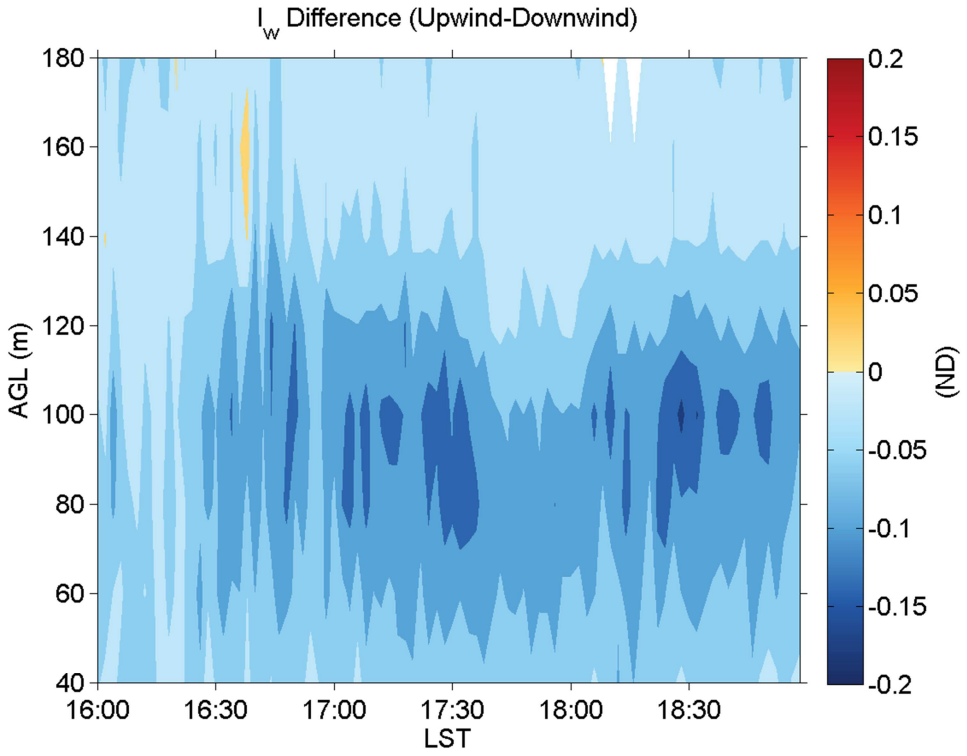

Figure 81: Convective time-height contours of upwind - downwind vertical turbulence intensity differences

5.2.6 Wind Speed Shear

Upwind convective wind speed shear is what we would expect with the turbulent mixing making the wind speed profile more uniform. The downwind convective wind shear (Figure 84) is similar to what we see in the stable boundary layer because positive shear exists above hub height and negative shear lies below the hub. As expected, the convective conditions decrease the severity of the wind shear downwind. Daytime wind shear is less persistent than what is seen in the nighttime case study.

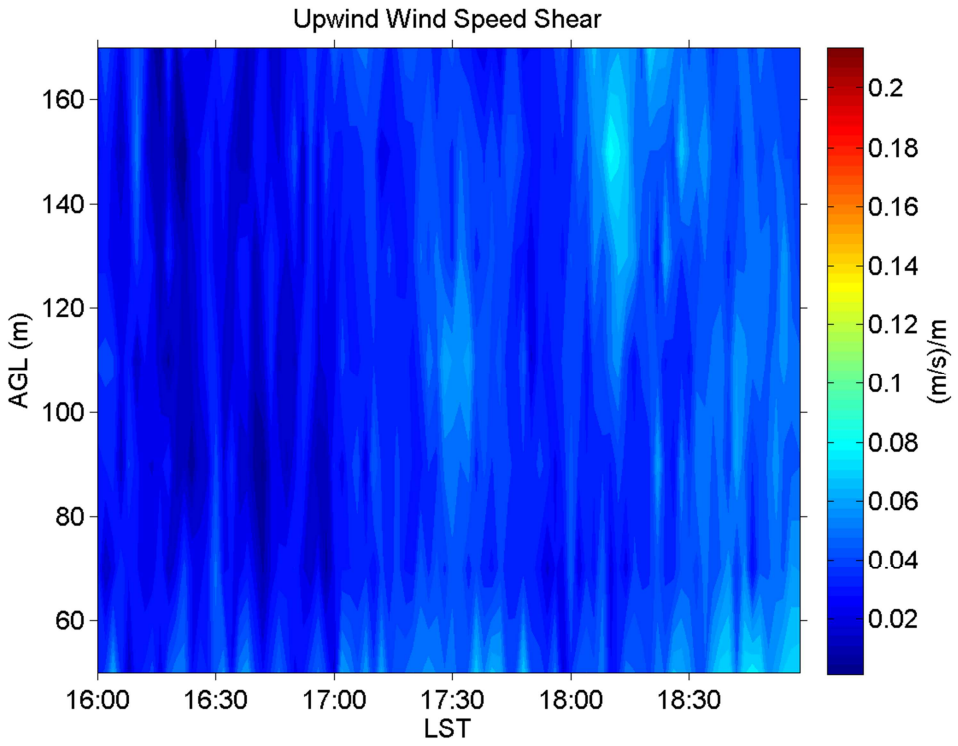

Figure 82: Convective time-height contours of upwind wind speed shear

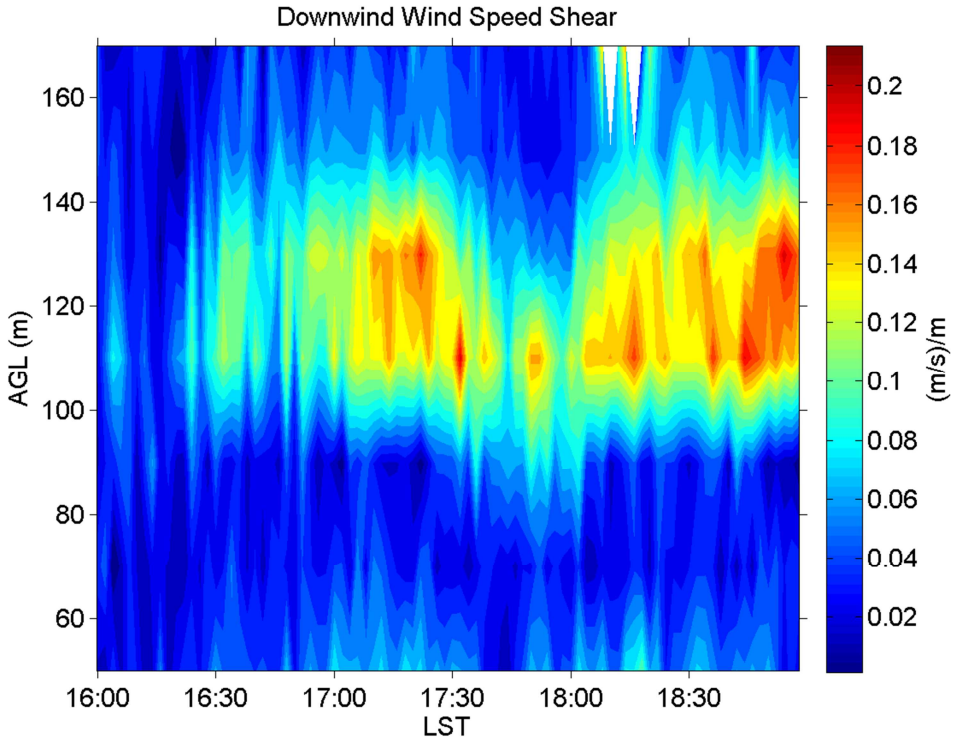

Figure 83: Convective time-height contours of downwind wind speed shear

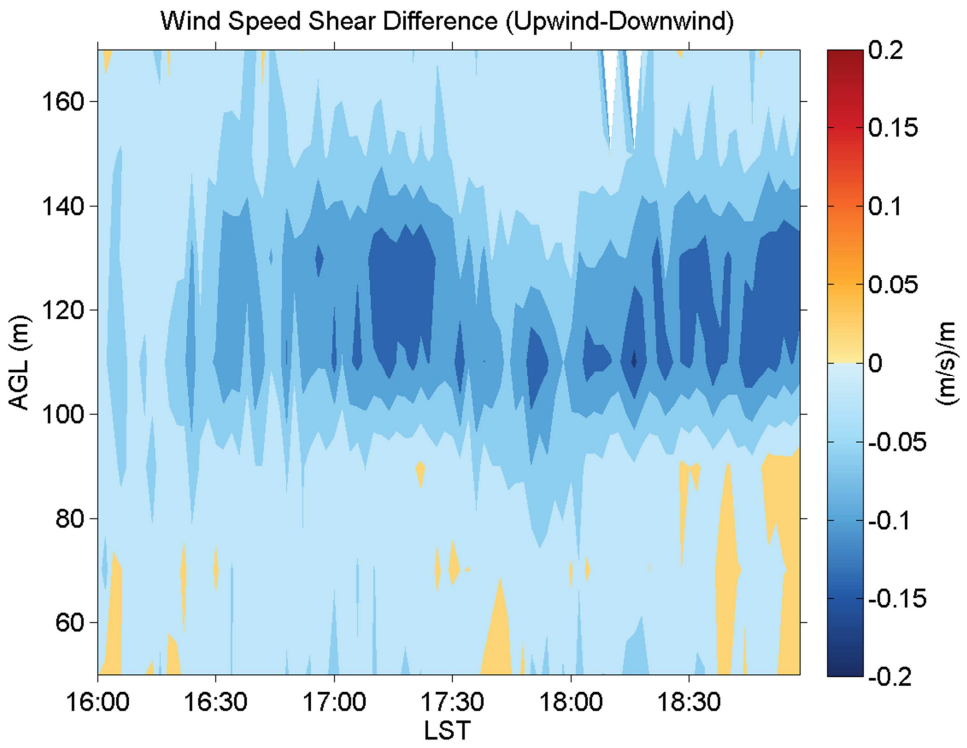

Figure 84: Convective time-height contours of upwind - downwind wind speed shear differences

5.2.7 Power law Coefficient, alpha

The power law coefficient profiles for the day and night cases are nearly identical upwind and downwind (Figure 87). The power law coefficient appears to be sensitive to wind direction at the lowest level detected by the Windcube. Wake data clearly show negative alpha values, while non-waked periods show behavior similar an upwind profile. The downwind alpha plot shows the effect of wind direction on values at the 60m level. Near the beginning of the case study period we were not sampling wake conditions, and throughout the night as wind direction shifted we sampled different parts of the wake with differing magnitudes of alpha.

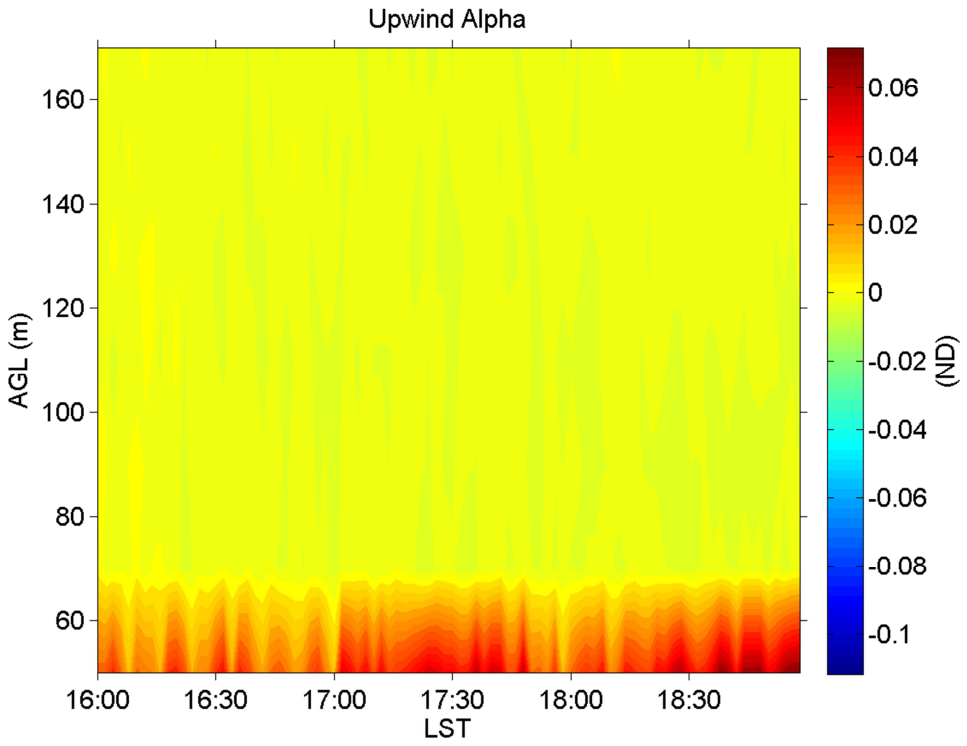

Figure 85: Convective time-height contours of upwind alpha, the power law coefficient

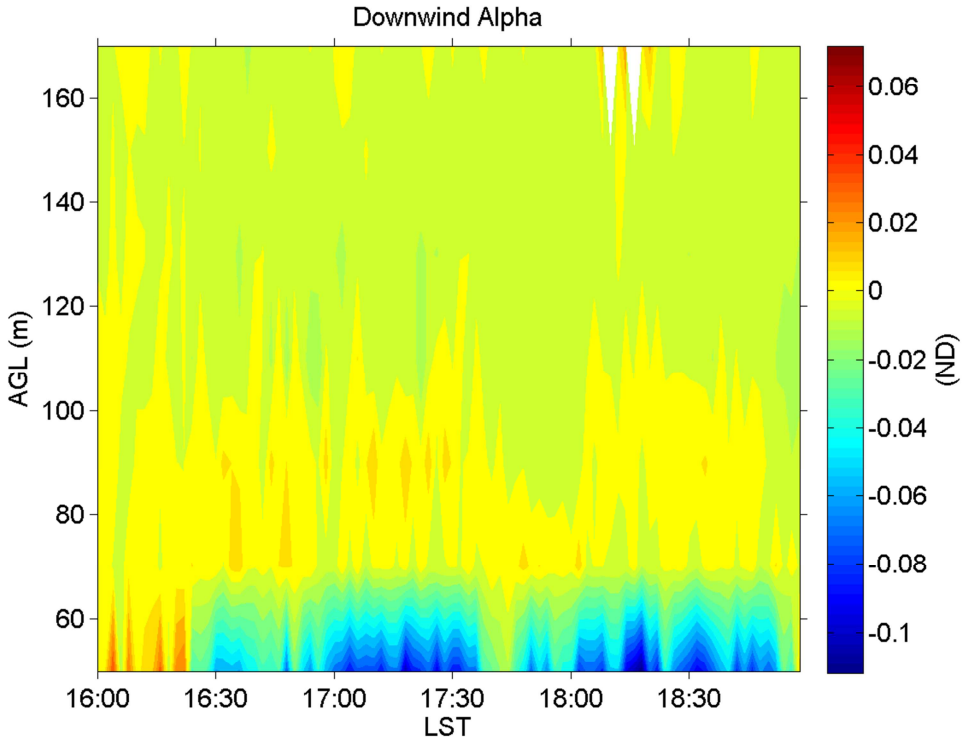

Figure 86: Convective time-height contours of downwind alpha, the power law coefficient

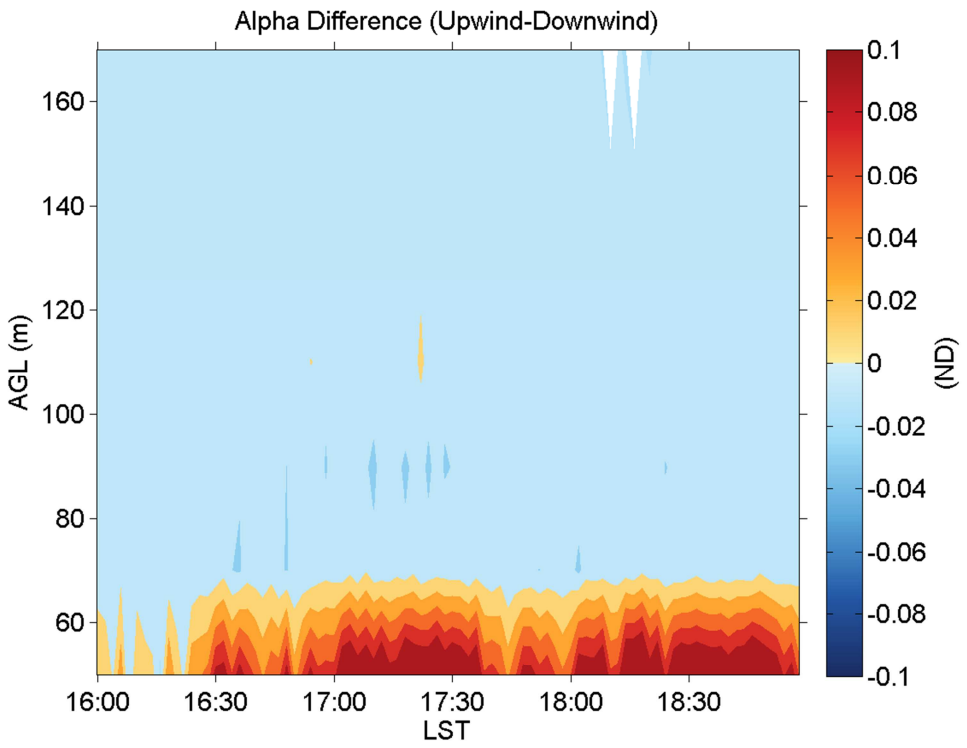

Figure 87: Convective time-height contours of upwind - downwind alpha differences

5.3 Case study summary and conclusion

The case study analysis of both nighttime stable conditions and daytime convective conditions allow us to explore in detail how the wind turbine affects the atmospheric flow over a shorter and continuous time periods. The data time averaging period for the case studies was 2 minutes for a single, real event, while the canonical day used 20 minute averaging periods over multiple days. Many of the turbine signatures present in the canonical day were also present in the case studies, such as increases in turbulence in the wake, decreases in horizontal momentum, and increases in vertical momentum for both nighttime and daytime cases. However, details about turbine and flow interaction are evident in the case studies that were not present in the canonical day analysis. The case study analysis shows turbine wake detection is highly sensitive to wind direction, and during the night time case study a wind direction shift near 3:00 caused the downwind LIDAR to observe atmospheric conditions outside the wake. We found that alpha was the most useful parameter to easily determine if downwind flow was waked or not, and the case studies reveal how quickly the wake could

shift between wake and non-wake conditions for relatively small differences in incoming wind direction. Using alpha instead of wind direction to determine wake periods may prove to be more useful for analysis of turbine wake behavior. Daytime wind direction shifts were not as dramatically captured in turbine variables because of the generally convective conditions. The other major difference between the two case studies is in the wind direction shear. Both day and night show a wake signature with positive shear capped by negative shear. However, the nighttime stability allowed the directional shear to remain strongly stratified for most the night, while the daytime shear structure does not persist due to convection.

6 Conclusions

Wind turbines have a measureable effect on atmospheric flow as measured 3 rotor diameters (240m) downwind of a multi-MW three-bladed horizontal axis turbine. Using two wind-profiling LIDARS, we have collected data to quantify those differences, finding patterns similar to those reported by other investigators in wind tunnel studies and high-resolution numerical simulations. Analysis of wind speed and turbulence intensity differences and their dependence on inflow wind speed shows that for upwind wind speeds between (4m/s and 10m/s) there is increased turbulence intensity and decreased wind speed downwind of the turbine rotor region.

One of our major findings was that the sign of alpha between 50-70 m is useful easy determinant of wake versus non-wake downwind conditions. Because alpha becomes negative downwind during wake conditions due to the momentum loss in the rotor disc region, alpha is a clear indicator of wind turbine wake and it could prove a more precise tool than upwind wind direction for definition of wake periods.

Our canonical day analysis shows that the main differences between upwind and downwind conditions also occur at rotor disc heights. Similar to the wind speed dependence study, the canonical day analysis shows decreased wind speeds but increased turbulence parameters and vertical velocities. However, we did note some differences over the course of the diurnal cycle due to varying stability through the day. To explore the diurnal impact on wake conditions, we examined a day and night case study, like the wind speed dependence and canonical day, these two case studies showed increases in turbulence but decreased momentum in the rotor disc area of the wake. However, the case studies reveal that observations of the wake are dependent on inflow wind direction and that during the day there is less directional shear than during the day due to convection. Finally, these case studies reinforced that the value of alpha was a good indication of wake conditions; when alpha values were negative at heights between 50m and 70m the conditions were waked, but when they were positive at the same heights conditions were not waked and these wake and non-wake conditions could change relatively quickly over the case study periods. Additionally, all three analyses show that in the turbine wake there were increases in turbulence, decreases in horizontal momentum, and increases in vertical momentum. Fluxes of heat and moisture depend strongly on turbulent and vertical

motions that move energy and moisture up and down in the atmosphere. Understanding how turbines impact nearby crops and other nearby environments will depend on quantifying how turbine wakes behave.

While we were able to investigate stable and convective conditions during the summer of 2011, the range of stability conditions does not span what might occur in other seasons. At this time we are unable to quantify differences between upwind and downwind variables based on stability alone, but further study might allow us to create a meaningful correlation. Additionally, the results are likely applicable only to this region, or other similar areas, since wind turbine wakes can vary depending on the geographic situation. Further study is needed to generalize the impacts of turbines on nearby environments beyond the Midwest. This data set can be used to help define the physical extent of turbine wakes for the Midwest.

The present work has provided insight into the impact of turbine wakes on the atmosphere at one location downwind of a turbine. To understand the spatial extent of turbine wakes and their evolution downstream, however, future field studies could incorporate scanning LIDAR to capture how a wake evolves downwind of a turbine. Scanning LIDAR can capture conical, constant azimuth vertical information. Scanning LIDAR can also take vertical scans that gives information across a vertical swath of the wake or horizontal scans that span wake and non-wake conditions simultaneously. Additionally, using a radiometer or tall tower measurements to measure temperature and moisture profiles of the atmospheric boundary layer would allow for better understanding of stability conditions and impacts of the turbine wake on moisture flux. *In situ* flux measurements of moisture, heat, or trace gases from met towers that span the distance between standard 10m met stations and the 40m lowest Windcube level would provide a more complete understanding of how wind turbine wakes propagate to and interact with the surface.

The CWEX 2011 LIDAR dataset answers important questions about the atmospheric boundary layer in a Midwest wind farm, and provides useful information for future development and prediction of wind farm performance in the region.

7 Bibliography

Acevedo, Otávio C., and David R. Fitzjarrald. 2001. "The Early Evening Surface-Layer Transition: Temporal and Spatial Variability." *Journal of the Atmospheric Sciences* 58 (17) (August): 2650–2667. doi:10.1175/1520-0469(2001)058<2650:TEESLT>2.0.CO;2.

Aitken, Matthew L., Michael E. Rhodes, and Julie K. Lundquist. 2012. "Performance of a Wind-profiling Lidar in the Region of Wind Turbine Rotor Disks." *Journal of Atmospheric and Oceanic Technology* (9): 120109134905004. doi:10.1175/JTECH-D-11-00033.1.

Albers, A., A.W. Janssen, and J. Mander. 2008. "Deutsche_windguard_report_windcube_evaluation.pdf". Deutsche WindGuard Consulting GmBH. http://www.leosphere.com/file/deusche_windguard_report_windcube_evaluation.pdf.

Baidya Roy, Somnath. 2011. "Simulating Impacts of Wind Farms on Local Hydrometeorology." *Journal of Wind Engineering and Industrial Aerodynamics* 99 (4): 491–498. doi:10.1016/j.jweia.2010.12.013.

Baker, R.W., and S.N. Walker. 1984. "Wake Measurements Behind a Large Horizontal Axis Wind Turbine Generator." *Solar Energy* 33 (1): 5–12.

Barthelmie, R. J., S. C. Pryor, S. T. Frandsen, K. S. Hansen, J. G. Schepers, K. Rados, W. Schlez, A. Neubert, L. E. Jensen, and S. Neckelmann. 2010. "Quantifying the Impact of Wind Turbine Wakes on Power Output at Offshore Wind Farms." *Journal of Atmospheric and Oceanic Technology* 27 (August): 1302–1317. doi:10.1175/2010JTECHA1398.1.

Chamorro, Leonardo P., and Fernando Porté-Agel. 2010. "Effects of Thermal Stability and Incoming Boundary-Layer Flow Characteristics on Wind-Turbine Wakes: A Wind-Tunnel Study." *Boundary-Layer Meteorology* 136 (June 6): 515–533. doi:10.1007/s10546-010-9512-1.

Chan, P. W. 2008. "Measurement of Turbulence Intensity Profile by a Mini-sodar." *Meteorological Applications* 15 (2) (June 1): 249–258. doi:10.1002/met.66.

Courtney, M., R. Wagner, and P. Lindelöw. 2008. "Commercial Lidar Profilers for Wind Energy: a Comparative Guide." In *Conference Proceedings of EWEC 2008*.

Frehlich, Rod, Yannick Meillier, Michael L. Jensen, and Ben Balsley. 2003. "Turbulence Measurements with the CIRES Tethered Lifting System During CASES-99: Calibration and Spectral Analysis of Temperature and Velocity." *Journal of the Atmospheric Sciences* 60 (20) (September): 2487–2495. doi:10.1175/1520-0469(2003)060<2487:TMWTCT>2.0.CO;2.

Hogstrom, D. Asimakopoulos, H. Kambezidis, C. Helmis, and A. Smedman. 1988. "A Field Study of the Wake Behind a 2 MW Wind Turbine." *Atmospheric Environment 1967* 22 (4): 803–820. doi:10.1016/0004-6981(88)90020-0.

Holton, James. 2004. *An Introduction to Dynamic Meteorology, Vol. 89*. 4th ed. Elsevier Science.

Jacobson, Mark Z., and Mark A. Delucchi. 2011. "Providing All Global Energy with Wind, Water, and Solar Power, Part I: Technologies, Energy Resources, Quantities and Areas of Infrastructure, and Materials." *Energy Policy* 39 (March): 1154–1169. doi:10.1016/j.enpol.2010.11.040.

Käsler, Yvonne, Stephan Rahm, Rudolf Simmet, and Martin Kühn. 2010. "Wake Measurements of a Multi-MW Wind Turbine with Coherent Long-Range Pulsed Doppler Wind Lidar." *Journal of Atmospheric and Oceanic Technology* 27 (September): 1529–1532. doi:10.1175/2010JTECHA1483.1.

Kelley, N., M Shirazi, D Jager, S Wilde, J Adams, M Buhl, P Sullivan, and E Patton. 2004. *Lamar Low-level Jet Project Interim Report*. National Renewable Energy Laboratory.

Kelley, ND, BJ Jonkman, and GN Scott. 2006. "The Great Plains Turbulence Environment: Its Origins, Impact and Simulation." In *AWEA WindPower Conference, Pittsburgh, USA*.

Kocer, G., M. Mansour, N. Chokani, R.S. Abhari, and M. Muller. 2011. "Full-Scale Wind Turbine Near-Wake Measurements Using an Instrumented Uninhabited Aerial Vehicle." *Journal of Solar Energy Engineering* 133 (4) (November): 041011–8. doi:10.1115/1.4004707.

Lee, S., M Churchfield, P Moriarty, J Jonkman, and J Michalakes. 2012. "Atmospheric and Wake Turbulence Impmacts on Wind Turbine Fatigue Loading." http://www.nrel.gov/docs/fy12osti/53567.pdf.

Lu, Hao, and Fernando Porté-Agel. 2011. "Large-eddy Simulation of a Very Large Wind Farm in a Stable Atmospheric Boundary Layer." *Physics of Fluids* 23: 065101. doi:10.1063/1.3589857.

Mikkelsen, T. 2009. "On Mean Wind and Turbulence Profile Measurements from Ground-based Wind Lidars: Limitations in Time and Space Resolution with Continuous Wave and Pulsed Lidar Systems." In *2009 European Wind Energy Conference and Exhibition: Wind Profiles at Great Heights 12*.

Milligan, M., D. Lew, D. Corbus, R. Piwko, N. Miller, K. Clark, G. Jordan, L. Freeman, B. Zavadil, and M. Schuerger. 2009. "Large-Scale Wind Integration Studies in the United States: Preliminary Results."

Pauliac, Romain. 2009. "Windcube V1 User's Manual". Leosphere, NRG.

Peña, Alfredo, Sven-Erik Gryning, Jakob Mann, and Charlotte B. Hasager. 2010. "Length Scales of the Neutral Wind Profile over Homogeneous Terrain." *Journal of Applied Meteorology and Climatology* 49 (April): 792–806. doi:10.1175/2009JAMC2148.1.

Rajewski, Daniel, Eugene Takle, Julie Lundquist, Steven Oncley, John Prueger, Thomas Horst, Michael Rhodes, et al. 2012. "CWEX: Crop/Wind-energy Experiment: Observations of Surface-layer, Boundary-layer and Mesoscale Interactions with a Wind Farm." *Bulletin of the American Meteorological Society* In Review.

Sathe, A., J. Mann, J. Gottschall, and M. S. Courtney. 2011. "Can Wind Lidars Measure Turbulence?" *Journal of Atmospheric and Oceanic Technology* 28 (July): 853–868. doi:10.1175/JTECH-D-10-05004.1.

Schwartz, M.N., and D.L. Elliott. 2006. *Wind Shear Characteristics at Central Plains Tall Towers*. National Renewable Energy Laboratory.

Stull, Roland B. 1988. *An Introduction to Boundary Layer Meteorology*. Springer.

Trujillo, Juan-José, Ferhat Bingöl, Gunner C. Larsen, Jakob Mann, and Martin Kühn. 2011. "Light Detection and Ranging Measurements of Wake Dynamics. Part II: Two-dimensional Scanning." *Wind Energy* 14 (January): 61–75. doi:10.1002/we.402.

Wharton, Sonia, and Julie K Lundquist. 2011. "Assessing Atmospheric Stability and Its Impacts on Rotor-disk Wind Characteristics at an Onshore Wind Farm." *Wind Energy* (July). doi:10.1002/we.483. http://onlinelibrary.wiley.com/doi/10.1002/we.483/abstract.

Wu, Yu-Ting, and Fernando Porté-Agel. 2010. "Large-Eddy Simulation of Wind-Turbine Wakes: Evaluation of Turbine Parametrisations." *Boundary-Layer Meteorology* 138 (December 14): 345–366. doi:10.1007/s10546-010-9569-x.